CHAPTER-5

RESULTS AND DISCUSSION

5.1 Calibration of glassware and instruments

5.1.1 *Calibration of thermometer*

The results of the thermometer calibration are mentioned in Table 5.1. The results were compared to the standard melting point of benzoic acid, which is 122 °C, according to IP 2014. The melting point observed was confirmed to be within the acceptable range. As a result, the thermometer was calibrated.

Table 5.1: Melting point of benzoic acid for thermometer calibration.

Observed melting point (°C)				Standard melting point of benzoic acid (°C)
1	**2**	**3**	**Mean**	
122.4	121.9	120.9	121.7	121 ± 2

5.1.2 *Calibration of measuring cylinder*

Calibrations of measuring cylinders were carried out by comparing the volume of the measuring cylinders to a standard volume. Results are summarized in Table 5.2.

Table 5.2: Calibration of volume for 10 mL and 100 mL measuring cylinders.

Observed volume (mL)				Standard volume (mL)
1	**2**	**3**	**Mean**	
10.1	10.2	10.2	10.2	10.0
100	99.8	100.1	100	1100.0

5.1.3 *Calibration of analytical balance*

The internal and exterior weights were adjusted as per the Standard Operating Procedure (SOP) to calibrate the analytical balance. Table 5.3 shows the results of external weights calibration of an analytical balance. The observed values were found to be within acceptable ranges and the analytical balance was calibrated.

Table 5.3: Interpretation of external weight with the standard weight.

S. No.	Weight (gm)	Standard weight (gm)	Observed weight (gm)	Standard deviation	Limit
1	100	100	99.73	0.38	±0.50
2	50	50.0096	50.0052	0.0025	±0.30
3	20	19.9906	19.9833	0.0037	±0.025
4	10	10.0015	10.0041	0.0004	±0.020
5	5	4.9946	4.9969	0.0006	±0.016

5.1.4 *Calibration of pipettes*

Pipettes (1 mL and 5 mL) were calibrated by measuring the volume of the pipette. The observed volume did not differ significantly from the standard volume and was deemed to be within acceptable limits. As a result, pipettes were calibrated. The results are summarized in Table 5.4.

Table 5.4: Interpretation of observed volume with standard volume for calibration of 1 mL and 5 mL pipettes.

Observed volume (mL)				Standard volume (mL)
1	**2**	**3**	**Mean**	
0.98	1.1	1.02	1.1	1.0
5.03	4.98	4.97	4.98	5.0

5.1.5 *Calibration of pH meter*

The pH of standard buffer solutions of pH 4 and pH 7 were used to calibrate the pH meter (Amar Enterprises, AI-102). Table 5.5 shows the calibration results for the pH meter. All of the recorded pH values were found to be within the permissible variation of 0.2. As a result, the pH meter was calibrated.

Table 5.5: Observed and accurate readings of pH meter using different buffers

S. No.	Buffer solution	Accurate pH	Observed pH
1.	A	4.14	4.00
2.	B	6.81	6.89

5.1.6 *Calibration of UV spectrophotometer*

UV spectrophotometer (Shimadzu, UV-1800) was calibrated for the limit of stray light, resolution power, and control of absorbance. The resulting values for these parameters were then compared to the IP, 2014 standard value, and the parameters were found to be within the acceptable range. As a result, the UV spectrophotometer (Shimadzu, UV-1800) was calibrated according to specifications.

5.1.6.1 *Limit of stray light*

The results are tabulated in Table 5.6. It was evaluated that absorbance of C at 200 nm was found to be > 2.0; thus, the UV spectrophotometer (Shimadzu, UV-1800) passed the test as per IP, 2014.

Table 5.6: Absorbance of KCl at 200 nm for the limit of stray light test.

Wavelength	Absorbance	Standard absorbance
200 nm	2.12	> 2.0

5.1.6.2 *Resolution power*

The results are tabulated in Table 5.7. The maximum absorbance at 269 nm was found to have a ratio of > 1.5 to the maximum (max) absorbance at 266 nm. Thus, according to IP, 2014, the UV spectrophotometer (Shimadzu, UV-1800) passed the resolution power test.

Table 5.7: Absorbance ratio for a resolution power test.

Wavelength (nm)	Absorbance (A)	Ratio=Max A at 269 nm / Max A at 266 nm	Standards limits
At 269 nm	2.34	1.647	**>1.5**
At 266 nm	1.42		

5.1.6.3 *Control of absorbance*

Results for this are shown in Table 5.8. All of the results were found to be within the parameters. As a result, the UV spectrophotometer (Shimadzu, UV-1800) passed the absorbance control test.

Table 5.8: Control of absorbance test.

S. No.	Wavelength (nm)	Absorbance (A)	∑	Maximum tolerance
1	235	0.744	123.34	122.9-126.2
2	257	0.869	144.36	142.8-145.7
3	313	0.297	49.88	47-50.3
4	350	0.641	106.9	104-108.2

5.2 Preformulation study

The physicochemical features of the obtained ART, such as physical appearance, melting point, solubility, and absorption maxima, were used to identify it. FT-IR, DSC, and XRD were used to evaluate the spectral interpretation of ART. The purity of the drug was confirmed by the findings of preformulation studies.

5.2.1 *Physical appearance*

ART was found to be a viscous creamy and odorless drug.

5.2.2 *Melting point*

The melting point of ART was found to be between 81°C – 83 °C ±1 °C as mentioned in Table 5.9, which complies with the standard given in IP, 2019. This confirmed the purity of the drug.

Table 5.9: Melting point of ART.

S.No.	Melting point of ART
1	81°C ±0.9°C
2	83°C±0.5°C
3	82 °C ±1°C

5.2.3 *Solubility studies*

In methanol, ART is freely soluble, but practically insoluble in water. The results are stated in Table 5.10. The results of ART solubility experiments revealed that the drug has a high solubility in organic solvents but a low solubility in aqueous media. Arteether is a relatively non-polar compound that contains a number of aromatic rings and long alkyl chains, which contribute to its low solubility in aqueous media, hence,

the drug is lipophilic. The collected data for determining solubility were found to comply with the literature (Chaturvedi *et al.*, 2010).

Table 5.10: Solubility data of ART.

S. No.	Solvents	Solubility	Inference
1	Methanol	250 mg/mL	Freely soluble
2	Dichloromethane	25 mg/mL	Sparingly soluble
3	Oleic acid	75 mg/mL	Soluble
4	Water	17µg/mL	Insoluble

5.2.4 *FT-IR spectroscopy*

5.2.4.1 *FT-IR analysis of ART*

The IR spectrum of ART is shown in Fig. 5.1. Various peaks observed were found to be concordant with the functional groups present in the structure of ART. FT-IR spectroscopy is a fast, non-destructive, and reliable method for confirming the purity of a procured drug. The wave number values for each peak have been explained in Table 5.11 and found to be similar to the reported data (Chadha *et al.*, 2011).

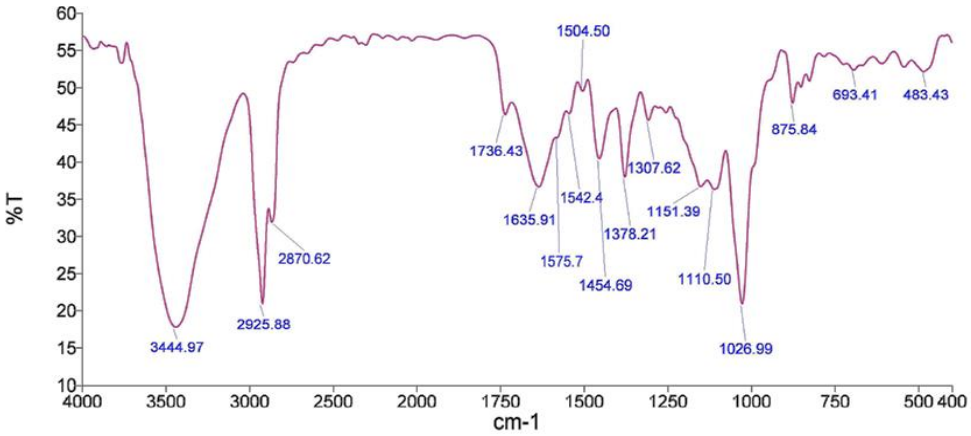

Figure 5.1: FT-IR spectrum of pure ART.

Table 5.11: Interpretation of FT-IR spectrum of pure ART.

Observed wave number (cm^{-1})	Standard wave number (cm^{-1})	Functional group
3444.97	3200 – 3450	OH
2925.88	2850 – 3000	-C-H
1454.69	1470	CH_2-
1110.50	1120 – 1260	Ether linkage
1026.99	1000 – 1300	C-O

5.2.5 *DSC analysis*

5.2.5.1 *DSC of ART*

The DSC thermogram of ART showed an endothermic peak at 177.57 °C and melting onset temperature at 174.14 °C and was found to be concordant with the reported literature (Chadha *et al.,* 2011). An enthalpy change (ΔH) of arteether was -1114.93J/g. The DSC thermogram confirms the crystalline nature of the drug as shown in Fig 5.2.

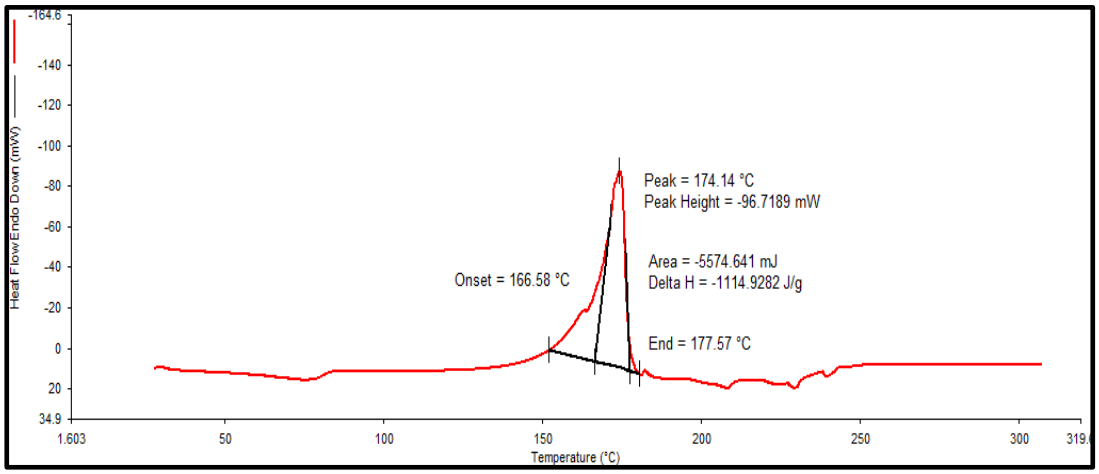

Figure 5.2: DSC thermogram of ART

5.2.6 *XRD analysis*

The XRD patterns of ART showed very strong characteristic diffraction peaks at 2θ of 9.19° or 9.29° as shown in Fig 5.3. It signifies that ART was purely a crystalline compound and was found concordant with the reported data (Gupta *et al., 2013*).

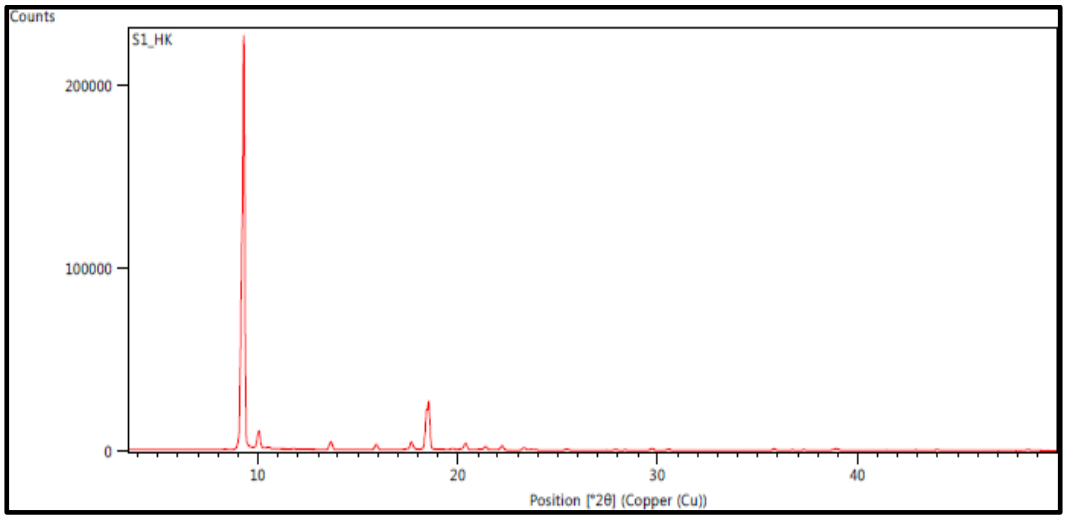

Figure 5.3: XRD pattern of ART.

5.2.7 *UV spectroscopy*

The identity and purity of the procured drug were confirmed through the degradation process and UV absorption. The use of 5M HCl to produce a chromophoric group that can absorb at 254±2 nm is a common method for detecting ART, as it has no UV absorption above 220 nm (Chadha *et al.*, 2014). The observed equation was a straight line in a slope-intercept form of ART in methanol, ethanol, and ethanolic phosphate buffer (pH 6.8) are depicted in Fig.5.4 A, Fig. 5.4 B, Fig.5.4 C, Fig.5.4 D respectively. The R^2 value was near 1indicating a very strong positive correlation between the two variables. This means that there was a high degree of association between the two variables and that the value of one variable can be used to predict the values of the other variable with a high degree of accuracy. Observed results complied with the reported values, thereby confirming the identity and purity of the procured drug (Chadha *et al.*, 2014).

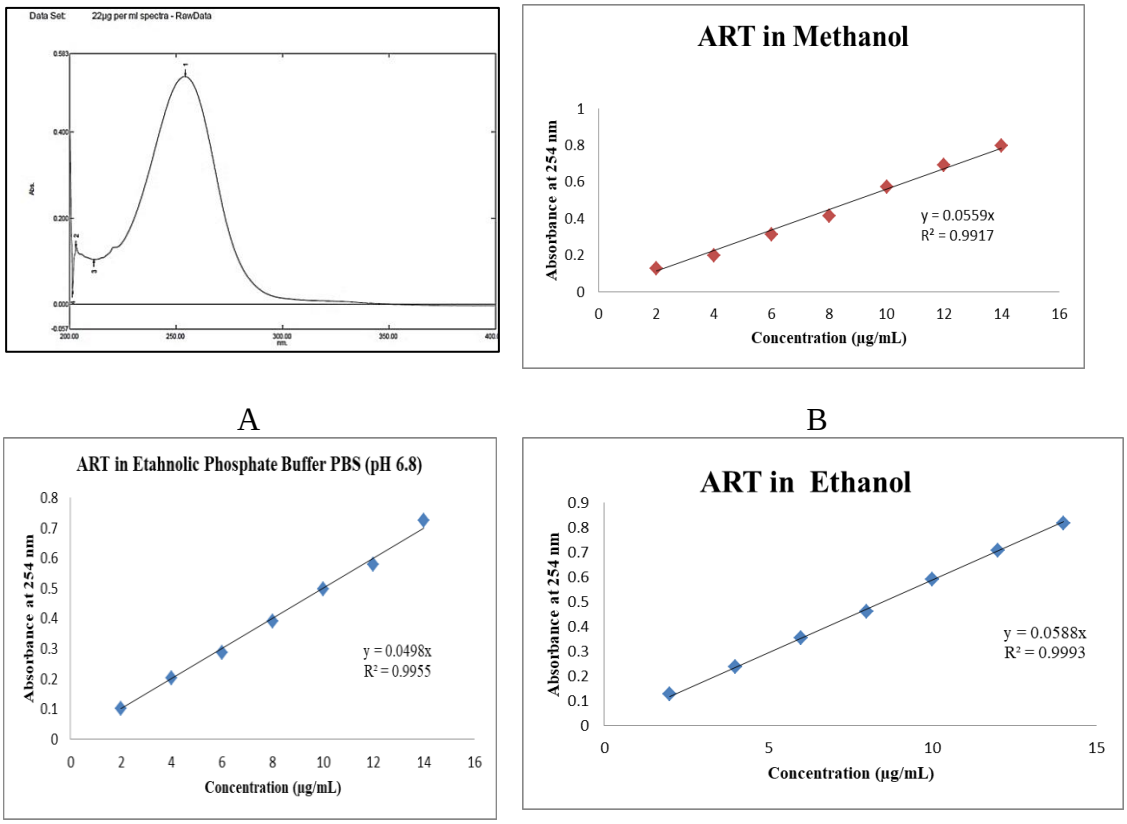

Figure 5.4: A) Spectrum of ART using UV spectroscopy B) Standard curve of ART in methanol, C) Standard curve of ART in ethanol, D) Standard curve of ART in ethanolic PBS 6.8.

5.2.7.1 *Determination of wavelength*

Fig.5.4 shows the spectrum and standard curve of ART in methanol, ethanol, and ethanolic phosphate buffer (pH 6.8), ART has no UV absorption above 220 nm, hence it was degraded using 5M HCl, resulting in a chromophoric group that can absorb at 254±2 nm. The observed findings matched the stated value, verifying the identification and purity of the drug.

5.2.7.2 *Experimental design*

Analytical Target Profile (ATP) was developed as a need for the QbD assisted UV spectrophotometric analytical method development by defining the desired quality attributes to the proposed method (Macintyre *et al.,* 2018). Table 5.12 lists potential ATP for development of UV spectrophotometric based methodology for estimation of ART.

Table 5.12: ATP for UV spectrophotometric method development of ART.

S. No.	ATP parameter	Objective/ Detail	Explanation
1.	Sample	ART	Quantitative assessment of drug molecule in a pharmaceutical dosage form utilizing a well-established analytical technique.
2.	Methodologies	UV spectrophotometric method	The UV spectrophotometric method is a simple way to assess drug molecules.
3.	Instrument requirement	UV spectrophotometer	UV spectrophotometer with high accuracy and precision.
4.	The nature of the analyte	Liquid (Solution)	In the case of liquid analyte (solution), uniform miscibility exists.
5.	Stock solution	Dilution of ART in ethanolic PBS 6.8	For proper dilution, ART should have 100% miscibility with required solvent.
6.	Sample preparation	Stock solution was used for sample preparation	As per the SoP, different concentrations of a solution containing ART were generated by manually weighing the required excipients and drug.
7.	Acid degradation	5M HCl was used for acid degradation	HCl was added in an appropriate amount to make the desired dilutions and then these were kept in water bath at 50±2 ºC for 30 min for acid degradation to get α, β-unsaturated decalone (8-methyl-5-(2-propanyl) decalin-4-ene3-one), a chromophoric derivative.
8.	Method utilization	Purity estimation and drug content of ART	The developed approach has been used to estimate the purity and drug content of ART in a variety of pharmaceutical formulations.

The aim of developing a novel UV spectrophotometric approach was to allow for rapid and straightforward drug analysis in comparison to previous sophisticated analytical methods. The absorbance of ART was chosen as the Critical Analyte Attribute (CAA) to achieve the predetermined goal profile (Madgulkar *et al.*, 2015).

The Ishikawa fishbone diagram (Fig 5.5) was created to demonstrate the correlation between the numerous process factors and essential analytical attributes (Magbool *et al.*, 2018), with absorbance at 254 nm chosen as the response. When the quantity of phosphate buffer pH 6.8 was raised, the absorbance increases, however, when the amount of 5N HCl was increased, drug degrades, resulting in a drop in absorbance.

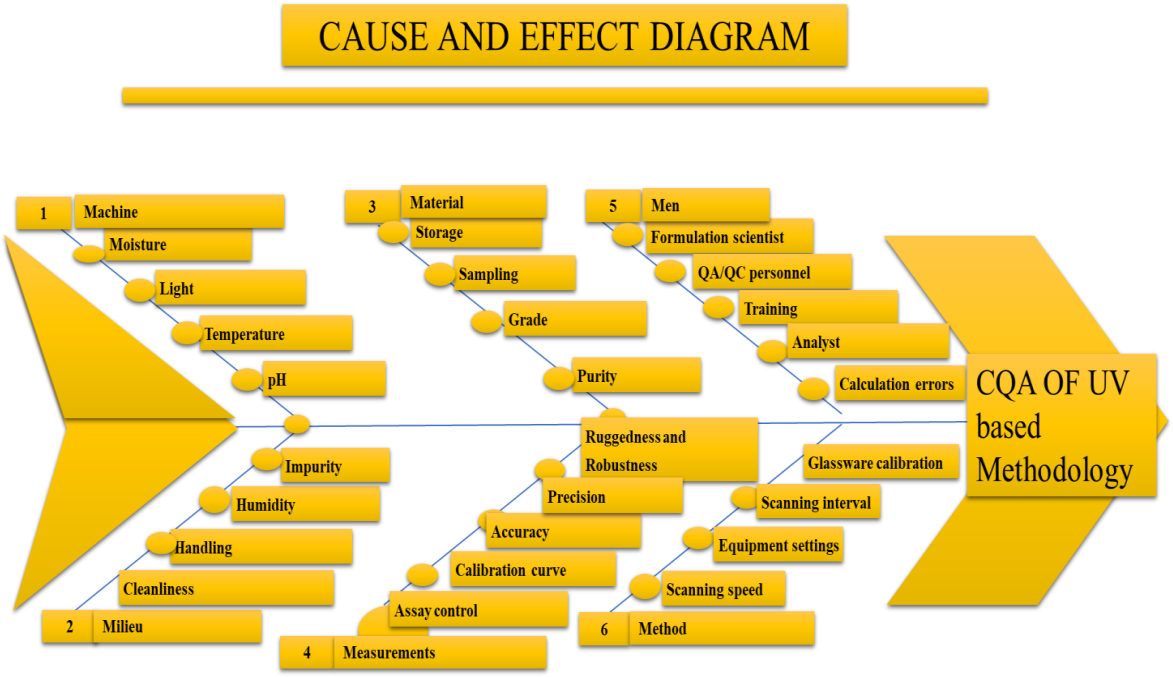

Figure 5.5: Ishikawa fishbone diagram for finding the probable factors that affect the method development.

Based on the results, absorbance at 254 nm was identified as the most important risk variable based on severity, which may be managed using the DoE technique. The remaining moderate and less effective risk variables were set to a constant value since they had a comparably less or moderate influence on the risk factors chosen (Marques-da-Silva *et al.*, 2020).

The mixture design was used to optimize crucial analytical variables. As responses or dependent variables, absorbance at 254 nm was used as shown in Table 5.13.

Table 5.13: Experimental design matrix obtained through mixture design.

Run	A:Amount of ethanol (mL)	B:Amount of HCl (mL)	C:PBS (pH 6.8) (mL)	Absorbance at 254 nm
1	6	2	2	0.922
2	5	2	3	0.848
3	5	1	4	0.595
4	5.51081	1.43437	3.05482	0.588
5	5	1.54236	3.45764	0.442
6	6	1	3	0.864
7	6	1.81241	2.18759	0.702
8	6	1	3	0.862
9	5.37796	1	3.62204	0.806
10	6	1.81241	2.18759	0.702
11	5	2	3	0.848
12	6	1.81241	2.18759	0.702
13	5	1	4	0.579

5.2.7.3 *Statistical optimization data analysis based on QbD*

After displaying the mathematical model using software, the experimental data was analyzed using the multiple linear regression analysis approach. A second-order quadratic model was built with the use of a coded equation that anticipated the link between the provided parameters and response (Mendoza-Muñoz *et al.,* 2021).

5.2.7.4 Equating *responses in terms of coded variables*

The correlation between the independent and dependent variables was predicted at different levels using equations in the form of coded factors. The lowest and highest levels were distinguished, with -1 (low level) and +1 (high level) respectively (higher levels).

The equation of selected responses is shown as Equation.

Absorbance at 254 nm = 0.153176 * A + 3.41772 * B + 0.58681 * C + -3.45762 * AB + 1.97128 * AC + -4.6167 * BC + -1.66614 * ABC……. (1)

Where, A is the amount of ethanol, B is the amount of HCl and C is the amount of PBS.

ANOVA was used to conduct a statistical analysis of the selected variables. A

significant model with a p-value less than 0.05 was selected and the suitability of the model was identified using the lack of fit, R^2, and modified R^2 values. The disparity between anticipated and exploratory data information points was not explained by the change judged by the imitates, according to a model with a significant 'Lack of Fit.' In ANOVA, R^2 values around 1 showed how well the predicted model matched the experimental model, and the value should be near 1 (Mirchandan *et al.,* 2021). Table 5.14 displays the results of different ANOVA studies of selected responses *i.e.* absorption at 254 nm, using various criteria such as p-value, lack of fit, and R^2 value.

Table 5.14: ANOVA analysis of response (absorbance of 254 nm).

Source	Sum of Squares	df	Mean Square	F-value	p-value	Inference
Model	0.2522	6	0.0420	1886.88	< 0.0001	Significant
Linear mixture	0.0503	2	0.0251	1128.30	< 0.0001	
AB	0.0167	1	0.0167	749.72	< 0.0001	
AC	0.0153	1	0.0153	685.41	< 0.0001	
BC	0.0657	1	0.0657	2948.04	< 0.0001	
ABC	0.0010	1	0.0010	42.76	0.0006	
Residual	0.0001	6	0.0000			
Lack of Fit	3.634E-06	1	3.634E-06	0.1398	0.7239	Not significant
Pure Error	0.0001	5	0.0000			
Cor Total	0.2523	12				

(1) Inference for linear mixtures uses Type I sums of squares.

The value obtained for model F was 1886.88, which indicated a significant model and this magnitude has a 0.01% probability of arising due to noise. The ANOVA model also showed that model terms with P-values were significant as the value was less than 0.0500. The F-value of 0.14 for the 'Lack of Fit' indicated that it was not significant in comparison to the pure error. There's a 72.39 % likelihood that a big Lack of Fit F-value was caused by noise. The non-significant lack of fit indicated that the model was perfectly validated. The Adjusted R^2 of 0.9989 was quite close to the Predicted R^2 of 0.9707; that is, the difference was less than 0.2. The signal-to-noise ratio was measured by adequate precision (Newton *et al.,* 1998). It was preferable to have a ratio of more than four. The signal-to-noise ratio of 138.316 suggested a good signal.

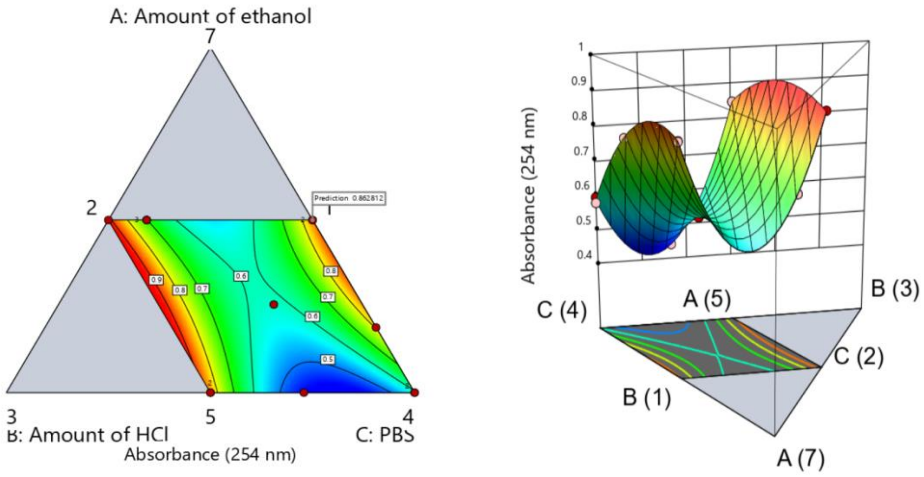

Figure 5.6: (a) 2D contour plot (b) 3D Response surface plot demonstrating the correlation between the specified variables.

To demonstrate the correlation between variables and response, 2D contour plots and 3D response surface plots were constructed using the Design Expert software, as shown in Fig. 5.6 (a) and (b). The absorbance started to decline at moderate and low values of both the specified variables, namely scanning speed and sample interval, according to the analysis of the aforementioned plots (Nontprasert *et al.*, 2019). To maximize selected essential aspects (amount of ethanol and HCl) in proportion to the desired response, it was critical to pick the design space from the experimental region (absorbance at 254 nm). Fig. 5.7 illustrated an overlay plot with the experimental area in grey and the design space in dark yellow. The light yellow zone denotes the region where several variables may be changed.

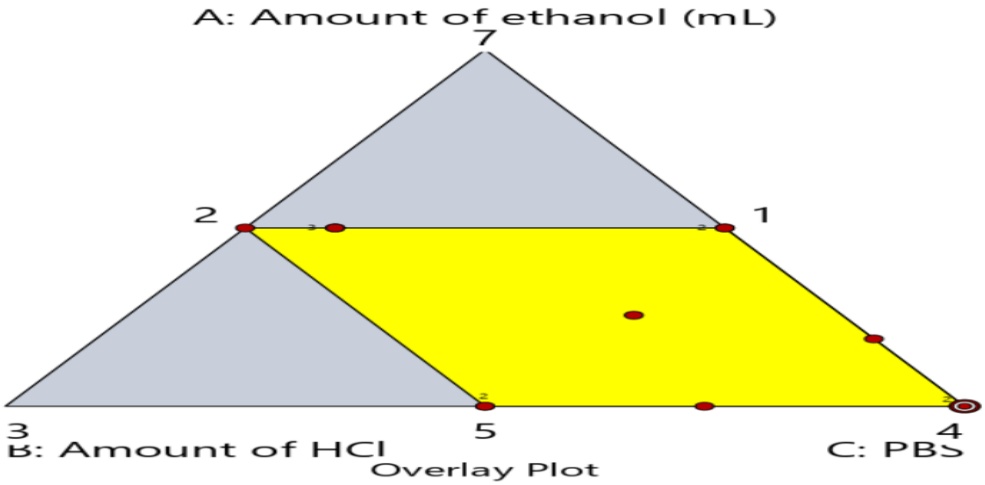

Figure 5.7: Overlay plot of the experimental area's design space (dark yellow).

5.2.7.5 *Experimental model validation*

The validation of the experimental design is also an essential criterion in the risk assessment and practical application of any analytical technique development based on the QbD and QRM principles. When the predicted value was compared to the experimental value, the developed model was found to be 98.1 % (0.702479 and 0.68923 was predicted and observed respectively) similar to the experimental value, confirming that the mathematical model can be acceptable for defining the interrelationship of selected variables to obtain the desired response within the identified design space as shown in Table 5.15 (Nureye *et al.,* 2020).

Table 5.15: Experimental validation of mathematical model.

Response	Predicted Mean	Predicted Median	Observed	Std Dev	n	SE Pred	95% PI low	95% PI high
Absorbance	0.702479	0.702479	0.68923	0.00471935	1	0.00531885	0.689464	0.715494

5.2.7.5.1 *Linearity*

The regression equations for the findings were determined using the least squares approach. Within the concentration range of 4-20 µg/mL, the Beer's Lambert law graph (n=6) was linear. Linear equation R^2 values vary from 0.9996 to 0.9999 ($p<0.001$), showing a good degree of linearity in the chosen solvent system.

5.2.7.5.2 *Precision*

Table 5.16 displayed repeatability results in three solvent systems during ART analysis validation investigations. The intraday and interday precision percent RSD values was observed around 0.612 % and 0.809 % respectively as shown in Table 5.16. In- terms of linearity, accuracy, and precision, the spectrophotometric analysis technique of, ART in diverse solvent systems was shown to be fairly excellent. The precision studies revealed appropriate sample stability and procedure dependability, with a percentage RSD of <2% (Mishra *et al.,* 2009).

Table 5.16: Precision of ART (4 µg/mL) in Ethanolic PBS 6.8.

S.No	Absorbance at λ_{max}	Calculated concentration (µg/mL)	Mean ±SD; RSD
Intraday (Ethanolic PBS 6.8)			
1	0.242	4.012	4.034±0.024; 0.612
2	0.246	4.061	
3	0.247	4.029	
Interday (Ethanolic PBS 6.8)			
1	0.245	3.964	3.996±0.032; 0.809
2	0.249	4.029	
3	0.247	3.996	

5.2.7.5.3 *Accuracy*

The percent accuracy of known concentrations (2, 4, 6 µg/mL) of ART in Ethanolic PBS 6.8 was found to be between 99.51 and 100.86 utilising the UV spectroscopy technique, as indicated in Table 5.17. The measured values are very comparable to the actual ones. The percent R.S.D. values were less than 2%, suggesting that the approach was accurate.

Table 5.17: Accuracy studies of ART in Ethanolic PBS 6.8.

Standard concentration (µg/mL)	Absorbance at λ_{max} (254 nm)	Calculated concentration (µg/mL)	% Accuracy	Mean ±SD; RSD
2	0.124	2.017	100.86	100.14±0.678; 0.677
4	0.247	4.002	100.05	
6	0.369	5.970	99.51	

5.2.7.5.4 *Robustness*

The novel method's resilience was validated using three duplicate trials with three different solvent ratios and three different wavelengths. The developed technique was shown to be robust, with a percent RSD of 0.539%. The results are summarised in Table 5.18.

Table 5.18: Robustness studies

Parameters	Alterations	% RSD (n=3) (Ethanolic PBS 6.8)
Solvent ratio (Ethanolic PBS 6.8: HCl)	8:2	0.539
Observed wavelengths	252 nm	0.507
	254 nm	0.498
	251 nm	0.431

5.2.7.5.5 *LOD and LOQ*

The calculations were done using conventional curve formulae. LOD is 3.3 times the standard deviation of the Y-axis intercepts, whereas LOQ is 10 times the standard deviation. Table 5.19 shows LOD and LOQ data, and it was proven that the suggested approach was sensitive and specific.

Table 5.19: Optimized parameters for UV estimation of ART.

Validation parameters	Values (Ehanolic PBS 6.8)
Absorption maxima (nm)	254
Linearity range	4-20 µg/mL
Standard regression equation	Y = 0.0014x + 0.0162
Correlation coefficient (R^2)	0.9969
Accuracy	100.14±0.678; 0.677
Precision	Intraday (0.536) Interday (0.553)
Robustness	1: 9 ratio (0.512) 2:8 ratio (0.539) 3: 7 ratio (0.315)
LOD	0.394 µg/mL
LOQ	1.263 µg/mL

Hence, the above results demonstrate the acceptability of the UV spectrophotometric method of analysis of ART in ethanolic PBS 6.8 with respect to linearity, accuracy, and precision.

5.2.8 Quantitation of ART using *HPLC method*

5.2.8.1 *Experimental design optimization using response surface methodology* for HPLC method

For optimizing chosen essential parameters such as pH of the mobile phase, concentration of the mobile phase, and flow rate in contrast to selected responses such as retention time and resolution, a central composite design was used, as depicted in Table 5.20. The primary composite design was chosen because it is a valuable optimization technique for determining the estimated relationship between independent and dependent variables (Alruwaili *et al.*, 2021). The fishbone diagram is as shown in Fig 5.8.

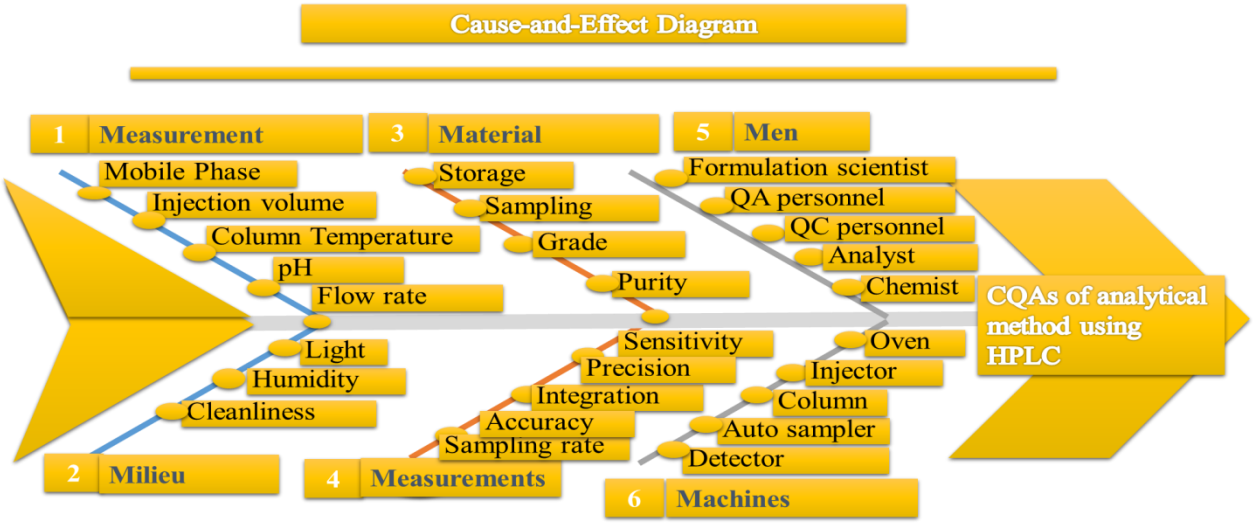

Figure 5.8: Ishikawa fish-bone diagram depicting various causes that affect the CQAs of the analytical method using HPLC.

Table 5.20: The experimental design for HPLC method using CCD.

Std	Run	A: pH of mobile phase	B: Flow rate (mL/min)	C:%ACN in water (%)	Retention time (min)	Resolution
14	1	5	0.55	76.8179	3.1	4.2
13	2	5	0.55	43.1821	1.9	5.3
15	3	5	0.55	60	5.2	4.6
19	4	5	0.55	60	5.6	4.5
20	5	5	0.55	60	5.2	4.6
4	6	7	1	50	2.4	4.5
6	7	7	0.1	70	3.3	3.7
9	8	1.63641	0.55	60	4.4	4.6
8	9	7	1	70	2	5.7
16	10	5	0.55	60	5.6	5.4
7	11	3	1	70	1.6	4.3
11	12	5	-0.206807	60	2.1	4.9
5	13	3	0.1	70	4.5	4.7
2	14	7	0.1	50	1.7	3.1
10	15	8.36359	0.55	60	3.9	3.8
12	16	5	1.30681	60	0.7	5.1
1	17	3	0.1	50	2.8	5.9
17	18	5	0.55	60	5.3	5.5
18	19	5	0.55	60	5.3	5.5
3	*20*	*3*	*1*	*50*	*2.1*	*5.7*

5.2.8.2 *ANOVA-based statistical analysis for HPLC method*

The appropriateness of the model was tested using an analysis of variance (ANOVA). Table 5.21 displays many ANOVA-based statistical parameters. The model was chosen after a thorough examination of several characteristics such as the f-value, p-value, R^2 value, anticipated R^2 value, Standard Deviation (SD) value, and good precision value, which were crucial in determining the model's relevance (Awotwe-Otoo et al., 2012). For a model to be significant, its p-value must be less than 0.5. The model's error was calculated using the "Lack of Fit" value. A substantial "Lack of Fit" indicates that the developed model did not distinguish between exploratory and anticipated data points (Bansal *et al*., 2016). The R^2 number indicates how well the predicted data points fit into the experimental data points, and it should be close to one. For a model to be significant, the anticipated R^2 value must deviate by more than 0.2. The adequate precision in the ANOVA measures the signal-to-noise ratio in the model, and a ratio of 4 or higher is required for a model to be noise-free as shown in Table 5.21. The SD of the developed model should have a lower value for the developed model's importance (Borman *et al*., 2006).

Table 5.21: ANOVA for quadratic model.

Source	Sum of Squares	Df	Mean Square	F-value	p-value	Inference
Model	48.05	9	5.34	222.69	< 0.0001	Significant
A-pH of mobile phase	0.4363	1	0.4363	18.20	0.0016	
B-flow rate	3.15	1	3.15	131.23	< 0.0001	
C-%ACN in water	1.43	1	1.43	59.62	< 0.0001	
AB	1.13	1	1.13	46.93	< 0.0001	
AC	0.0000	1	0.0000	0.0000	1.0000	
BC	2.21	1	2.21	91.98	< 0.0001	
A^2	2.59	1	2.59	108.05	< 0.0001	
B^2	28.09	1	28.09	1171.91	< 0.0001	
C^2	14.62	1	14.62	609.98	< 0.0001	
Residual	0.2397	10	0.0240			
Lack of Fit	0.0664	5	0.0133	0.3830	0.8421	Not significant
Pure Error	0.1733	5	0.0347			
Cor Total	48.29	19				

The Model F-value of 222.69 indicated that the model was statistically significant. An F-value of this magnitude had a 0.01% probability of occurring due to noise.

Model terms with P-values less than 0.0500 were significant. A, B, C, AB, BC, A^2, B^2, and C^2 were essential to model terms in this situation. The model terms are unnecessary if the value is more significant than 0.1000 (Dejaegher *et al.*, 2011). Model reduction may enhance statistical model if there are numerous inconsequential model terms (not including those essential to maintain hierarchy).

The F-value of 0.38 for the Lack of Fit indicated that it was not significant compared to the pure mistake. A significant Lack of Fit F-value had an 84.21% probability of occurring owing to noise. To fit the model slight lack of fit is required (Hibbert *et al.*, 2012).

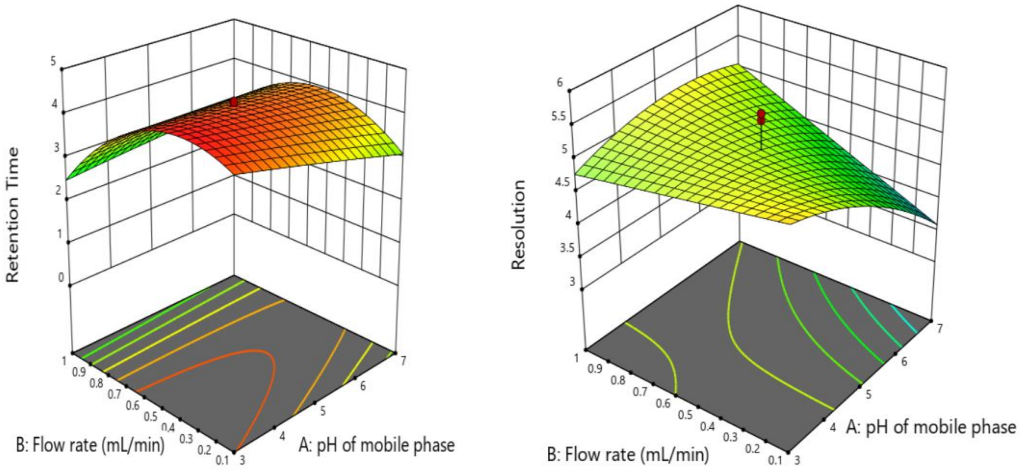

Figure 5.9: 3-D response surface plots portraying the effect of flow rate and pH of the mobile phase on retention time and resolution.

The 3D surface plot (Fig 5.9) for retention and resolution time revealed a decrease in retention time with increasing flow rate and pH, but somewhat that the effect diminishes after saturation. In contrast, the impact of the resolution was not significant. The response surface diagram was used to demonstrate the inter-variation, interdependence, and co-dependence among the chosen independent variables and their probable interaction with the response/dependent variable (Monks K *et al.*, 2012).

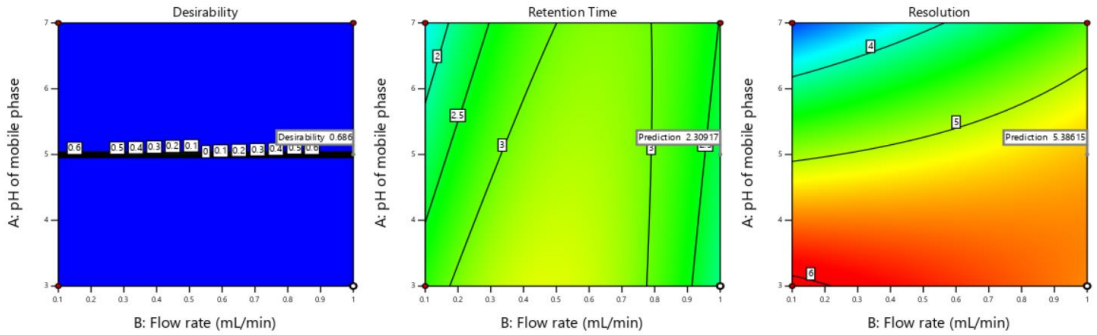

Figure 5.10: The standard plots of residuals for all the selected independent variables showing that irregular distribution of the data points to that of the best-fit line.

The data around the best-fit line demonstrated the generated QbD model's applicability for optimizing chosen independent variables, as shown in Fig 5.10.

The generated model operated in an experimental domain (Fig 5.11) was built using various independent variables. However, it is vital to establish the design space, which aids in creating an analytical method's ultimate quality profile (Musters *et al.*, 2013).

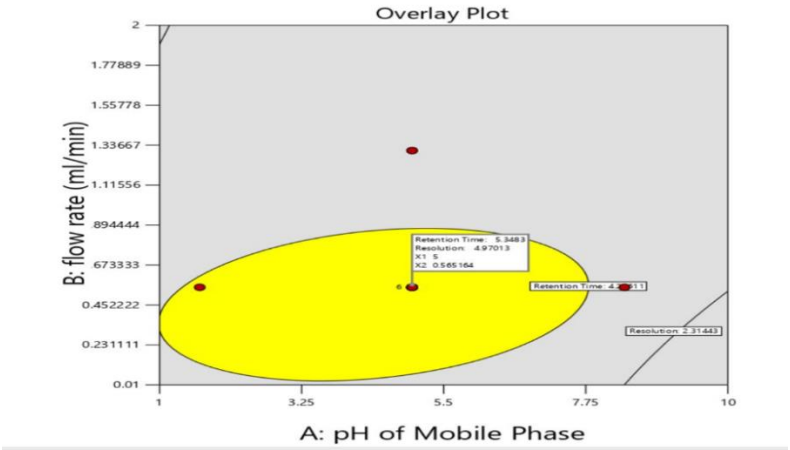

Figure 5.11: Overlay plot presenting the optimized analytical data as depicted by flag with the design space demarcated by the yellow region.

5.2.8.3 *The proposed model's point prediction and validation*

The Design-Expert software's point prediction feature was used to determine the optimal value of independent variables for meeting the quality goal profile, as shown in Table 5.22 below.

Table 5.22: Point prediction and confirmation/observed feature for determining the optimized independent variable values.

Response	Predicted Mean	Predicted Median	Observed	Std Dev	SE Mean	95% CI low for Mean	95% CI high for Mean	95% TI low for 99% Pop	95% TI high for 99% Pop
Retention Time	5.74784	5.74784	5.6	0.15483	0.0631385	5.20716	5.48852	4.59806	6.09762
Resolution	4.97024	4.97024	4.85	0.396039	0.11331	4.72545	5.21503	3.25427	6.68621

In the optimized mobile phase, an HPLC chromatogram of ART was produced and displayed in Fig. 5.10. For the linearity range of 1- 40 ng/mL, the retention time for ART was 5.687 min, with a correlation value of 0.999 and 97.4% similarity was observed.

A variety of criteria, many of which are within the researcher's control, affect a chromatographic method's capacity to correctly separate, identify, and quantify species. To determine the significance of these variables concerning the response, the ED/DoE provides a comprehensive set of statistical techniques capable of evaluating the impacts of each element alone and in combination. Flow rate, pH of the mobile phase A, percent acetonitrile in mobile phase B, and flow rate were selected as Critical Method Parameters (CMPs) for experimental design.

5.2.8.3.1 *Linearity (HPLC method)*

Linearity is an essential requirement for adopting any analytical technique in an HPLC study. The peak area (Mean SD) recorded at various ART concentrations after linear regression analysis.

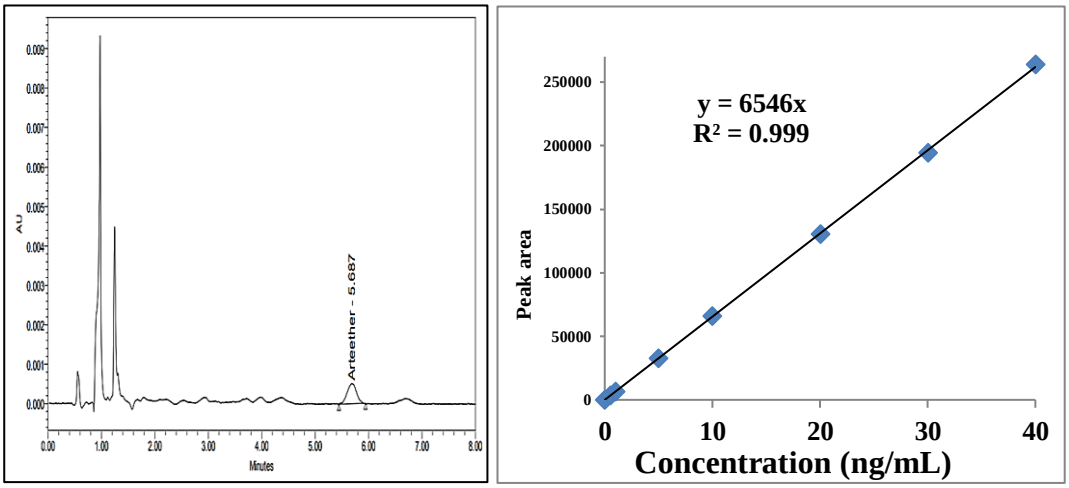

Figure 5.12: The typical HPLC chromatogram and linear calibration curve of ART.

RSD (2%) values were relatively low for all drug concentrations examined, indicating high technique repeatability.

Linearity was detected between peak regions at varying concentrations in the test concentration range (1-40 ng/mL), as illustrated in Fig 5.12. The linearity of the calibration plot was characterized by the equation y= 6546 x; r^2 = 0.999 ($p<0.001$), where y and x are the response and concentration, respectively. The slope's RSD was determined to be 1.322%.

5.2.8.3.2 *Accuracy (HPLC method)*

The accuracy data of ART acquired for analytical technique validation are shown in Table 5.23. The analytical investigations assessed accuracy by comparing measured values to actual concentrations at four different mobile phase concentrations. The percent accuracy for concentration (5, 10, and 20 ng/mL) with an RSD of 0.45%. It denoted a high degree of similarity between the measured and actual values.

Table 5.23: Results of accuracy study at concentrations (5, 10, 20 ng/mL).

Concentration (ng/mL)	Peak area (ART in mobile phase)	ART concentration recovered ± S.D	% Recovery	% RSD
5	33138	5.05±0.01	101.18	0.23
	33183			
	33033			
10	65456	10.02±0.03	100.20	0.39
	65434			
	65897			
20	132563	20.27±0.14	101.38	0.73
	133785			
	131865			
Average			100.92	0.45

5.2.8.3.3 *Precision (HPLC method)*

When a procedure is used repeatedly to different sampling sites of a homogenous sample, precision refers to the degree of consistency among the findings of individual tests.

As reported in Table 5.24, the system repeatability data for ART showed that the measured RSD values were in the range from 0.79% to 1.18 %.

Table 5.24: Results of system repeatability study at different concentrations.

Concentration (ng/mL)	Peak area	Mean concentration ± SD	RSD (%)
10	66574	10.20±0.08	0.79
	67389		
	66389		
20	132664	20.30±0.04	0.23
	132785		
	133245		
40	262349	40.36±0.47	1.18
	262456		
	267833		

5.2.8.3.4 *Precision (Intraday and interday) (HPLC method)*

Table 5.25 displays the mean drug concentrations, SD and RSD values, and data from the precision study. The percent RSD values for intra-day and inter-day investigations ranged from 0.24 to 0.40% for intra-day and 0.12 to 1.52% for inter-day studies, indicating good repeatability of the analytical procedure. As a result, the observed levels were deemed within permissible limits (ICH 1996; USP XXXII/NF-XXVII 2009).

Table 5.25: Results of precision at different concentrations of ART

S. No.	ART concentration (ng/mL)	Mean peak area±SD	Mean DIF concentration ± SD	% RSD
Intra-day precision				
1.	5	32449.33±111.59	4.95± 0.01	0.34
2.	20	133137.3±399.6	20.33 ±0.08	0.40
3.	40	263826.7±641.14	40.30 ±0.09	0.24
Inter-day precision				
1.	5	33016.67±503.32	5.04 ± 0.07	1.52
2.	20	132603±167.26	20.25 ± 0.02	0.12
3.	40	264212.3±707.51	40.36 ± 0.10	0.26

5.2.8.3.5 *Limit of detection (LOD) and limit of quantification (LOQ) (HPLC method)*

0.251 ng/mL and 0.762 ng/mL were estimated as the LOD and LOQ, respectively. These limitations imply that even short amounts of ART may be identified and measured (ICH 2005).

Overall, it can be stated that the established HPLC technique was quick, easy, reliable, selective, and repeatable and satisfies ICH Q2 R1 guidelines.

5.3 Solubility enhancement

5.3.1 *Characterization of prepared hydrotropic solid dispersions*

5.3.1.1 *Solubility studies of the prepared solid dispersions*

Various hydrotropic agents were tested to see whether they might improve aqueous solubility of ART. The aqueous solubility of ART was increased by 50.7 times using a hydrotropic mix of 40% nicotinamide solution. The solubility values of several hydrotropic mixes are shown in Table 5.26.

Table 5.26: Solubility enhancement in various hydrotropic blends.

S. No.	Hydrotropic agent	Solubility (mg/mL)	Solubility enhancement
1.	40% Sodium benzoate	0.625	36.76±1.2 times
2.	40% Nicotinamide	0.863	50.7±2.8 times
3.	40% Urea	_	Not enhanced
4.	40% Sodium citrate	_	Not enhanced
5.	20% Nicotinamide + 20% Sodium benzoate	_	Not enhanced
6.	30% Nicotinamide + 10% Sodium benzoate	_	Not enhanced
7.	10% Nicotinamide + 30% Sodium benzoate	_	Not enhanced

*Aqueous solubility of pure arteether = 17 µg/mL.

The hydrotropic solid dispersions with sodium benzoate and nicotinamide with maximum enhancement in aqueous solubility were further selected for the conformational studies.

5.3.2 *Differential scanning calorimetry of the prepared solid dispersions*

Pure ART has a normal crystalline thermal curve, with an endothermic peak at 177.57^{o} C and an exothermic peak at 174.14^{o} C as reported in Fig. 5.2. The endothermic peak of ART was completely absent from DSC curves of hydrotopic solid dispersions. The removal of the endothermic peak was a significant indicator of amorphous entity development and appropriate drug fit in solid dispersion. The DSC thermogram of the produced hydrotropic solid dispersions is shown in Fig. 5.13.

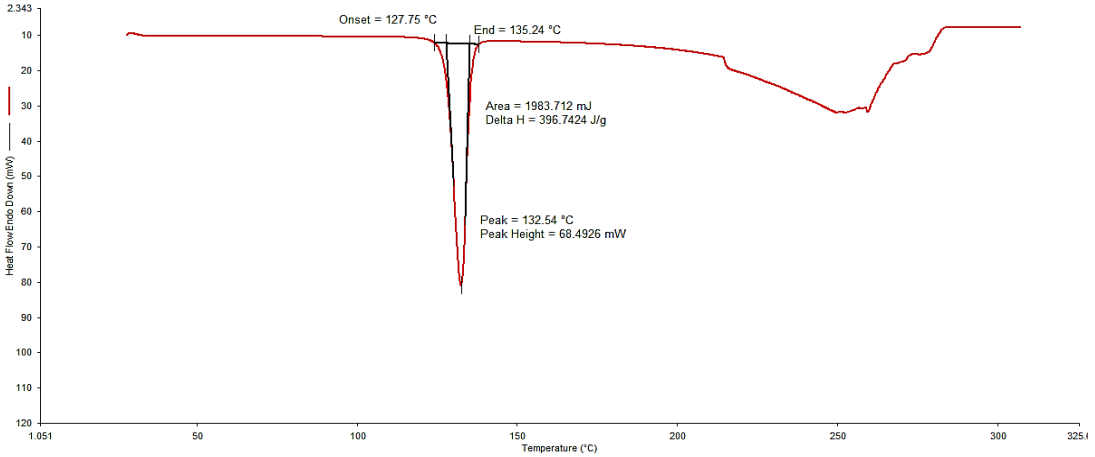

(a)

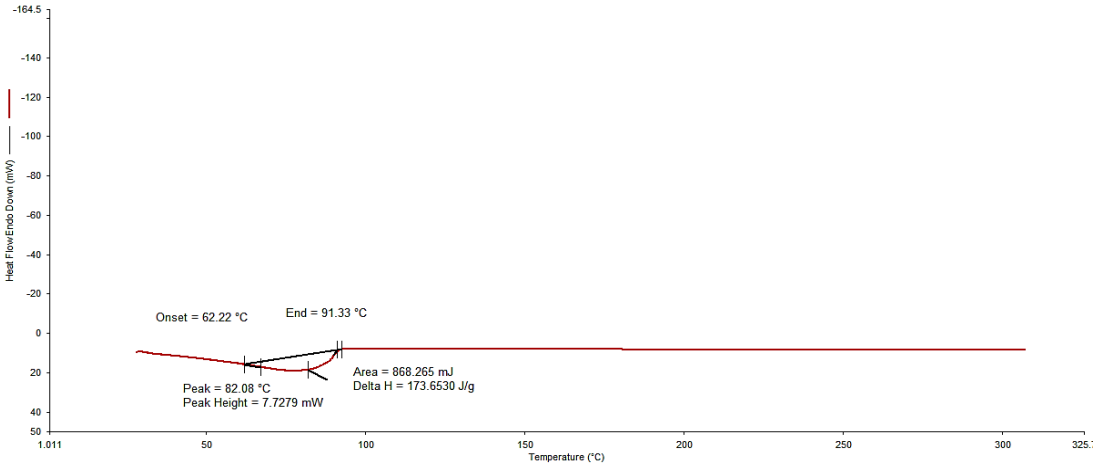

(b)

Figure 5.13: DSC thermogram of (a) AE-NIC-HSD (40 %) (b) AE-SB-HSD (40%).

5.3.3 *FT-IR spectroscopy of the prepared solid dispersions*

The typical peaks of ART were either displaced or disappeared, indicating that the environment had changed owing to the creation of solid dispersion between arteether and hydrotropic agents. ART FTIR spectra revealed distinct peaks at 1026.99, 1635.91, 3444.97, and 2925.88 cm^{-1}, respectively as reported in Fig. 5.1. The amorphous nature of prepared hydrotropic solid dispersion was shown by the lack of distinctive peaks in both ART-NIC-HSD and ART-SB-HSD hydrotropic solid dispersion (Fig. 5.14).

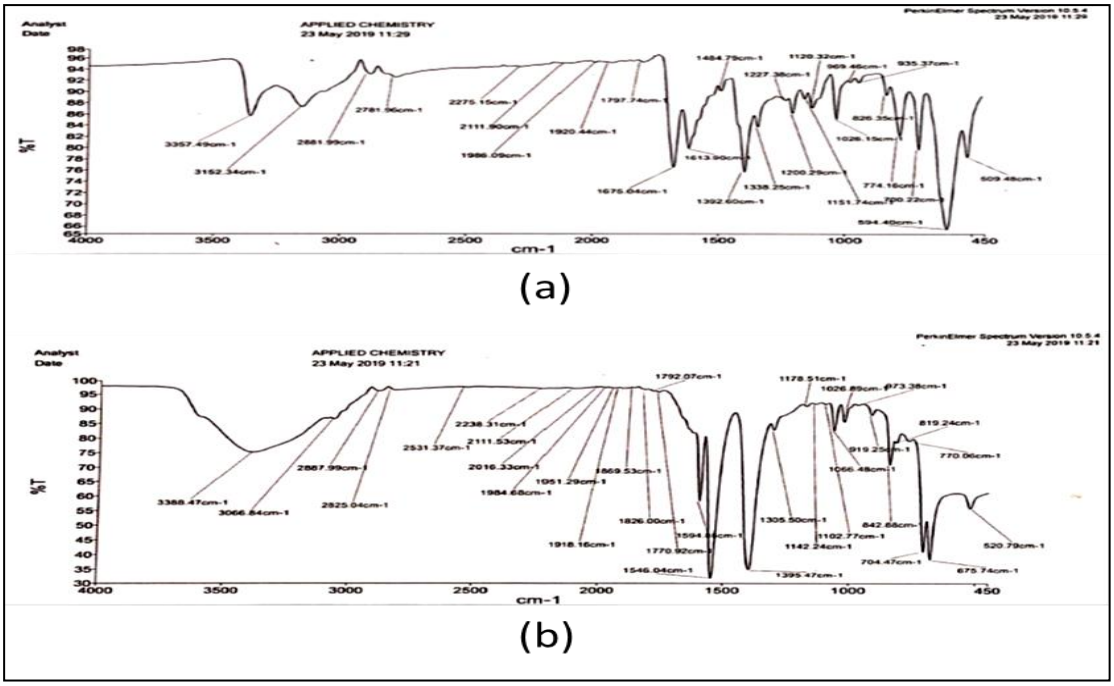

Figure. 5.14: FT-IR spectrum of (a) ART-NIC-HSD (40%) (b) ART-SB-HSD (40%).

5.3.4 *X-Ray diffraction studies of the prepared solid dispersions*

ART has extremely strong distinctive diffraction peaks at 2 θ of 9.19^{o} or 9.29^{o} in its XRD patterns as reported in Fig. 5.3. It denoted the fact that ART was a pure crystalline substance. After preparing solid dispersion development, all ART distinctive peaks were present at a lesser intensity for both ART-NIC-HSD and ART-SB-HSD (Fig. 5.15). The amorphous nature of solid dispersions was shown by the reductions in the intensity of distinctive peaks.

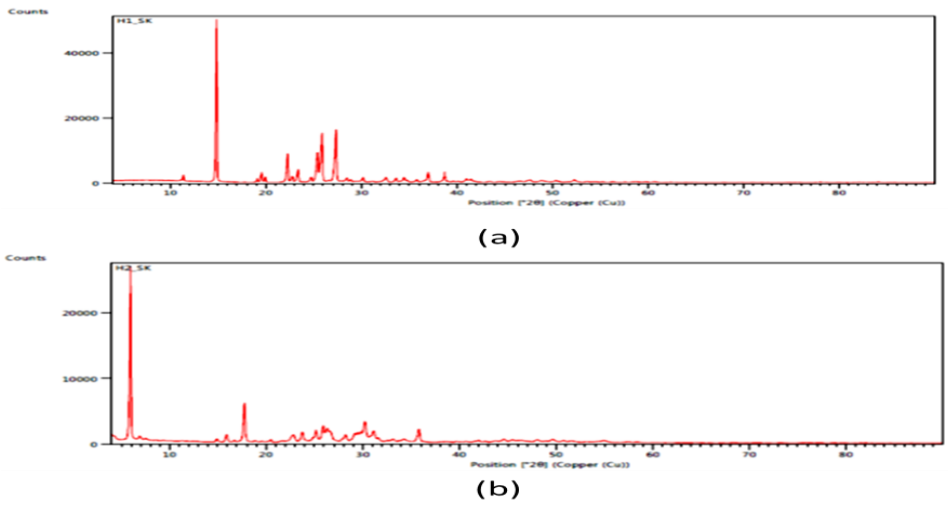

Figure 5.15: XRD pattern of (a) ART-NIC-HSD (40 %) (b) ART-SB-HSD (40%).

5.3.5 *Characterization of prepared solid dispersion*

The melting process and solvent evaporation procedure were used to create diverse solid dispersions utilizing various carriers. Table 5.27 summarizes the percentage yield of different solid dispersions generated.

Table 5.27: Percentage yield of prepared solid dispersion.

Composition	Ratio	Theoretical yield (mg)	Practical yield (mg)	% Yield
ART:PVP K-30	1:1	20	17	85
ART:HPMC E 15LV	1:5	60	53	88.3
ART:HPMC K 1OOM	1:4	50	47	94
ART:Sucrose	1:4	50	44	88
ART-Mannitol	1:2	30	27	90
ART:PEG-6000	1:4	50	45	90
ART:Poloxamer-188	1:2.5	35	32	91.4
ART:Poloxamer-407	1:3.5	45	41	91.1
ART:PEG-6000, Poloxamer 407, HPMC K 100M	1:4:3:4	120	109	90.8
ART:PEG-6000, Poloxamer-407, HPMC K 100M	1:1.4:1.2:1.4	50	43	86
ART:PEG-6000, Poloxamer-407, HPMC K 100M	1:2.9:2.2:2.9	90	84	93
ART:PEG-6000, Poloxamer-407	1:2.1:1.9	50	45	90
ART:PEG-6000, Poloxamer-407	1:4.3:3.7	90	85	94.4
ART: D-Fructose	1:3	36	28	77.7
ART: Dextrose	1:3	47	42	89.3
ART: Saccharin sodium	1:5	50	42	84
ART: D-tartaric acid	1:2	32	26	81.25
ART: Starch soluble	1:3	40	36	90
ART: Succinic acid	1:3	62	58	93.5
ART: β CD:PEG600:Poloxamer -407	1:1:3.7:4.3	89	85	95.5

The prepared solid dispersions were characterized based on the following techniques:

5.3.5.1 *Solubility studies of the prepared solid dispersions*

The aqueous solubility of ART was tested using a variety of solid dispersions prepared in the study. The solubility of the solid dispersion created using the melting process approach was the highest. Table 5.28 shows the solubility data while Table

5.29 provides the maximum solubility enhancement data for different solid dispersions.

Table 5.28: Solubility data of various prepared solid dispersions.

Composition	Method	Ratio	Solubility enhanced (times)
ART:PEG-6000	Melting	1:1, 1:2, 1:3, 1:4, 1:5	4.2, 4.1, 6.7, 5.8, 5.4 (± 0.6)
ART:Poloxamer-188	Melting	1:0.5, 1:1.5, 1:2.5, 1:3.5, 1:4.5	3.8, 4.5, 5.1, 6.2, 4.8 (±0.1)
ART:Poloxamer-407	Melting	1:0.5, 1:1.5, 1:2.5, 1:3.5, 1:4.5	3.5, 6.2, 7.3, 3.1, 3.8 (±0.5)
ART:PVP K-30	Solvent evaporation	1:0.25, 1:0.5, 1:1, 1:2, 1:3,1:4	3.2, 2.9, 3.7, 2.6, 1.4, 0.8 (±0.2)
ART:HPMC E 15LV	Solvent evaporation	1:1, 1:2, 1:3, 1:4, 1:5	3.2, 4.6, 4.9, 5.9, 7.9 (±0.4)
ART:HPMC K 100M	Solvent evaporation	1:1, 1:2, 1:3, 1:4, 1:5	4.2, 6.1, 7.8, 8.9, 9.1 (±0.5)
ART:Sucrose	Solvent evaporation	1:1, 1:2, 1:3, 1:4,1:5	1.8, 2.1, 3.4, 1.2, 2.6 (±0.2)
ART:Mannitol	Solvent evaporation	1:1, 1:2, 1:3, 1:4, 1:5	4.3, 4.8, 3.7,2.8,1.3 (±0.3)
ART:D-Fructose	Solvent evaporation	1:1, 1:2, 1:3, 1:4, 1:5	1.6, 1.4, 5.58, 2.05, 1.5 (±0.5)
ART:Dextrose	Solvent evaporation	1:1, 1:2, 1:3, 1:4, 1:5	9.35, 6.66, 10.142, 11.07, 6.12 (±0.1)
ART:Saccharin sodium	Solvent evaporation	1:1, 1:2, 1:3, 1:4, 1:5	19.4, 28.03, 28.03, 48.91, 61.06 (±0.6)
ART:D-tartaric acid	Solvent evaporation	1:1, 1:2, 1:3, 1:4, 1:5	2.08, 12.15, 11.02, 8.86, 4.62 (±0.3)
ART:Starch soluble	Solvent evaporation	1:1, 1:2, 1:3, 1:4, 1:5	18.03, 16.31, 18.76, 13.08, 15.53 (±0.7)
ART:Succinic acid	Solvent evaporation	1:1, 1:2, 1:3, 1:4, 1:5	6.5, 6.64, 7.48, 6.0, 3.4 (±0.4)
ART: β CD:PEG600:Poloxamer -407	Melting method	1:1:3.7:4.3	67 (±1)

*Aqueous solubility of pure ART = 17 μg/mL.

Table 5.29: Maximum solubility enhancement data of various solid dispersions.

Composition	Method	Ratio	Solubility enhanced (times)
ART:PVP K-30	Solvent evaporation	1:1	3.7±0.5
ART:HPMC E 15LV	Solvent evaporation	1:5	7.9±0.4
ART:HPMC K 1OO	Solvent evaporation	1:5	9.1±0.5
ART:Sucrose	Solvent evaporation	1:3	3.4±0.2
ART:Mannitol	Solvent evaporation	1:3	3.7±0.3
ART:PEG-6000	Melting	1:3	6.7±0.6
ART:Poloxamer-188	Melting	1:3.5	6.2±0.1
ART:Poloxamer-407	Melting	1:2.5	7.3±0.5
ART:PEG-6000:Poloxamer-407:HPMC K 100M	Melting	1:3:2.5:5	19.62±0.5
ART:PEG-6000, Poloxamer-407	Melting	1:3:2.5	39.6±0.4
ART:D-Fructose	Solvent evaporation	1:3	5.58±0.5
ART:Dextrose	Solvent evaporation	1:4	11.07±0.1
ART:Saccharin sodium	Solvent evaporation	1:5	61.06±0.6
ART:D-tartaric acid	Solvent evaporation	1:2	12.15±0.3
ART:Starch soluble	Solvent evaporation	1:3	18.76 ±0.7
ART:Succinic acid	Solvent evaporation	1:3	7.48±0.4
ART: β CD:PEG600:Poloxomer-407	Melting method	1:1:3.7:4.3	67±1

*Aqueous solubility of pure ART = 17 µg/mL.

For conformational investigations, solid dispersions with drug:carrier ratios of 1:3:2.5:5 (ART:PEG-6000, Poloxamer-407, HPMC K 100), 1:3:2.5 (ART:PEG-6000, Poloxamer-407), ART: CD:PEG 600:Pol -407 (1:1:3.7:4.3), and ART: Saccharin sodium (1:5) with the highest increase in solubility were used.

5.3.5.2 *Dissolution studies of the prepared solid dispersions*

Solid dispersion's hallmark behavior is rapid disintegration. The dissolution rate of both the solid dispersion and the liquid dispersion did not vary significantly. The dissolution profile of prepared solid dispersions as shown in Fig. 5.16. The combination of PEG-6000 and Poloxamer-407 results in a greater drug amorphization, which means that it had a disordered molecular structure that allowed

it to dissolve more easily in a solvent (Schweitzer *et al*., 2010). The increase in drug amorphization and combination solubility efficiency of PEG-6000 and Poloxamer-407 resulted in a faster dissolving rate of the produced solid dispersion. The solid dispersion made with PEG-6000 and Poloxamer-407 had a greater dissolving rate of ART with a weight ratio of 1:3:2.5:5 because both PEG-6000 and Poloxamer-407 are hydrophilic polymers that can enhance the solubility and dissolution rate of poorly water-soluble drugs like ART. Cyclodextrins are cyclic oligosaccharides that can form inclusion complexes with drug molecules, thereby improving their solubility and bioavailability.

When a solid dispersion is prepared using cyclodextrin as a carrier matrix, the drug molecules are encapsulated within the cyclodextrin cavity, which protects them from degradation and improves their stability (Peraman *et al*., 2015).

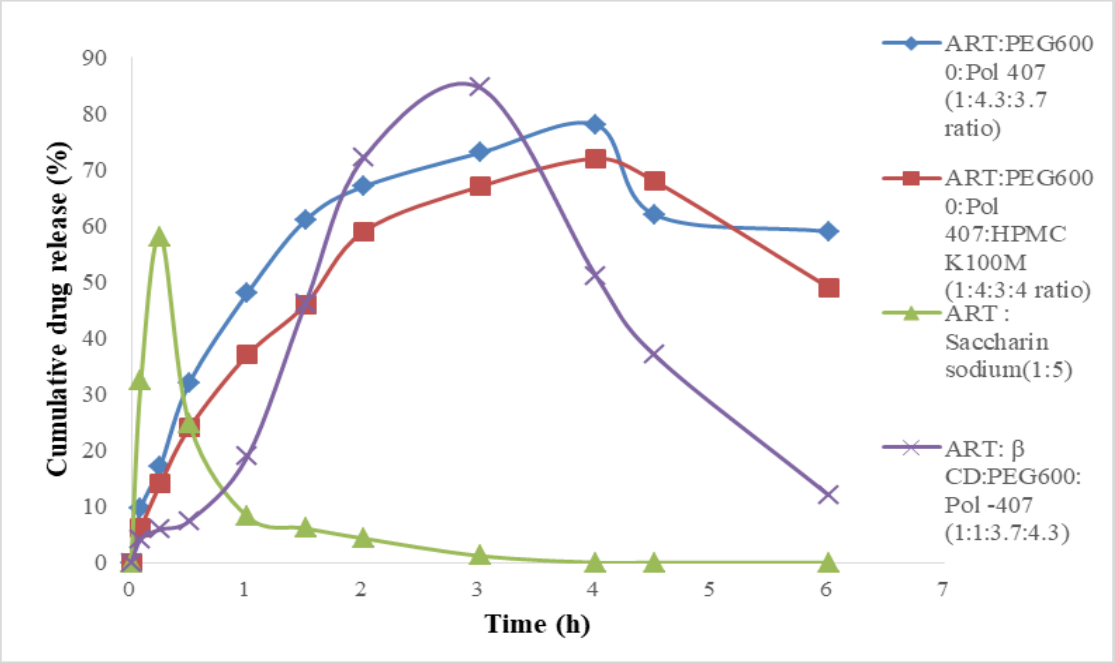

Figure 5.16: Dissolution profiles of prepared solid dispersions.

As the solid dispersion of ART with saccharin sodium showed burst release and not controlled release may be due to enhancement in solubility, they easily got dissolved in aqueous medium so it is not used for further studies.

5.3.5.3 *Differential scanning calorimetry of the prepared solid dispersions*

Pure ART has a normal crystalline thermal curve, with an endothermic peak at 166.58º C and an exothermic peak at 83.24º C. The DSC curves of both solid dispersion preparations showed no significant differences. The endothermic peak of

ART was completely absent from DSC curves of solid dispersions. The removal of the endothermic peak was a significant indicator of amorphous entity development and appropriate drug fit in solid dispersion. The DSC thermogram of pure drug and produced solid dispersions is shown in Fig. 5.17.

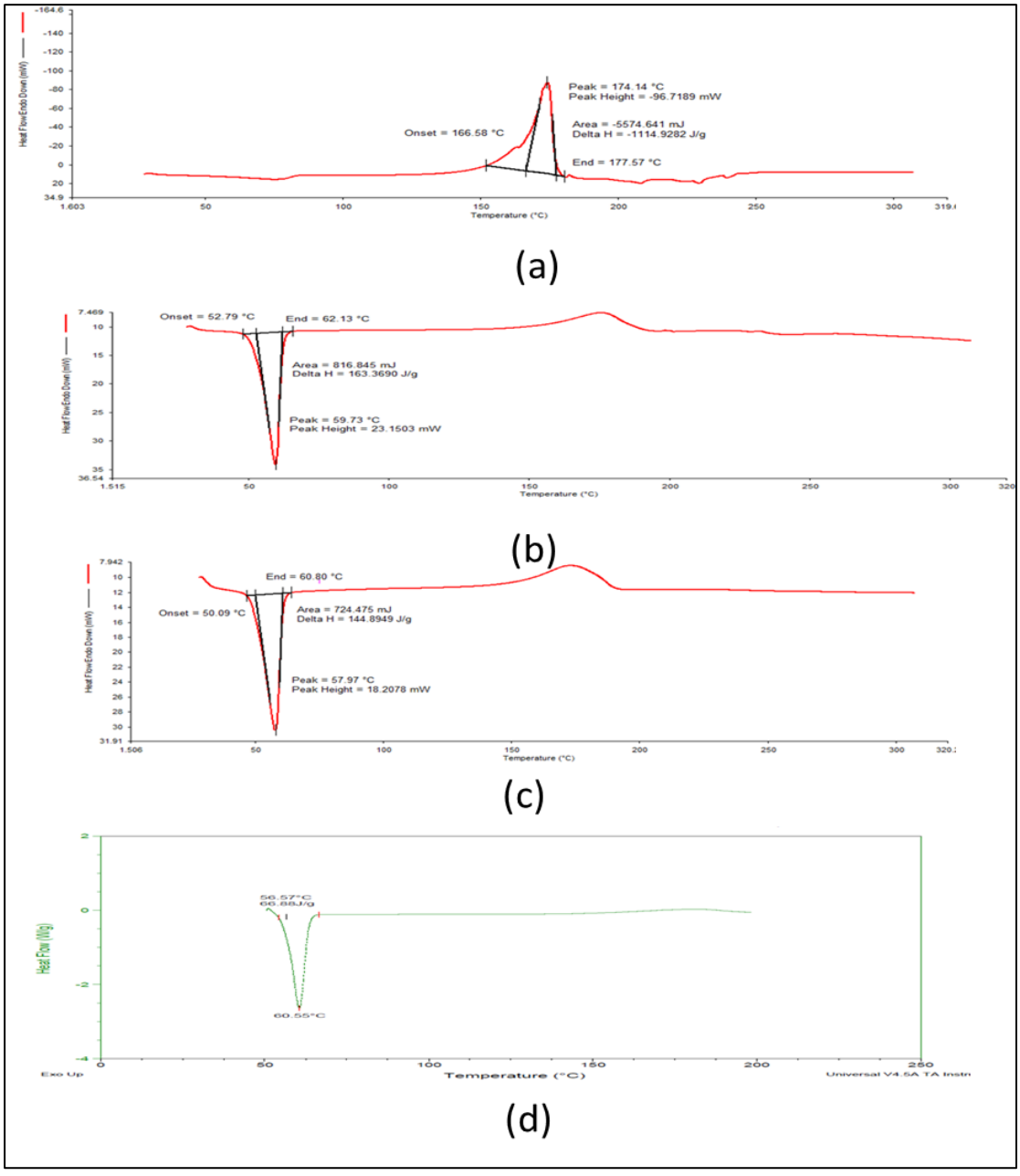

Figure 5.17: DSC thermogram of (a) ART (b) ART:PEG6000:Poloxamer 407 (1:3:2.5:5 ratio) **(c) ART:PEG6000:Poloxamer407:HPMC K100M (**1:3:2.5 ratio**) (d) ART: β CD:PEG600:Poloxamer -407 (**1:1:3.7:4.3 ratio**).**

5.3.5.4 *FT-IR spectroscopy of the prepared solid dispersions*

The typical peaks of ART were either displaced or missing, indicating that the environment had changed owing to the creation of solid dispersion between arteether and carriers. For both ART:PEG 6000:Poloxamer 407 (1:3:2.5:5 ratio), the C-O-, CH_2, CH_3, and C-H- stretching of pure ART moved to the the low frequency of 1143 cm^{-1}, 1463 cm^{-1}, 1342 cm^{-1}, and 2881 cm^{-1} (c) Solid dispersions of ART:PEG 6000:Poloxamer 407:HPMC K100M (1:3:2.5 ratio) (Fig. 5.18). The frequency of observed bands is shown in Table 5.30 along with their interpretation.

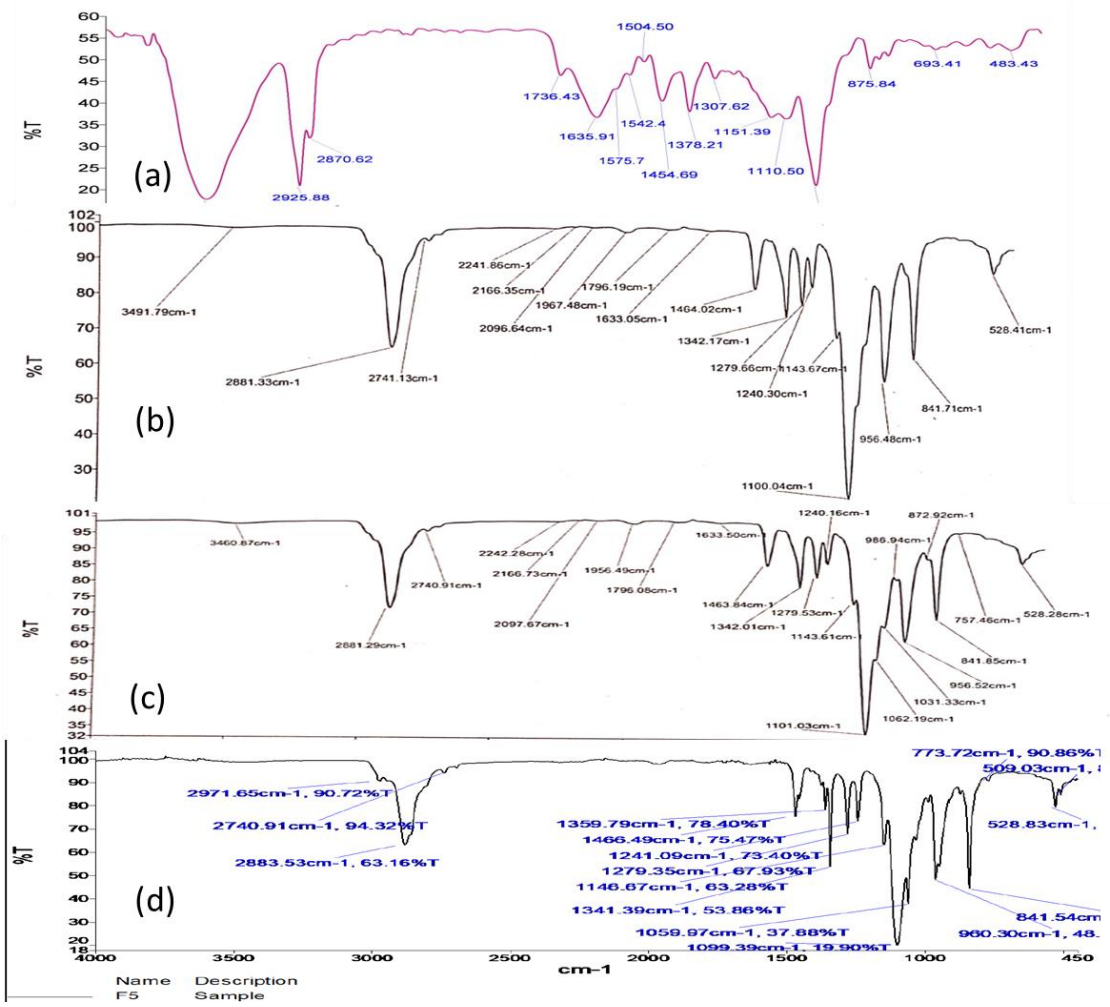

Figure 5.18: FT-IR spectrum of (a) ART (b) ART: PEG 6000:Poloxamer 407 (1:3:2.5:5 ratio**) (c) ART: PEG 6000:Poloxamer407:HPMC K100M (**1:3:2.5 ratio**) (d) ART: βCD: PEG 600:Poloxamer -407 (**1:1:3.7:4.3 ratio**).**

Table 5.30: Interpretation of FT-IR spectrum of solid dispersions

S. No.	Interpretation	Standard wave number (cm^{-1})	ART	SD-1	SD-2
1.	OH- (stretch)	3200 – 3450	3595.79 cm^{-1}	3491.79 cm^{-1}	3460.87 cm^{-1}
2.	C-O- (stretch)	2850 – 3000	2925.58 cm^{-1}	1100.04 cm^{-1}	2881.29 cm^{-1}
3.	CH_2 - (stretch)	1470	1454.69 cm^{-1}	1464.02 cm^{-1}	1463.84 cm^{-1}
4.	Ether linkage (stretch)	1120 – 1260	1143.67 cm^{-1}	1143.60 cm^{-1}	1101.03 cm^{-1}
5.	C-H- (stretch)	1000 – 1300	1110.50 cm^{-1}	2881.33 cm^{-1}	2741.13 cm^{-1}

5.3.5.5 *X-Ray diffraction studies of the prepared solid dispersions*

ART has extremely strong distinctive diffraction peaks at 2 of 9.190 or 9.290 in its XRD patterns. It denotes the fact that ART was a pure crystalline substance. After solid dispersion formation, all of the ART distinctive peaks were present at a lesser intensity for both ART:PEG 6000:Poloxamer 407 (1:3:2.5:5) and ART:PEG 6000:Poloxamer 407:HPMC K100M (1:3:2.5 ratio) (Fig. 5.19). The amorphous nature of solid dispersions was shown by the reductions in the intensity of distinctive peaks.

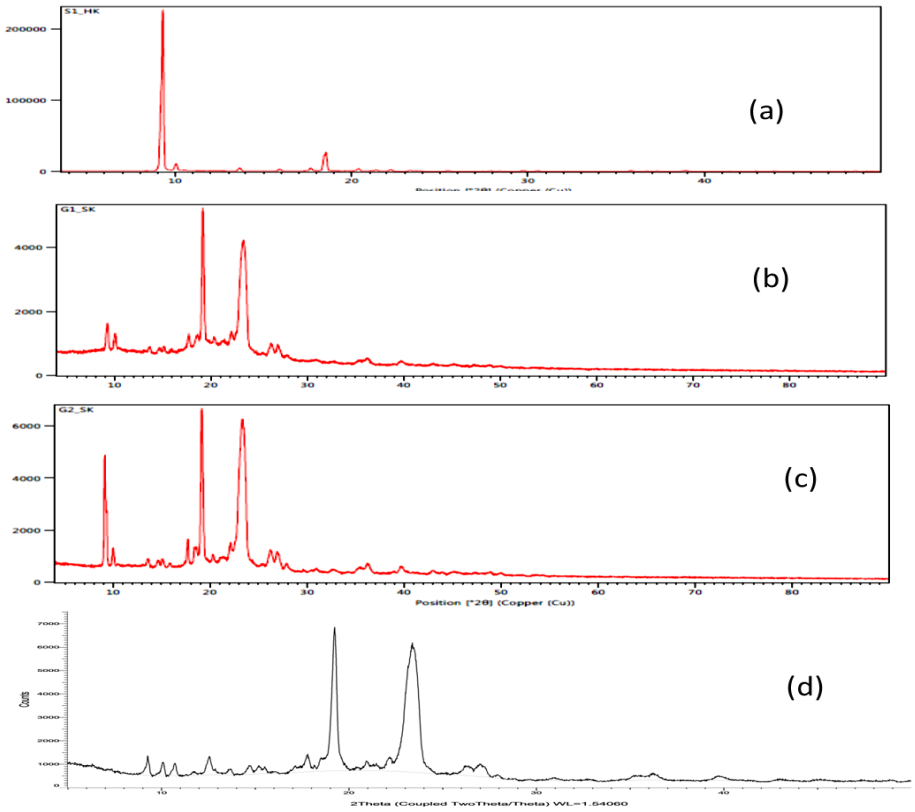

Figure 5.19: XRD pattren of (a) ART (b) ART:PEG 6000:Poloxamer 407 (1:3:2.5:5 ratio**) (c) ART:PEG 6000:Poloxamer 407:HPMC K100M (**1:3:2.5 ratio**) (d) ART: β CD:PEG 600:Poloxamer -407 (**1:1:3.7:4.3 ratio**).**

5.3.5.6 *Permeability studies of the prepared solid dispersions*

The Franz dispersion cell approach was used to establish if the formulated SDs of ART are effectively increasing its permeability through the tissue of the gut, resulting in improved bioavailability as a component of increased immersion dissolvability and disintegration rate (Rozet *et al*., 2013). In contrast to ART, (Fig. 5.20) displays the concentration of ART distributed over the colon of a pig for ART-loaded SDs.

The findings showed a significant improvement in the permeated measure of ART, with produced SDs displaying a 6.75-fold (0.648± 0.90 mg/mL) increase in permeability compared to ART plain drug (0.096± 0.23 mg/mL). Because the drug was contained in the cyclodextrin cavity, the permeability of ART: CD: PEG600:Pol - 407 (1:1:3.7:4.3) was only 4.42%. Surfactants such as PEG 6000 and poloxamer 407 were used to increase ART dissolvability and produce a supersaturated state in the gut by increasing wettability and dispersibility (Mahapatra *et al*., 2020).

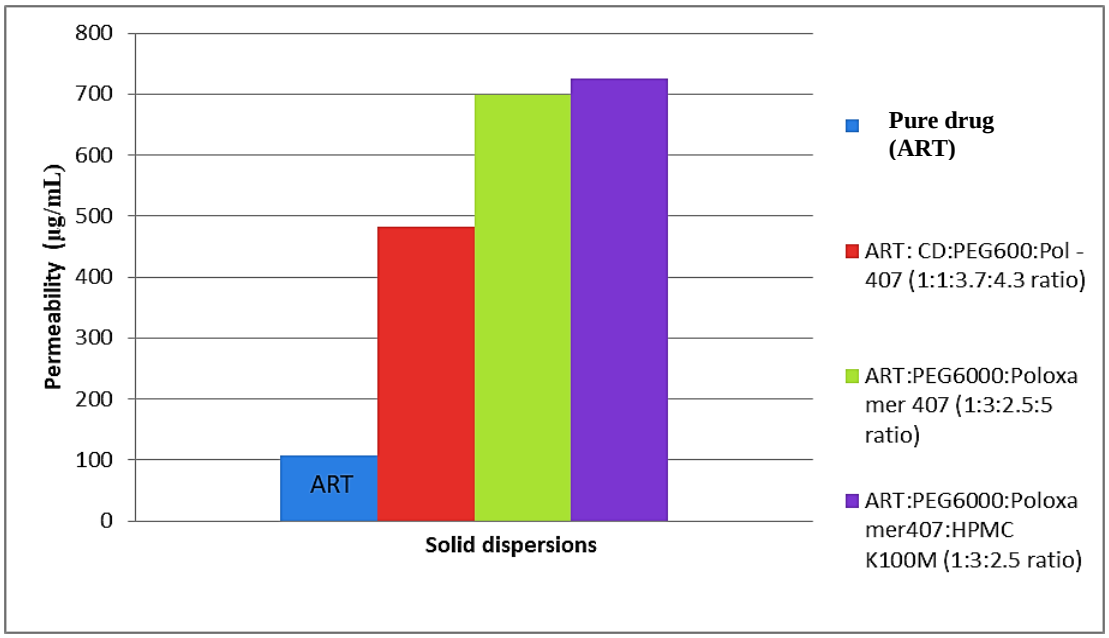

Figure 5.20: The permeability data of various solid dispersions.

5.3.6 *Preparation and characterization of inclusion complexes*

Binary and ternary inclusion complexes of β-CD were prepared by employing physical mixing, kneading method, and freeze-drying method. The percentage yield of various complexes formed is summarized in Table 5.31.

Table 5.31: Percentage yield of ART-β-CD.

Complex	Theoretical yield (g)	Practical yield (g)	% Yield
β – CD – ART (physical mixture)	4.6	4.12	89.13
β – CD – ART 3° (kneading method)	4.8	4.39	89.58
β– CD – ART 3° (lyophilisation)	1.8	1.23	68.33

The prepared complexes were characterized based on the following techniques:

5.3.6.1 *Solubility studies of inclusion complexes*

The prepared binary and ternary complexes were evaluated for enhancement in the aqueous solubility of ART. The complex formed with the spray drying technique had shown a maximum increase in solubility. As spray drying is an energy-intensive process, rapid solvent evaporation leads to amorphization of the drug as very less time is offered for crystal building process along with the inclusion of the drug in the cavity of the cyclodextrin and thus resulting in solubility enhancement. The maximum enhancement in solubility was observed with β-CD, as it is having maximum cavity size which leads to proper inclusion of the drug. Table 5.32 depicts the solubility data of the complex formed.

Table 5.32: Solubility data of binary complexes

Sr. No.	Complex	Aqueous solubility (µg/mL)	Enhanced solubility (in times)
1	ART – β – CD (PM) 2°	39.27	2.3
2	ART – β – CD (PM) 3°	41.86	2.4
3	ART– β – CD (KN) 2°	52.68	3.09
4	ART– β – CD (KN) 3°	60.0	3.53
5	ART– β – CD (FD) 2°	869.55	51.15
6	ART– β – CD (FD) 3°	1298.45	75.249

*Aqueous solubility of pure ART = 17 µg/mL.

5.3.6.2 *Dissolution studies of inclusion complexes*

Rapid dissolution is the characteristic behavior of inclusion complexes but the comparative release of drugs from complexes is strongly affected by the method of preparation. Fig. 5.21 depict the dissolution profile of complexes. The stronger drug amorphization and better inclusion were caused by the combined action of β-CD and

the hydrophilic polymers. The enhanced dissolution rate of ternary complexes was due to an increase in the complexation and solubility efficiency of CD.

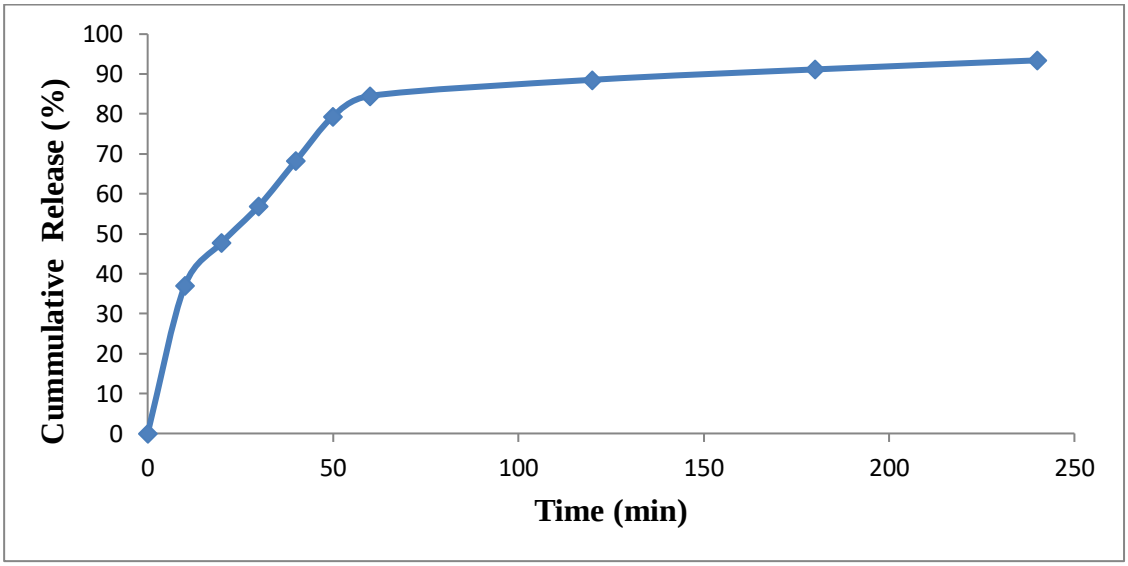

Figure 5.21: Dissolution profile of ART-β-CD ternary inclusion complex.

5.3.6.3 *FT-IR spectroscopy of inclusion complexes*

The characteristic peaks of ART and CD were either shifted or absent which suggested the change in environment due to the inclusion of complex formation between ART and CD. The O-H stretching of pure CD shifted to the low frequency of 3356.09 cm^{-1} for AE-β-CD binary (SD) 2^0 after inclusion complex formation (Fig. 5.22). It might be due to involvement of β-CD hydroxyl groups in hydrogen bonding with ART groups. Bands of the included part of the guest molecule are masked by the bands of the spectrum of CDs. Table 5.33 shows the frequency of observed bands and interpretation.

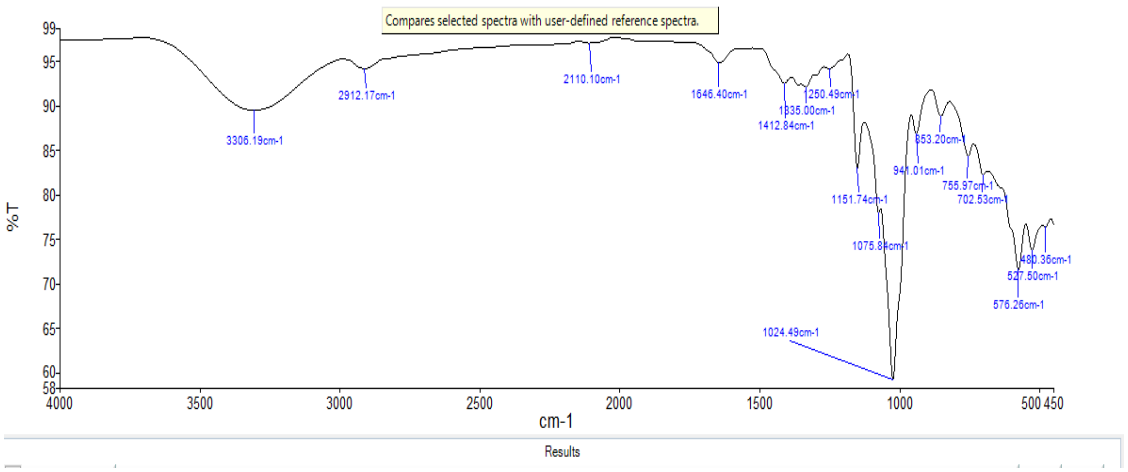

(a)

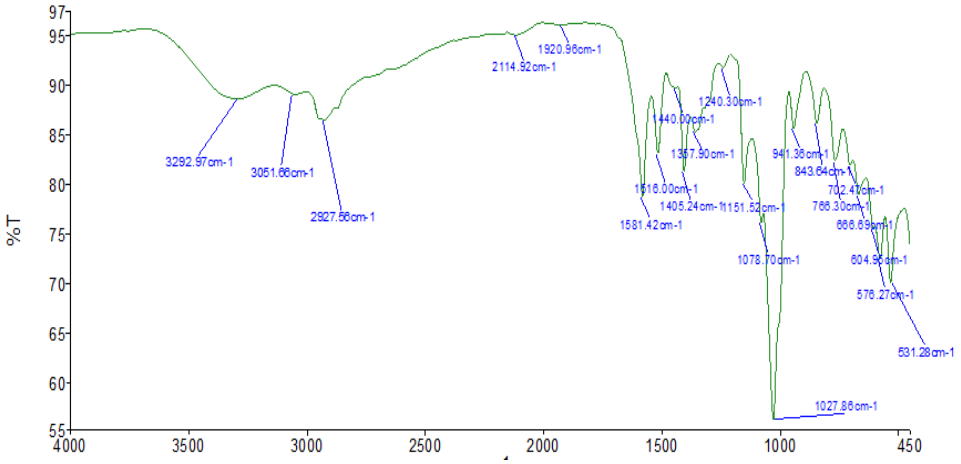

(b)

Fig. 5.22: FT-IR spectrum of ART-β-CD binary and ternary complex.

Table 5.33: Interpretation of IR spectral data of ART-β-CD binary and ternary complexes

Observed wave number (cm^{-1}) (ternary)	Observed wave number (cm^{-1}) (binary)	Standard wave number (cm^{-1})	Functional group
3292.97	3306.19	3200 – 3450	OH
2927.56	2912.17	2850 – 3000	-C-H
1581.42	1412.84	1450-1590	CH_2-
1151.52	1151.72	1120 – 1260	Ether linkage
1024.49	1027.88	1000 – 1300	C-O

5.3.6.4 *Mass spectroscopy of inclusion complexes*

ES-MS spectroscopy allows us to provide evidence of complexation and stoichiometry of the molecular complexes based on their molecular weights in the vaporized form. Peaks observed in mass spectra of ART and ART-β-CD 3° complex at m/z 1448, 1558, 2113, 2357, 2640 correspond to the charged (AE + H^+), (AE + β -CD + 1 monomer units of PVP), (AE + β-CD+8 monomer units of PVP–endoperoxide bridge (28))$^+$. Thus, these peaks confirmed the formation of a 1:1 inclusion complex. The mass spectra recorded are depicted in Fig. 5.23 for lyophilized conclusion complexed pure drug.

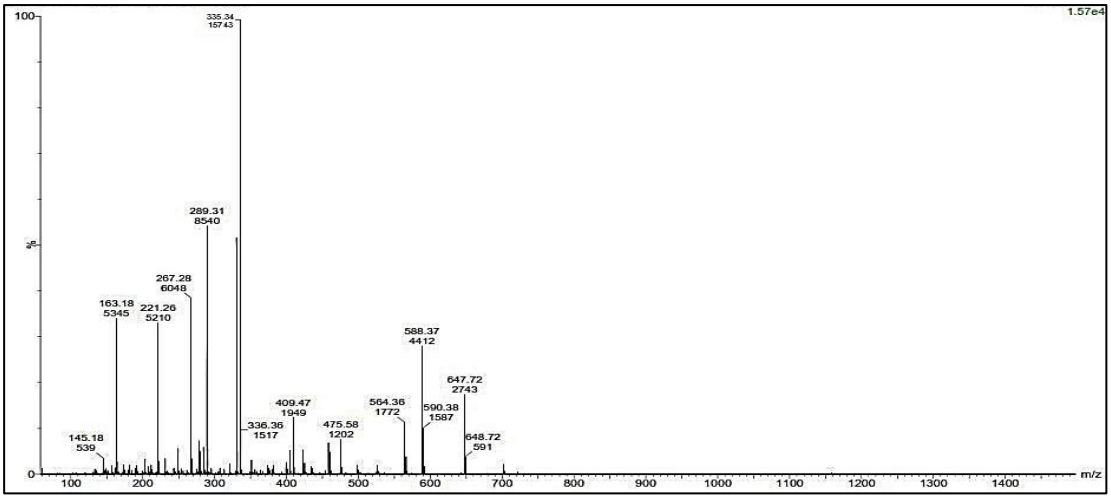

(a)

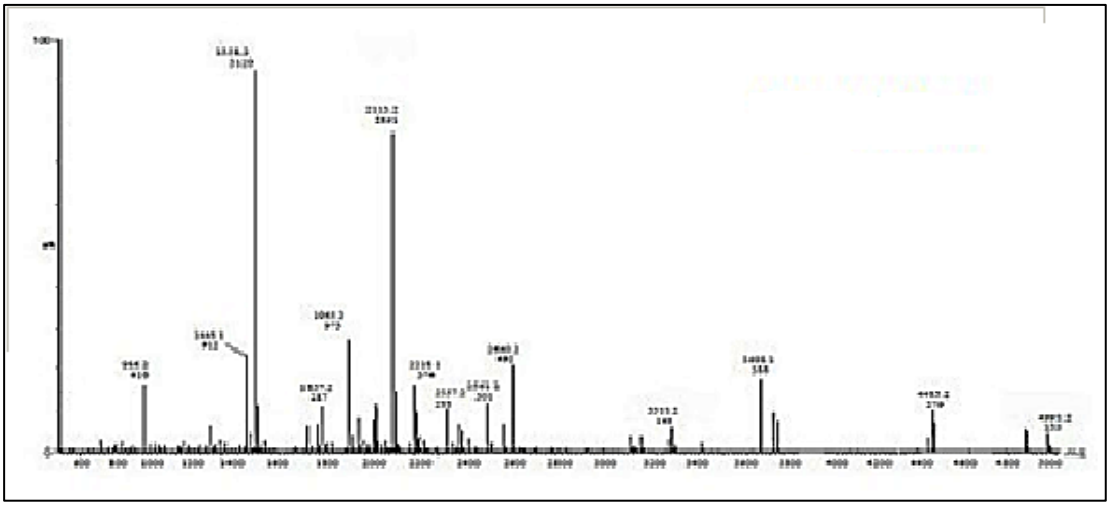

(b)

Figure 5.23: Mass Spectra of (a) ART (b) ART-CD (ternary complex)

5.3.6.5 *Differential scanning calorimetry of inclusion complex*

The thermal curve of pure ART was a typical crystalline substance with an endothermic peak at 107.53 °C and an exothermic peak at 82.19 °C in the case of the complex exothermic peak at temperature 81.60 °C. The DSC curves of the complex exhibited the complete disappearance of the endothermic peak of α, β-arteether. The disappearance of the endothermic peak gave a strong indication of the formation of amorphous entities and the proper fit of the drug inside the cavity indicating the true inclusion (Chadha *et al.*,2011). Fig. 5.24 (a) and (b) depict the DSC thermogram of the ART, and prepared ternary complex.

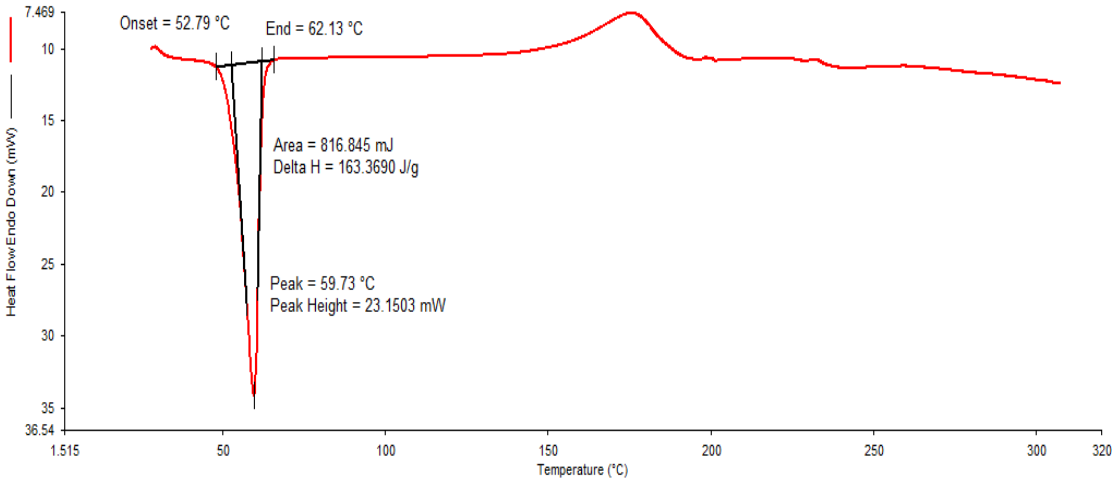

(a)

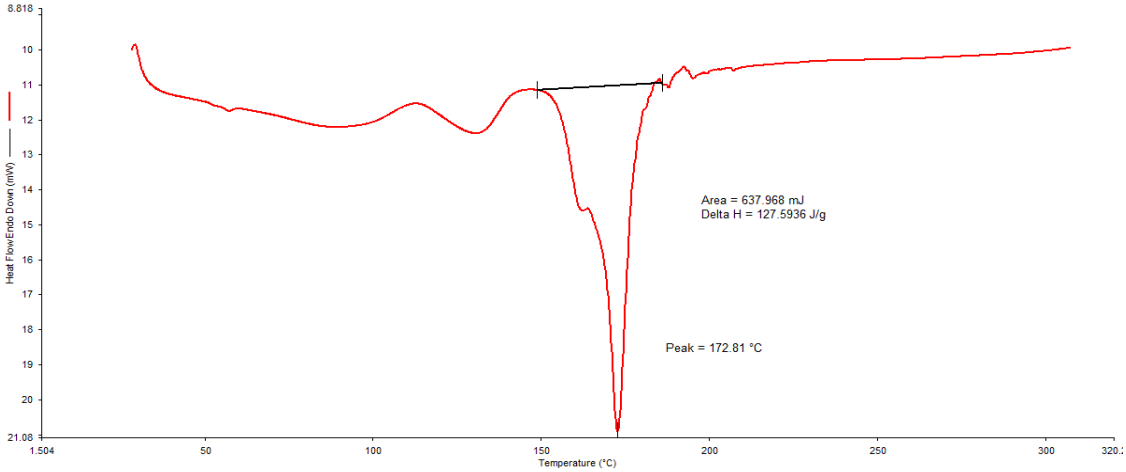

(b)

Figure 5.24: DSC thermogram of (a) ART (b) ART- CD (ternary complex).

5.3.6.6 *SEM image analysis of ART-CD inclusion complexes*

ART, CD, physical mixture of CD-ART, and lyophilized (ternary) CD-ART complex were examined by scanning electron microscope (SEM) to visualize the surface topography. Samples were prepared by preparing the film on the aluminium stub. The stubs were then coated with gold to the thickness of 200-500Å under the argon atmosphere using a gold sputter module in a high vaccum evaporator. The coated samples were scanned and photographs were taken with SEM camera (Jeol-1761, Cambridge, UK).

Fig.5.25-5.28 illustrated the surface morphology of pure ART, pure CD, physical mixture ART-CD ternary inclusion complex, and lyophilized ternary inclusion complex. Fig. 5.25 assures the existence of only the amorphous product indicated the drug was in amorphous form, while Fig. 5.26 showed exhibited the presence of regular size crystalline particles which indicated its crystalline form. The surface morphology of the physical mixture of ART and CD exhibited as expected showed the presence of crystalline as well as amorphous particles as depicted in Fig. 5.27. However, in the case of lyophilized ART-CD complex (Fig 5.28), assured the existence of only amorphous particles.

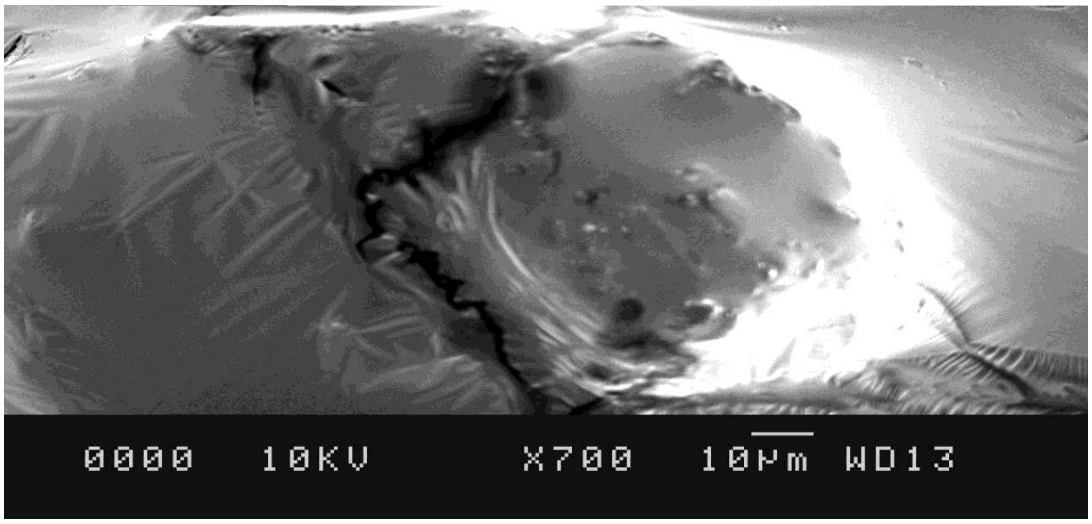

Figure 5.25: Scanning electron microscopy of ART. The image assures the existence of only the amorphous product indicating that the drug is in amorphous form.

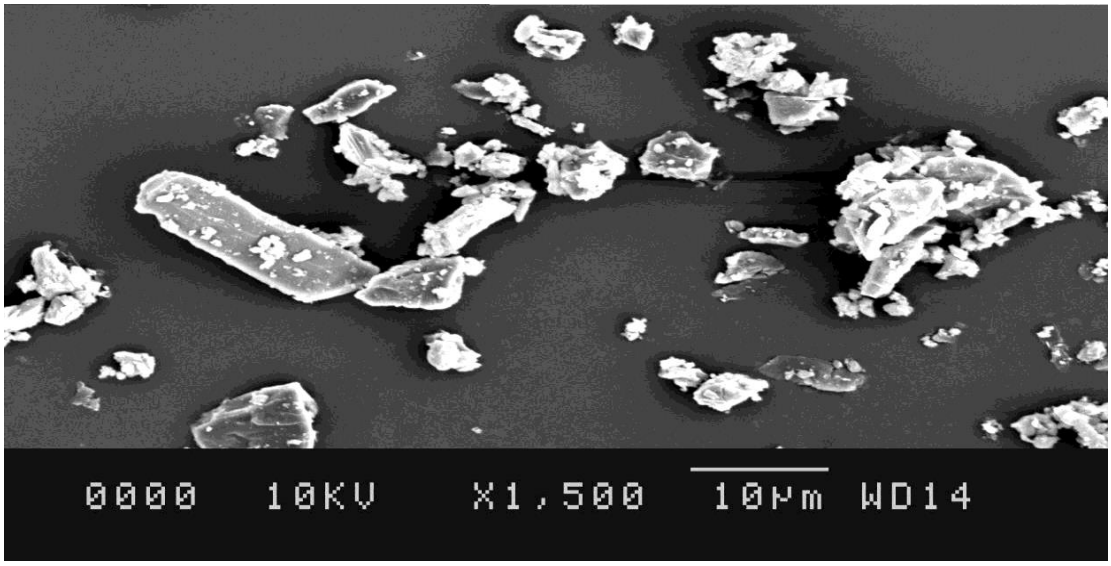

Figure 5.26: Scanning electron microscopy of CD exhibits the presence of

regular-size crystalline particles, indicating its crystalline form.

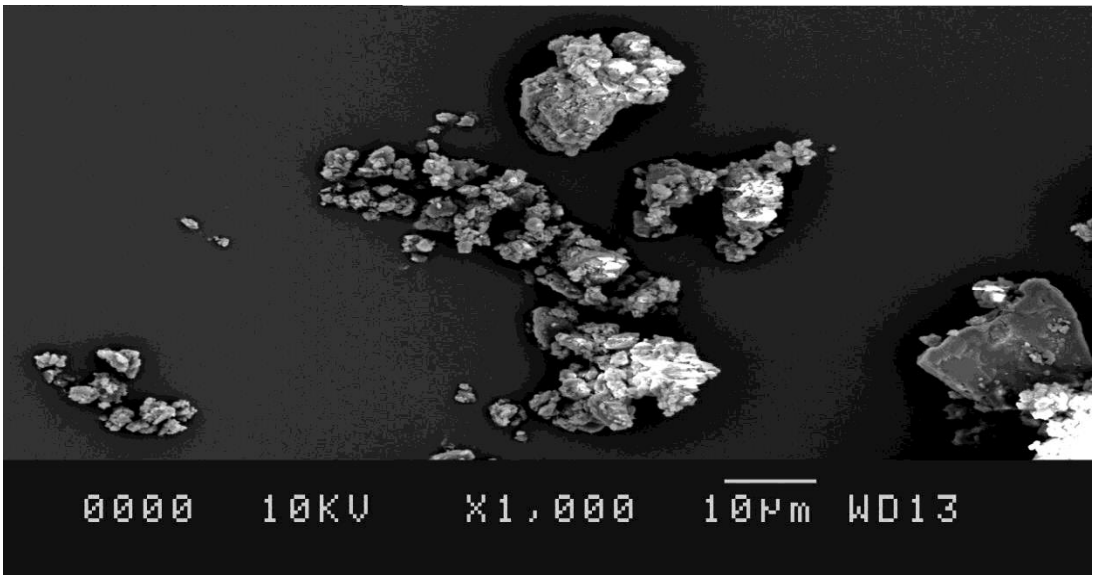

Figure 5.27: Scanning electron microscopy of the physical mixture of ART and CD exhibits the presence of crystalline as well as amorphous particles.

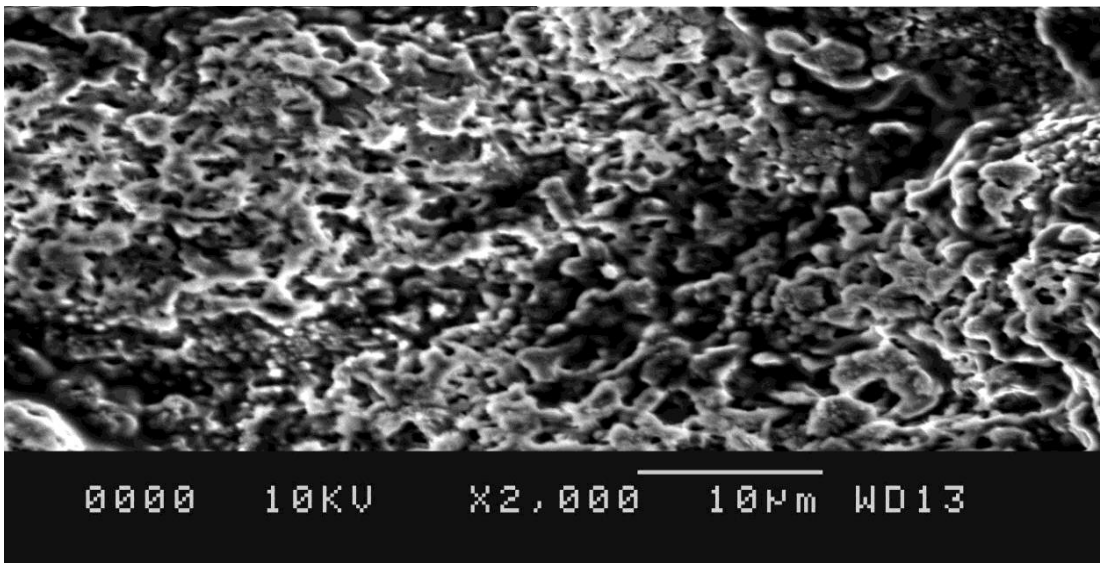

Figure 5.28: Scanning electron microscopy of lyophilized ART and CD complex exhibits existence of only amorphous particles.

5.4 Formulation development

5.4.1 Formulation development, optimization, and characterization of SLNs

5.4.1.1 Formulation optimization and development of SLNs

5.4.1.1.1 *Analysis of SLNs using QbD approach*

The main objective of risk assessment was to identify the plausibility of risks/failures. To do so, the Ishikawa fish-bone diagram was constructed with the aid of Minitab 17 statistical software (M/s Minitab Inc., Philadelphia, PA) to depict a cause-effect relationship among the possible material attributes that were going to affect the CQAs of the formulation. The obtained fishbone diagram depicted the influence of various process parameters and material specifications for the development of ART-CD complex-loaded SLNs. Furthermore, a risk assessment matrix (RAM) was carried out for prioritization of selecting high-risk factors, to demonstrate the potential risks involved with different material specifications and process parameters of ART –CD complex loaded SLNs on potential CQAs by designating a low, medium, and high grade to each of the studied factors.

5.4.1.1.2 *Outlining Quality target product profile (QTPP) and CQAs of SLN*

QTPP is a primary step towards QbD-oriented development of ART-loaded SLNs, and is defined as 'the imminent glossary of the quality attributes of a drug product that will be achieved exemplary to ensure the desiderate quality, along with safety and efficacy of the drug product'. To meet the QTPP, various CQAs were allocated such as particle size, and drug entrapment. Table 5.34 enlists the QTPP elements and CQAs for products/processes affecting the performance of ART-SLNs.

Table 5.34: QTPP elements and CQAs for SLNs-based formulations and their justification.

QTPP elements	**Target**	**Justification**	
Dosage form	Liquid	To enhance bioavailability	
Novel drug delivery system designed	SLNs	Selection of SLNs helps in improved drug loading and enhances bioavailability	
Route of administration	Oral	The proposed route of delivery is to improve patient compliance	
Strength	0.04% w/w	This strength is within the minimum effective concentration range of ART as per literature and preclinical investigations	
Packaging	Suitable for dosage form	Suitable packaging is required for proper extrusion and consumer acceptability.	
Stability	At least 12 months at refrigerated storage	To maintain the optimum strength of ART for the therapeutic efficacy of the drug during the storage period	
Quality attribute of the drug product	**Target**	**Justification**	**Is this a CQA?**
Physical appearance	Smooth & uniform no unpleasant color or odor	Physical appearance is not considered critical as it is not directly linked to safety and efficacy	No
Total drug content	100%	It is a vital parameter for dosage form design. Since SLNs are not a unit dose system it is considered moderately critical	No
Particle size	Nanometer range (50-200 nm)	It is a very critical parameter as particle size will significantly affect the bioavailability and solubility	Yes
PDE	80-100%	Higher value of PDE will provide good formulation stability and as well drug stability. Hence, it is a very critical attribute	Yes
Entrapment efficiency	More than 90%	Higher value of % EE will significantly effect the dose loading and dose delivery	Yes
In vitro drug release	pH-dependent drug release	Minimum drug release in an acidic environment and maximum in basic pH.	Yes

5.4.1.1.3 *Preparation of SLNs*

ART-loaded SLNs were prepared by the spontaneous nanoprecipitation method with some modifications. Briefly, ART (6 mg) and stearic acid (6 mg) were dissolved in an acetone/ethanol mixture (1:1) to obtain an organic phase. Then, the organic phase (was added drop wise using a syringe to 120 mL with 70 ^{o}C temperature of the aqueous phase under continuous stirring at a magnetic stirrer for half an hour. The nanoparticle suspension was then lyophilized. After lyophillization the SLNs were redispersed in water by sonication which was used to determine the particle size and supernatant was collected to evaluate entrapment efficiency (%).

5.4.1.1.4 Selection of lipids of SLNs

The solid lipid selected was stearic acid (290±0.9 mg/mL) as ART showed maximum solubility in it. Equilibrium solubility studies were done in various organic solvents like ethanol, and acetone. The solubility of ART was maximum in ethanol (232±0.8 mg/ ml) and acetone (301±0.7 mg/ mL). Hence, based on the results of solubility studies, stearic acid, ethanol, and acetone were selected as lipid and organic solvents respectively for the development of SLNs.

5.4.1.1.5 Risk assessment studies of SLNs

Fig. 5.29 demonstrates the Ishikawa fish bone diagram depicting the various causes that affect the CQAs of SLNs formulations. The 6Ms probably affecting the CQAs like, machines, men, material (API & excipients), measurements, methods, and milieu/environment were depicted by the fish-bone diagram. The risk assessment matrix (RAM) was also constructed to observe the possible causes affecting the CQAs. The risk matrix for SLNs enlightening the low, medium, and high-risk levels related to each of the process parameters/material specifications are illustrated in Table 5.35. RAM suggested that the concentration of solid lipid, liquid lipid, and surfactant, PL were high-risk levels as assigned with red color and the aqueous phase was associated with medium risk as assigned with brown color while the stirring speed, stirring time, and temperature were associated with medium to low levels of risk as assigned with green color.

Table 5.35: Initial RAM for ART-loaded SLNs.

CQAs of SLNs	**Risk Estimation Matrix**						
	Concentration of solid lipid	**Concentration of S_{mix}**	**Concentration of organic solvent**	**Ratio of Solid:liquid lipid**	**Stirring Time**	**Stirring speed**	**Temperature**
Particle size	High	High	High	Medium	Medium	Medium	Low
PDE	High	High	High	High	Low	Low	Low
% EE	High	High	High	High	Low	Low	Low

*Red color = High risk parameter, Yellow color = Medium risk parameter, Green = Low risk parameter.

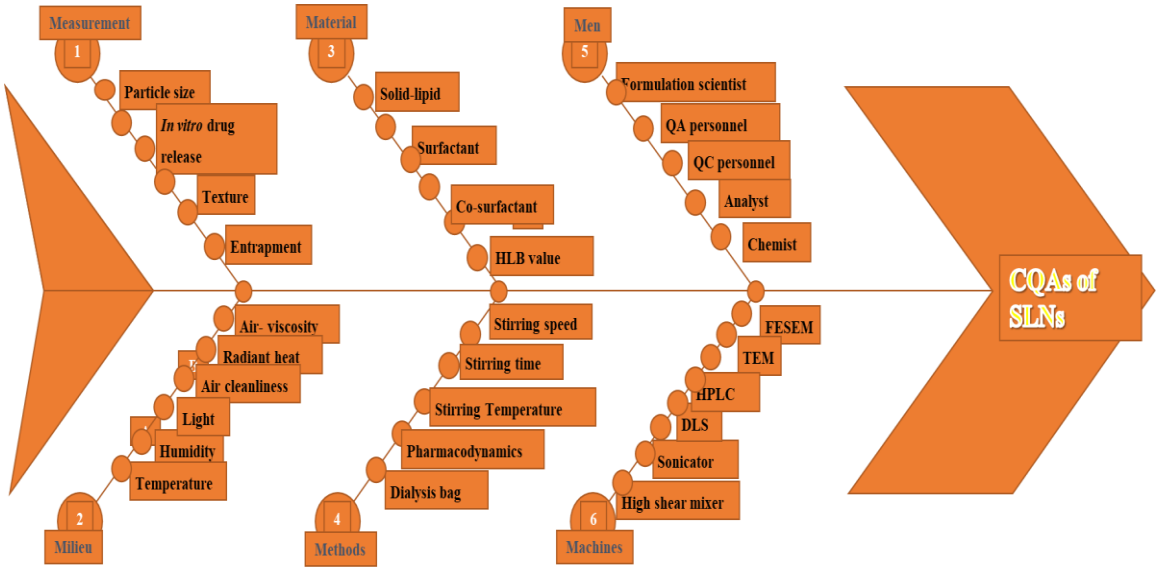

Figure 5.29: Ishikawa fishbone diagram depicting various causes that affects the CQAs of SLNs formulation.

5.4.1.1.6 *Design of Experiments (DoE) for SLNs*

The randomized CCD was employed to optimize ART-loaded SLNs. Surfactant concentration and acetone to ethanol volume ratio in the organic phase were selected as independent variables. Particle size and entrapment efficiency were selected as responses. The statistical analysis of the factorial design formulations was performed using Design-Expert® software (Version 13, Stat-Ease Inc.). Thirteen batches were prepared as suggested by the software using a CCD with three levels, two factors, and two responses.

For optimization of these factors, CCD was used with the help of Design Expert software. CCD was selected because of its capability to give a lesser number of experimental runs in comparison to other experimental design. Table 5.36 show the low high value of the factors selected by DoE.

Table 5.36: Low and high values of selected factors.

A	Surf	mg	50.00	100.00	-1 ↔ 50.00	+1 ↔ 100.00	75.00	17.68
B	organic phase	ml	3.00	12.00	-1 ↔ 3.00	+1 ↔ 12.00	7.50	3.18

5.4.1.2 Optimization and development

5.4.1.2.1 *DoE-based optimization of selected factors of SLNs*

DoE was employed for the optimization of the selected independent variables i.e., the

concentration of surfactant and amount of organic phase with respect to entrapment efficiency (EE) and particle size (PS) as the selected response. CCD gave 13 experimental runs for different values of independent variables and the value of response is shown in Table 5.37.

Table 5.37: Experimental runs and value of response as per experimental runs.

Std	Run	A: Surfactant concentration	B: Organic phase	Entrapment efficiency	Particle size
		(mg)	(mL)	(%)	(nm)
2	1	100	3	88.75	340.4
1	2	50	3	81.01	293
10	3	75	7.5	84	402.3
11	4	75	7.5	79.58	443.4
7	5	75	3	85.98	461.8
13	6	75	7.5	86.52	465.3
8	7	75	12	95.5	513.6
3	8	50	12	92.37	519.6
6	9	100	7.5	80.7	211.2
9	10	75	7.5	87.65	366.7
4	11	100	12	98.55	334.3
5	12	50	7.5	86.03	479.9
12	13	75	7.5	84.45	436.8

5.4.1.2.2 *Statistical analysis of data of SLNs*

ANOVA was involved in the statistical data analysis of the information generated through the help of software for better optimization of selected variables for the evaluation of the significance of the model. A significance model will have a p-value less than 0.05. The adequacy of our defined model was calculated based on Lack of fit or P-value and R^2 value. The R^2 value exhibited closeness of predicted data and came closer to experimental data and the value should be closer to 1 (Newton *et al.,* 1998). ANOVA statistics shown in Table 5.38 suggested that our p-value for both responses. i.e., EE and PS were near about 0.0343 and 0.0265 respectively (much lesser than 0.05) showing the significance of the developed model. The same result was

confirmed by the value of R^2 for both responses were found to be 0.9767 and 0.9198 respectively which is much nearer to 1 (Bhoop *et al.,2013)* .

Table 5.38: ANOVA-based statistical parameters for SLNs.

	EE (%)		**PS**		**Inference**
Source	**F-value**	**p-value**	**F-value**	**p-value**	
Model	4.65	0.0343	5.17	0.0265	Significant
A-Surfactant	0.9636	0.3590	8.99	0.0200	
B-Organic phase	12.29	0.0099	4.03	0.0846	
AB	0.0477	0.8334	4.42	0.0737	
A^2	0.1495	0.7105	8.30	0.0236	
B^2	9.27	0.0187	1.92	0.2080	
Residual					
Lack of Fit	1.77	0.2925	3.44	0.1319	Not significant
R^2	0.7687		0.7868		
Adjusted R^2	0.6035		0.6345		
Adeq Precision	5.822		7.585		

5.4.1.2.3 *Effect of the variables on entrapment efficiency of SLNs*

Entrapment efficiency, defined as the amount of drug entrapped in SLNs, is one of the important parameters that can affect the final quality target profile of SLNs. Design of Experiment gave a quadratic mathematic model to depict the effect of a different variable on EE.

$$EE = +84.37+1.43\ A +5.11B-0.3900AB-0.8312A^2+6.54\ B^2 \quad \text{……..(2)}$$

Where A and B are the selected variables i.e. surfactant concentration and organic phase.

The relationship between the independent variable and entrapment efficiency was determined by plotting 2D contour plot and 3D response surface plot as shown in Fig. 5.30.

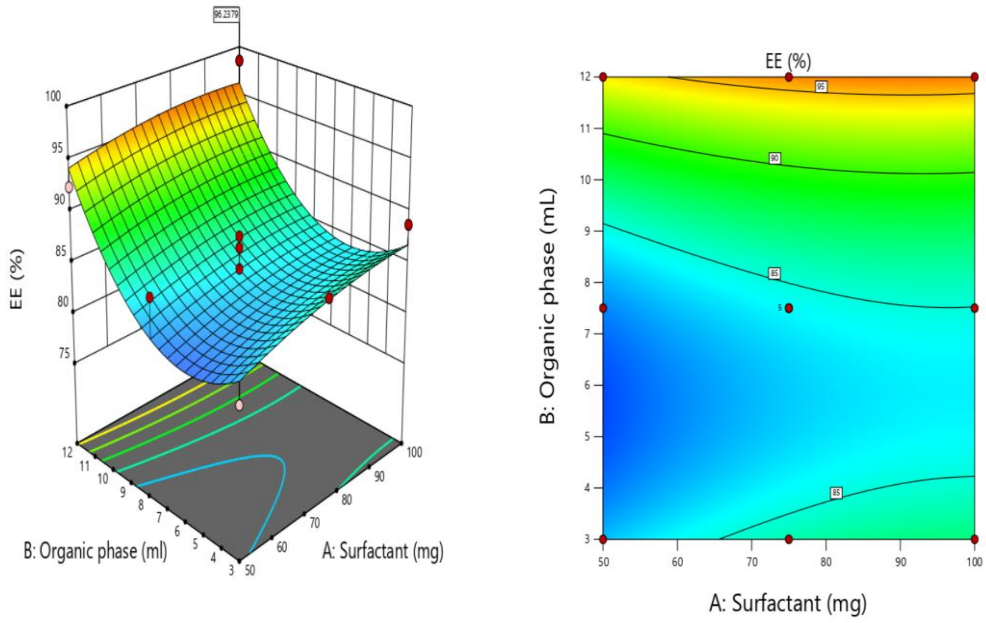

Figure 5.30: The 2-dimensional contour plot and 3-dimensional response surface plot for entrapment efficiency.

As per the above, EE started increasing with an increasing amount of organic phase, but it decreased when the value of the organic phase and surfactant continuously increases. The value of entrapment efficiency again starts increasing with the increasing value of the organic phase after a certain point. Thus, EE was more in higher and lowest values of organic solvent.

5.4.1.2.4 Effect of the variable on particle size of SLNs

Particle size is one of the important parameters that can affect the final quality profile of SLN.

The below-given equation shows the relationship between the particle size and the selected independent variable as shown in Fig 5.31**.**

PS= 428.21 -67.77A-45.38B - 58.17AB-95.95 A^2 + **$B^2$46.20** …….(3)

Where A and B are the selected two variables.

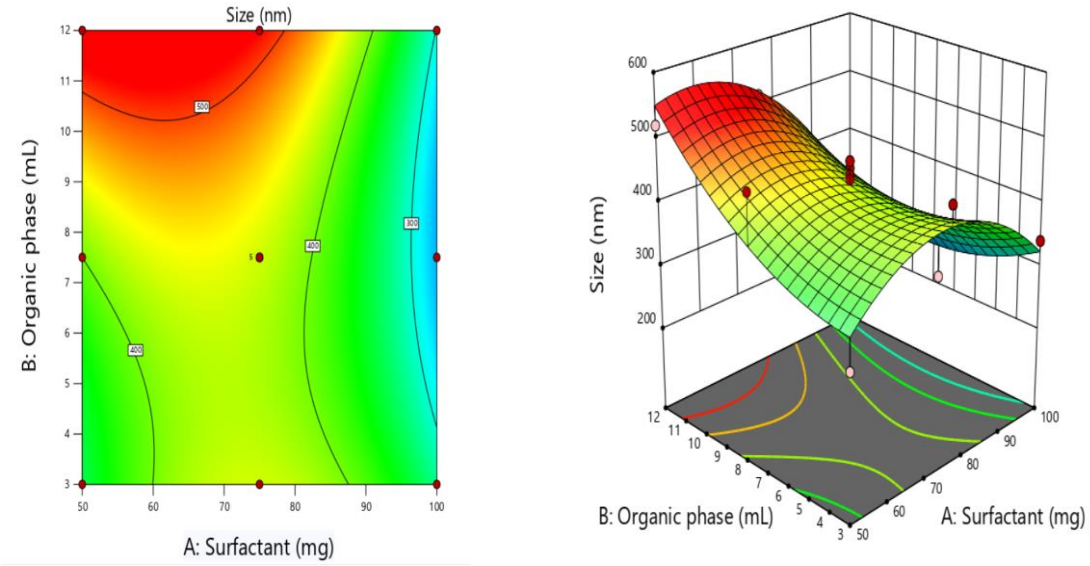

Figure 5.31: The 2-dimensional contour plot and the 3-dimensional response surface plot for particle size.

According to Fig. 5.31, particle size continuously increased with the increase in the concentration of the organic phase. But with an increase in the concentration of surfactant particle size increased to a certain extent, then start decreasing if the concentration of surfactant further increases.

5.4.1.2.5 Overlay plot and validation of model

It is important to determine the design space from all the experimental areas so that the desired quality profile of the final product can easily achieve. So, an overlay plot with the help of Design Expert software was generated showing the design space in the yellow region and the whole experimental region in the grey background as shown in Fig 5.32.

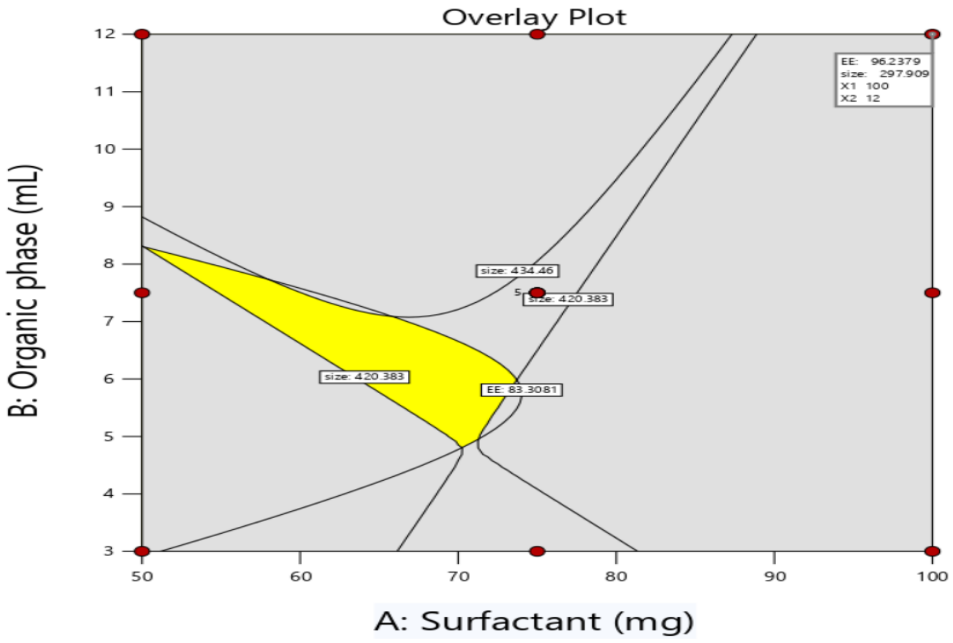

Figure 5.32: Overlay plot showing the design space in the yellow region and the whole experimental region in the grey background.

Validation of the model is important aspect of QbD based formulation development as it ensures that the design is capable of replicating the experimental region. So validation of the above-developed model was done by comparing the result of responses at the lab experimental level to that value suggested by the design itself. The above design was 92.4% (197.90 nm predicted and 109 observed) and 93.8% (96.23% predicted and 93.4 % observed) nearest in predicting both responses i.e., particle size, and entrapment efficiency.

5.4.1.2.6 *Preparation of SLNs*

ART-loaded SLN was prepared by spontaneous nanoprecipitation method with some modifications. Briefly, ART (6 mg) and stearic acid (50 mg) were dissolved in 12 mL of an acetone/ethanol mixture (1:1) to obtain an organic phase. Then, the organic phase (12 mL) was added dropwise using a syringe to 120 mL with 70^{o}C temperature of the aqueous phase under continuous stirring at a magnetic stirrer for half an hour. The nanoparticle suspension was then lyophilized conditions. After lyophillization the SLNs were redispersed in water by sonication which was used to determine the particle size and supernatant was collected to evaluate % entrapment efficiency.

5.4.1.2.7 *Physicochemical characterization of ART-loaded SLN*

The key advantage of ART-SLN is the protection of ART from enzymatic

degradation, which delays its metabolism. The endoperoxide ring of ART; which is mainly responsible for its antimalarial activity, has been reported to get cleaved in the acidic environment of the stomach, which can decrease its activity and absorption. The incorporation of the ART in SLN can reduce its exposure to the acidic pH of the stomach preventing its degradation, thus increasing its bioavailability and activity.

5.4.1.2.7.1 *Particle size distribution*

The result shows the formation of a homogeneous ART- SLN having a polydispersity index of less than 0.2. Fig 5.32 illustrated its and particle size and its distributions of ART-SLN measured by DLS. The results demonstrate that ART-SLNs have been prepared successfully the mean diameter of ART-SLN was 109.2±15 nm. The zeta potential of the SLN (-29.1) was determined so that the contribution of charge distribution can also be assessed as shown in Fig. 5.33.

The particle size of ART-SLN was less than 200 nm and the PDI was found to be < 0.5, which provides a large surface area for the absorption of ART.

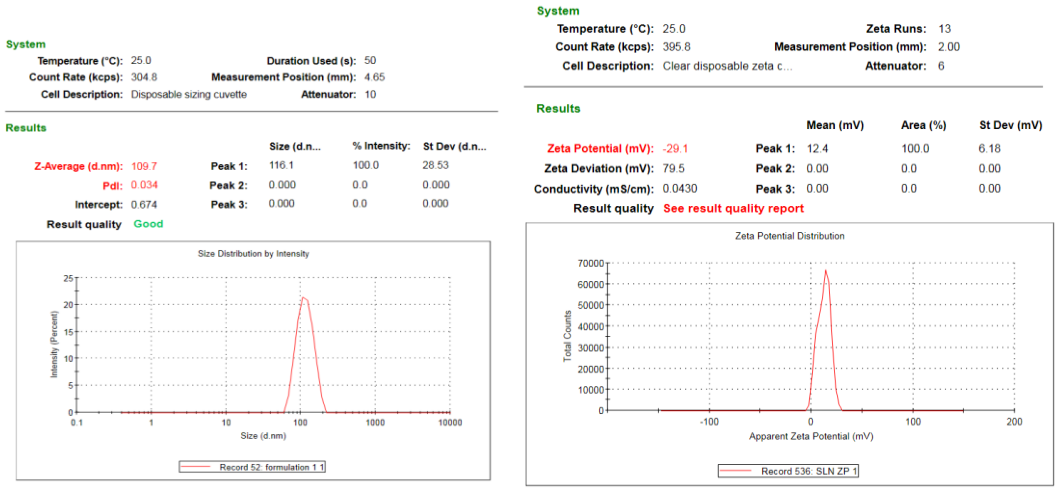

Figure 5.33: Particle size and zeta potential of prepared SLNs.

5.4.1.2.7.2 *Surface morphology of SLNs*

The particle size of the ART-SLN was further confirmed by HR-TEM, and the results revealed that the particle size was less than 200 nm (Fig. 5.34). FESEM photomicrograph revealed spherical nanoparticles with a smooth and uniform surface. TEM photomicrograph also indicated the presence of spherical nanoparticles.

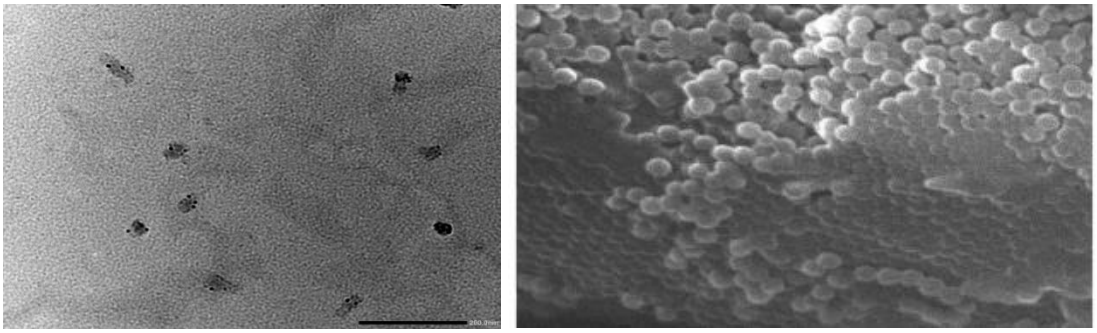

Figure 5.34: TEM image and SEM image of prepared SLNs.

5.4.1.2.7.3 *XRD of SLNs*

The PXRD spectra of lyophilized optimized ART-loaded SLN formulations showed the absence of all the ART characteristics peaks as shown in Fig. 5.35. The absence of characteristic ART peaks demonstrated the successful incorporation of ART into the SLNs.

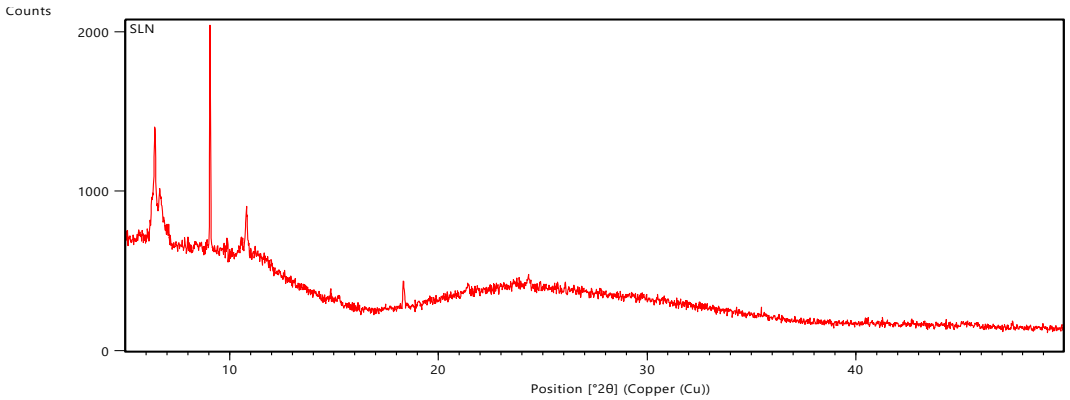

Figure 5.35: The PXRD spectra of prepared SLNs.

5.4.1.2.7.4 *Entrapment efficiency % of SLNs*

The maximum entrapment efficiency (% EE) in ART-SLN was found 93.7±6.2%. The drug loading of the optimized SLNs was found to be 78.54±0.62%.

5.4.1.2.7.5 pH

The pH of ART-SLNs was found to be 7.2, which is somewhat neutral. This is important because substances that are too acidic or too basic can cause irritation or damage to the skin or other tissues. Therefore, the fact that the ART-SLNs have a neutral pH confirmed that they are not likely to cause any irritation or harm to the gastrointestinal tract.

5.4.1.2.7.6 Particle size distribution of lyophilized SLNs

The prepared SLN were lyophilized to get powder SLN, the flow properties of powdered SLN was further analyzed. The particle size distribution of powdered SLN are as shown in Table 5.39.

Table 5.39: Particle size distribution.

S.No.	Sieve No.	% weight retained (uncoated)
1	18	0
2	22	1.2
3	25	5.4
4	30	89

5.4.1.2.7.7 *Shape of lyophilized SLNs*

The shape of solid SLN was found to be spherical when seen under a motic microscope. The spherical nature of the spheroid was calculated by pellips (which is a characteristic of pellet shape). A powder with pellips equal to 1.0 is considered good for pharmaceutical processing as shown in Fig 5.36.

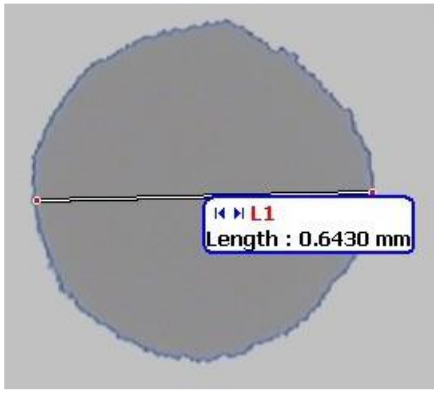

Figure: 5.36: Shape of *lyophilized* SLN.

$P_{ellips} = p/\pi\ d\ max = 1$(Spherical)

Where; p = perimeter, $\Pi = 27/7$, d_{max} = maximum diameter of SLNs

Bulk density of lyophilized SLNs

Bulk density and tapped density were used for the calculation of Hausner's ratio and compressibility index. These help in determining the flow property and the compressibility of ingredients. A negligible variation in bulk density was observed. The bulk density of solid SLNs, was found to be 0.81.

Tapped density of lyophilized SLNs

A negligible difference was experimentally observed in the tapped density and was found to be 0.89.

Carr's Index (%) of lyophilized SLNs

Results of the compressibility study showed that the compressibility index of the solid SLN was having excellent flowability as the results fell in the range of ≤10 %. The compressibility index was found to be 7.2 which showed excellent flow.

Hausner's ratio of lyophilized SLNs

According to USP 2000, powder with Hausner's ratio between 1.12 and 1.18 had good flow, and above 1.35 showed poor flow properties. The result was found to be 1.14.

Angle of repose of lyophilized SLNs

The angle of repose of freeze dried SLNs was found to be 29 According to I.P. this is a very good flow.

5.4.1.2.7.8 *In-vitro drug release of lyophilized SLNs*

Fig. 5.37 depicts the cumulative ART release from ART- SLN, at 37 ^{o}C. Around 40 % of the drug was released from ART-SLN within the first 12 h. Following that, the ART release rate increased to 30 h, with a maximum drug release of 79.1 %. The results show that the % drug release of all formulations was less than 10 % in the acidic pH, while at 50 h, the maximum drug release was attained.

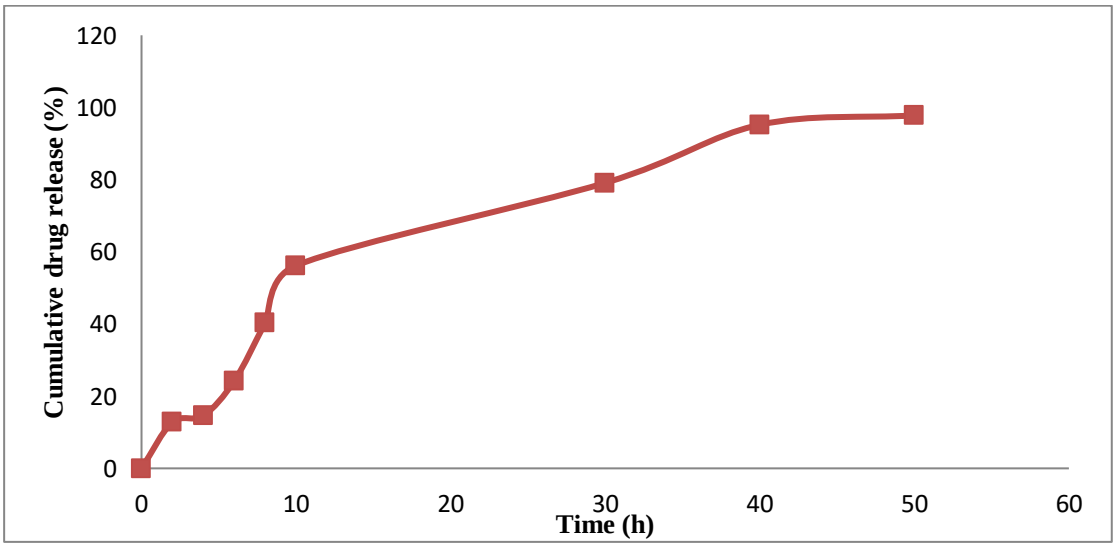

Figure 5.37: The % drug release of ART-SLN.

5.4.1.3 *Discussion on SLN formulation*

Additional oral nanoformulations of different kinds were created to improve the solubility and bioavailability of ART. Although SLNs can administer drugs through parenteral and oral routes (Yang *et al.*, 1999), the oral route is usually preferable due to patient compliance. Since ART is not well soluble in water, administering it through SLNs may be preferable. With modest adjustments, the spontaneous nanoprecipitation process was used to formulate ART-loaded SLNs. To create the organic phase, ART and stearic acid were briefly mixed in an acetone/ethanol combination. The organic phase was then injected dropwise using a syringe into 120 mL of the 70°C aqueous phase while being continuously stirred on a magnetic stirrer for 30 min. The suspension of nanoparticles was lyophilized after that. This method has the benefit of minimizing lipid melting, which prevents medication loss or degradation. The main benefit of ART-SLN is the defense against enzymatic degradation of ART, which postpones its metabolism. In the acidic environment of the stomach, the endo peroxide ring of ART, which is primarily responsible for its antimalarial action, has been observed to cleave, which may reduce its activity and absorption. By incorporating the ART into SLN, it may be protected from the stomach's acidic pH and prevented from degrading, boosting its bioavailability and action (Venkatesan *et al*. 2006). The polydispersity index of ART-SLN was determined to be 0.034 and the particle size of the material was smaller than 200 nm, providing a significant surface area for ART absorption. It has been shown by ART release from ART-SLN that the concentration of the surfactants had an impact on the release. In the instance of SLN, it was found that ART was released more quickly. The absolute bioavailability of ART has been greatly increased by ART-SLN, according to the statistical analysis of pharmacokinetic data.

The increased oral bioavailability of ART-SLN is justified by the discovery of substantially higher AUC and C_{max} values for ART-SLN. These parameters, which are characteristics of the drug formulation and are crucial for comparative bioavailability studies, describe the amount of drug absorption and C_{max} is a crucial component of the blood level profile. This might be related to the ART-strong SLN's lipid shielding, which prevents enzymatic and chemical destruction of the ART. According to some previous study (Song *et al.*, 2005, Venkatesan *et al.*, 2006) surfactants also improve the permeability of ART through intestinal membranes and

establish the affinity of lipid particles for these membranes (Holm *et al*., 2001, Nishimukai *et al*., 2003). The discovered formulation's enhanced oral bioavailability may be used to treat multidrug-resistant malaria with higher patient compliance.

5.4.2 *Formulation development, optimization, and characterization of NLCs*

5.4.2.1 Formulation optimization and development

5.4.2.1.1 *Selection of lipids for NLC preparation*

Soya lecithin was chosen as a solid lipid, while stearic acid was selected as the ART with the most excellent solubility. Various oils (liquid lipids) such as oleic acid were studied for equilibrium solubility. The highest solubility of ART was 75.1512±0.13 mg/mL in oleic acid. Stearic acid and oleic acid were chosen as solid and liquid lipids to form NLCs, respectively, as a consequence of the solubility studies.

5.4.2.1.2 *Risk assessment studies for NLC preparation*

The Ishikawa fishbone diagram demonstrating the many reasons that impact the CQAs of NLC formulations is shown in Fig.5.38. Machines, procedures, material (API & excipients), measurements, personnel, and milieu/environment were all depicted as fishbones in the fishbone graphic. To track potential sources of CQAs, the risk assessment matrix (RAM) was created. The risk matrix for NLCs is shown in Table 5.40, with low, medium, and high-risk categories related to process parameters/material specifications. As indicated by the red hue, RAM suggested that the concentrations of solid lipid, surfactant, and liquid lipid, PL, were high-risk levels. Assigned with brown colour, stirring speed, and stirring duration, the aqueous phase was a medium risk. The temperature ranged from medium to low risk, as shown by the green color.

Table 5.40: Initial RAM for ART-loaded NLCs

CQAs of NLCs	RISK ASSESMENT ESTIMATION MATRIX						
	Concentration of solid lipid	**Concentration of S_{mix}**	**Concentration of liquid lipid**	**The ratio of Solid: liquid lipid**	**Stirring time**	**Stirring speed**	**Temperature**
Particle size	High	High	High	Medium	Medium	Medium	Low
PDE	High	High	High	High	Low	Low	Low
% EE	High	High	High	High	Low	Low	Low

*Orange color = High risk parameter, Red color = Medium risk parameter, Blue = Low risk parameter.

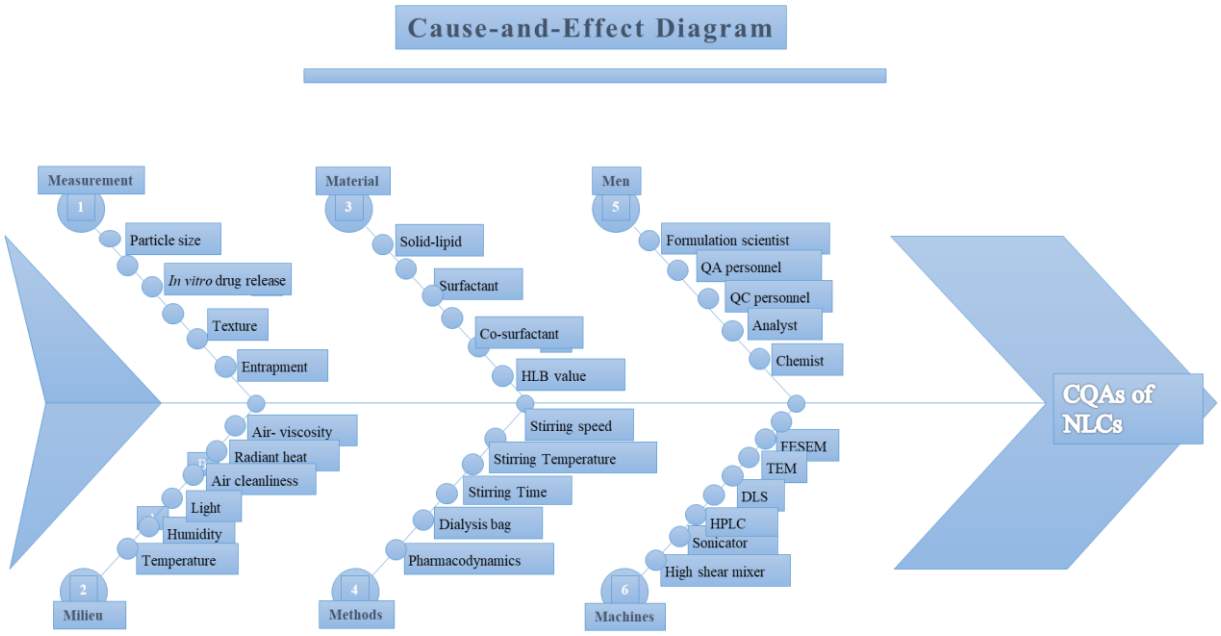

Figure 5.38: The Ishikawa fishbone diagram shows the numerous factors that influence the CQAs of NLC formulation.

Table 5.41 enlists the essential QTPP and CQA parameters for formulation development of NLCs.

Table 5.41: QTPP elements and CQAs for NLC-based formulations and their justification

QTPP elements	**Target**	**Justification**	
Dosage form	Liquid	To enhance bioavailability	
Novel drug delivery system designed	NLCs	The selection of NLCs helps in improved drug loading and enhances bioavailability	
Route of administration	Oral	The proposed route of delivery is to improve patient compliance	
Strength	0.04% w/w	This strength is within the minimum effective concentration range of ART as per literature and preclinical investigations	
Packaging	Suitable for dosage form	Suitable packaging is required for proper extrusion and consumer acceptability.	
Stability	At least 12 months at refrigerated storage	To maintain the optimum strength of ART for the therapeutic efficacy of the drug during the storage period	
Quality attribute of the drug product	**Target**	**Justification**	**Is this a CQA?**
Physical appearance	Smooth & uniform No unpleasant color or odor	Physical appearance is not considered critical as it is not directly linked to safety and efficacy	No
Total drug content	~ 100%	It is a vital parameter for dosage form design. Since NLCs are not a unit dose system it is considered moderately critical	No
Particle size	Nanometer range (50-200 nm)	It is a very critical parameter as particle size will significantly affect the bioavailability and solubility	Yes
PDE	80-100%	Higher value of PDE will provide good formulation stability and as well drug stability. Hence, it is a very critical attribute	Yes
Entrapment efficiency	More than 90%	Higher value of % EE will significantly effect the dose loading and dose delivery	Yes
In vitro drug release	pH-dependent drug release	Minimum drug release in an acidic environment and maximum in basic pH.	Yes

As indicated in Table 5.42, the CCD was applied using Design-Expert version 13 software to screen out components from two independent variables: surfactant (Tween 80) and lipid (soya lecithin) concentration. Entrapment efficiency and particle size were chosen as dependent response variables. The low and high values of selected factors i.e. surfactant and lipid (low (-1 to 50), high (+1 to 150)) the maximum limit for both lipid and surfactant was selected as 150.

Table 5.42: Design matrix for factor screening as per CCD.

Std	Run	A:Surfactant (mg)	B:Lipid concentration (mg)	Entrapment Efficiency (%)	Particle size (nm)
6	1	150	100	63.211	190.45
3	2	50	150	4.85	227.378
10	3	100	100	78.2	205.51
4	4	150	150	28.9	227.378
11	5	100	100	78.6	190.302
1	6	50	50	18.02	166.4
12	7	100	100	78.4	202.12
8	8	100	150	40.6	227.3
5	9	50	100	44.19	203.39
9	10	100	100	78.1	206.2
2	11	150	50	31.8	153.225
13	12	100	100	78.2	204.9
7	13	100	50	48.7	156.4

5.4.2.1.3 ***Reduced quadratic model – ANOVA for preparation of NLC***

The ANOVA method was used to determine the model's significance. A significant value is one with a p-value of less than 0.005. The model's adequacy was determined by the lack of fit and R square value. The ANOVA data for % EE is shown in Table 5.43. The data shows that the model was quadratic. The coding of factors was done. The model's F-value of 17344.49 suggested that it was statistically significant. A F-value of 0.01% may be due to noise (Alruwaili *et al.*, 2021).

Model terms with P-values of less than 0.0500 were also significant. Basic model terms in this circumstance were A, B, AB, A^2, and B^2. The F-value of 4.12 suggested that the Lack of Fit was not statistically significant when compared to the pure error. The F-value for Lack of Fit had a 10.26% chance of occurring due to noise. It is desired that the model should be as accurate as possible. As a result, a minor mismatch is beneficial.

Table 5.43: ANOVA response of % EE of NLCs.

Source	Sum of Squares	df	Mean Square	F-value	p-value	Inference
Model	8103.53	5	1620.71	17344.49	< 0.0001	Significant
A-Surfactant concentration	538.67	1	538.67	5764.78	< 0.0001	
B-Lipid concentration	97.36	1	97.36	1041.98	< 0.0001	
AB	26.37	1	26.37	282.19	< 0.0001	
A^2	1616.55	1	1616.55	17300.01	< 0.0001	
B^2	3052.27	1	3052.27	32664.82	< 0.0001	
Residual	0.6541	7	0.0934			
Lack of Fit	0.4941	3	0.1647	4.12	0.1026	Not significant
Pure Error	0.1600	4	0.0400			
Cor Total	8104.18	12				

The coding of factors was done. The statistical significance of the model was indicated by the Model F-value of 46.66. Due to noise, an F-value of this magnitude had a 0.01% chance of occurring. Model terms with P-values under 0.0500 were significant. In this case, B is a critical model term. If the value is greater than 0.1000, the model terms are not required (Newton *et al.,* 1998). The Lack of Fit had an F-value of 0.36, indicating that it is not statistically significant when compared to the pure error. Observed value of noise is 78.51% likely to be the source of a significant Lack of Fit F-value as shown in Table 5.44.

Table 5.44: ANOVA response for particle size of NLCs.

Source	Sum of Squares	df	Mean Square	F-value	p-value	Inference
Model	7416.46	5	1483.29	46.66	< 0.0001	Significant
A-Surfactant Concentration	113.67	1	113.67	3.58	0.1005	
B-Lipid Concentration	7074.80	1	7074.80	222.55	< 0.0001	
AB	43.40	1	43.40	1.37	0.2809	
A^2	7.84	1	7.84	0.2466	0.6347	
B^2	126.02	1	126.02	3.96	0.0868	
Residual	222.53	7	31.79			
Lack of Fit	47.49	3	15.83	0.3617	0.7851	Not significant
Pure Error	175.04	4	43.76			
Cor Total	7638.99	12				

The 2D and 3D response surface diagrams, as shown in Fig. 5.39, were used to define the dependent, co-dependence, and inter-variation between the independent parameters selected, i.e., surfactant and lipid concentrations; established responses or CQA, i.e., particle size and entrapment efficiency across the entire experiment domain.

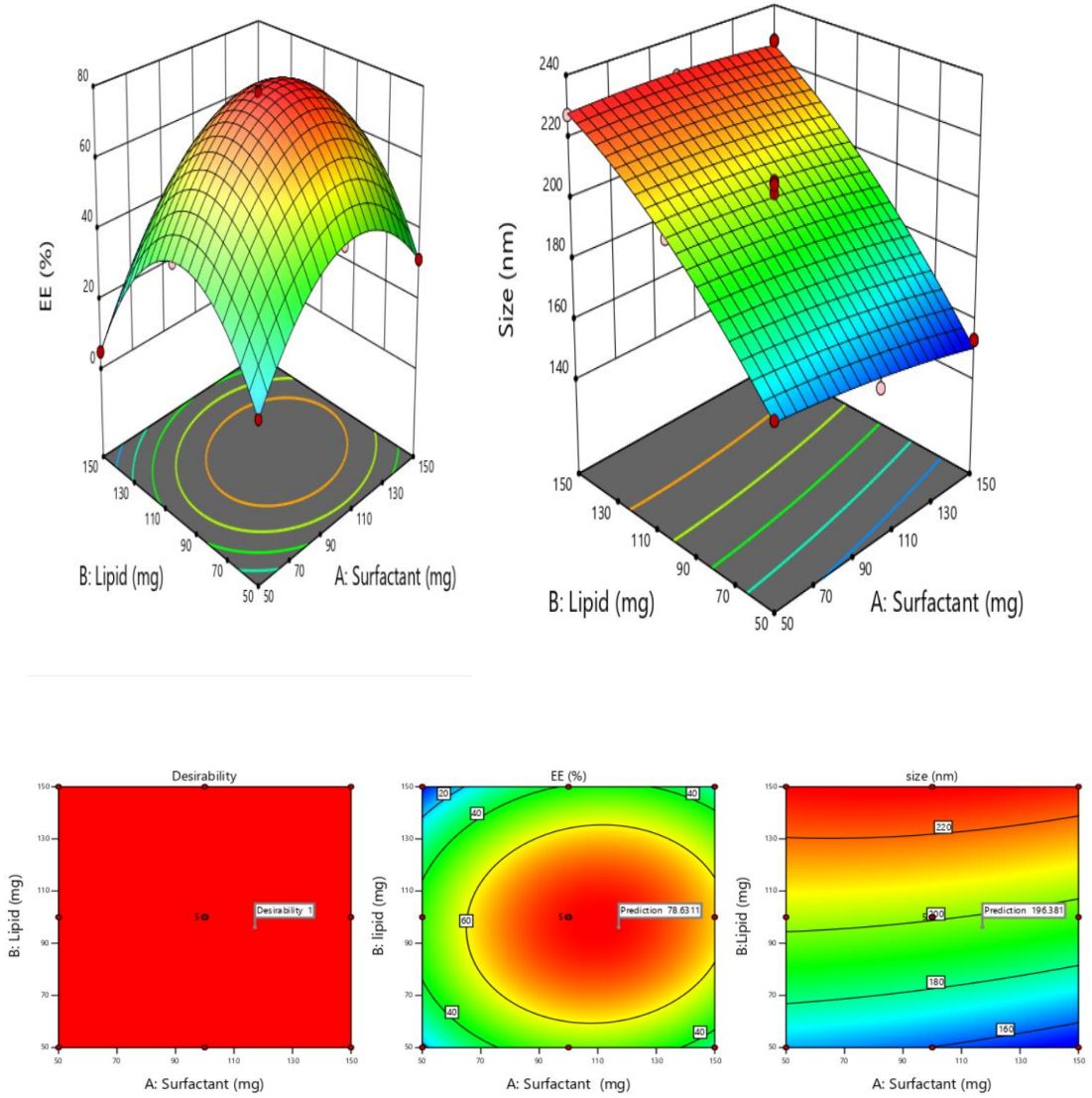

Figure 5.39: 3D response plot and 2D response plot portraying the influence of concentration of surfactant and lipid on entrapment efficiency and particle size.

It's crucial to use an overlay plot to define the experimental domain. The conditions for finding the optimum formulation become more constrained in an overlay plot, as shown in Fig. 5.40. An overlay plot of the observed region is in the yellow shade, also known as design space or configuration space, with an optimum lipid and surfactant

concentrations. The rest of the light background serves as a testing ground. The counter lines represent CPP limits/ranges as far as possible.

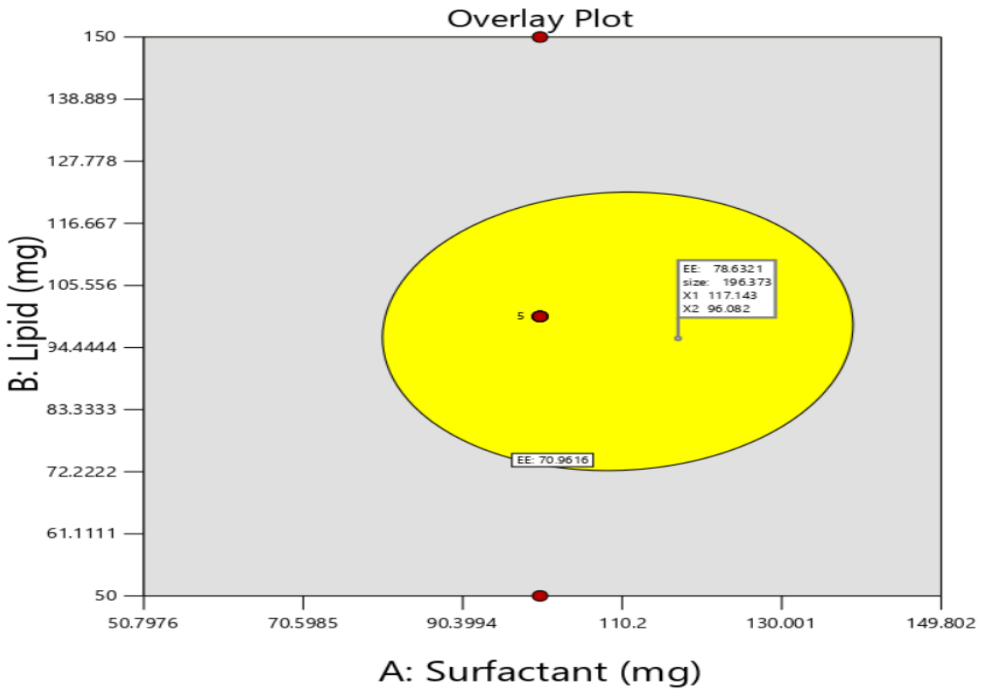

Figure 5.40: Overlay plot design space for NLCs in 2D regions.

5.4.2.1.4 *Validation of the proposed model for NLC preparation*

To establish the optimal concentration, three replication tests with the best combination of primary factors and responses were carried out to confirm the predicted NLC formulation. The observed (62.967% for EE and 189.7 nm for size) and predicted value (65.3268 % EE and 213.621 nm for particle size) was calculated and % validation was calculated on the basis of the results. The verified experimental model's output includes a comparison of observed and projected CQA values and percentage prediction error, indicating that the generated model can roughly explain the connection of selected factors and quality characteristics, as shown in Table 5.45.

Table 5.45: Validation of experimental model for the preparation of NLCs.

Solution 1 of 100 Response	Predicted Mean	Predicted Median	Observed	Std Dev	SE Mean	95% CI low for Mean	95% CI high for Mean	95% TI low for 99% Pop	95% TI high for 99% Pop
EE	65.3268	65.3268	62.967	0.305683	0.127516	65.0253	65.6283	63.6701	66.9834
Size	213.621	213.621	189.7	5.63824	2.352	208.059	219.183	183.065	244.177

5.4.2.1.5 *Formulation development of NLCs*

The ART-NLC was made using the solvent diffusion approach. Adding OA to SA yielded 6 mg ART+ ethanol (6 mL) + stearic acid (100 mg) + oleic acid (0.5 mL) + soya lecithin (100 mg). The resultant organic solution was immediately distributed into 120 mL distilled water containing 1% Tween 80 after mechanical agitation (DC-40), Hangzhou Electrical Engineering Instruments, China) at 400 rpm in a water bath at 70°C for 5 minutes. After obtaining the pre-emulsion (melted lipid droplet), the drug-loaded NLC dispersion was chilled at 27±2 ºC. NLCs of a milky white color were formulated. The NLCs that were created were then lyophilized. To avoid the acidic breakdown of the drug, the powdered NLCs were analyzed and were then put into enteric-coated capsule shells.

5.4.2.1.6 *Characterization of NLCs*

5.4.2.1.6.1 *Morphology of NLCs*

The particle size of the enhanced ART-NLC formulation was determined using Zetasizer. Fig. 5.41 shows a normal distribution map of optimized ART-NLC dispersion with an average particle size of 150.3 nm and a PDI of 0.016. The low PDI value suggested that NLC dispersion was homogeneous. The zeta potential of the ART-NLC dispersion was -32.28 mV, showing that the colloidal dispersion of produced NLCs was stable and devoid of aggregation and settling.

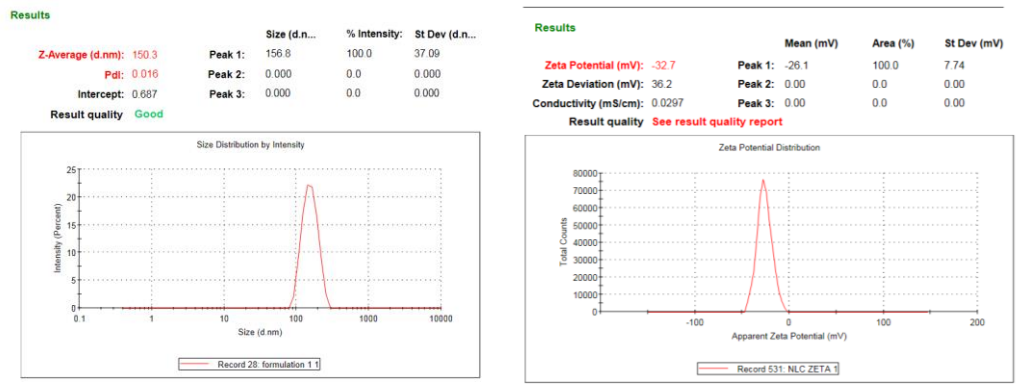

Figure 5.41: Zeta potential and particle size of prepared NLCs.

Fig. 5.42 shows how TEM and SEM were used to study the morphology of the improved formulation. SEM pictures showed that the nano lipid carriers were spherical.

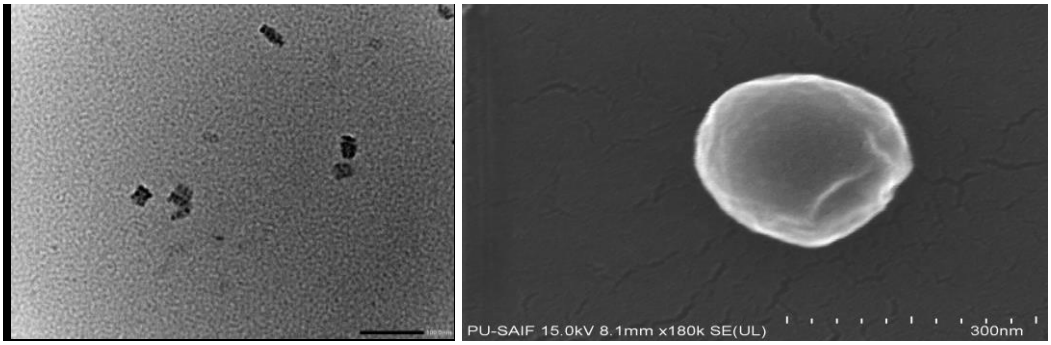

Figure 5.42: TEM and SEM image of prepared NLCs.

5.4.2.1.6.2 *Particle size distribution of lyophilized NLCs*

The NLCs were lyophilized to get powder NLCs. Further the flow properties of powdered NLCs were analyzed. The particle size distribution of powdered NLCs is illustrated in Table 5.46.

Table 5.46 Particle size distribution.

S.No.	Sieve No.	Weight retained (uncoated) (%)
1	18	0
2	22	1.7
3	25	5.2
4	30	89

5.4.2.1.6.3 Shape of lyophilized NLCs

The shape of the powdered NLCs was found to be spherical when seen under a motic microscope. The spherical nature of the lyophilized NLCs was calculated by P_{ellips} (which is a characteristic shape) as shown in Fig. 5.43. A pellet with P_{ellips} equal to 1.0 is considered spherical and good for pharmaceutical processing.

$$P_{ellips} = p/\pi\ d\ max = 1(Spherical)$$

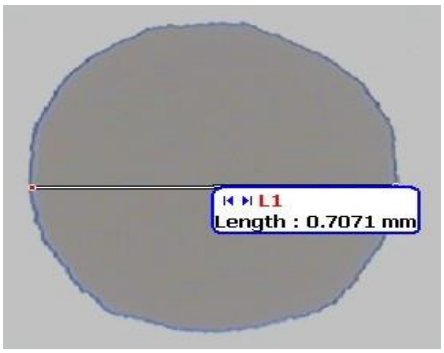

Figure 5.43: Shape of *lyophilized* NLCs.

Bulk density of lyophilized NLCs

Bulk density and tapped density were used for the calculation of Hausner's ratio and compressibility index. These help in determining the flow property and the compressibility of ingredients. A negligible variation in bulk density was observed. The bulk density of lyophilized NLCs was found to be 0.79.

Tapped density of lyophilized NLCs

A negligible difference was experimentally observed in the tapped density and was found to be 0.87.

Carr's Index of lyophilized NLCs

Results of the compressibility study showed that the compressibility index of the lyophilized NLCs was having excellent flowability as the results fell in the range of ≤10 %. The compressibility index was found to be 7.2, which shows excellent flow.

Hausner's ratio of lyophilized NLCs

According to USP 2000, lyophilized NLCs with Hausner's ratio between 1.12 and 1.18 had good flow, and above 1.35 showed poor flow property. The result was found to be 1.02.

Angle of repose of lyophilized NLCs

The angle of repose of lyophilized NLCs was found to be 22 According to I.P. this is a very good flow.

5.4.2.1.6.4 *Efficiency of entrapment in lyophilized NLCs*

ART loaded lyophilized NLC was shown to have four times the entrapment efficiency of empty NLCs. The effectiveness of entrapment was 68.2% of ART-NLCs.

5.4.2.1.6.5 *In vitro drug release of* lyophilized NLCs

The lyophilized NLCs were encapsulated in enteric coated capsule shell, which were further used for *in-vitro* and *in-vivo* studies. Fig. 5.44 depicts the cumulative ART release from ART-NLC at 37^{o} C. Around 46.8% of the drug was released from ART-NLC within the first 12 h. Following that, the AE release rate increased to 52 h, with a maximum drug release of 93.1 %. The results show that the % drug release of all formulations is less than 10% in the acidic pH, while at 52 h, the maximum drug release is attained.

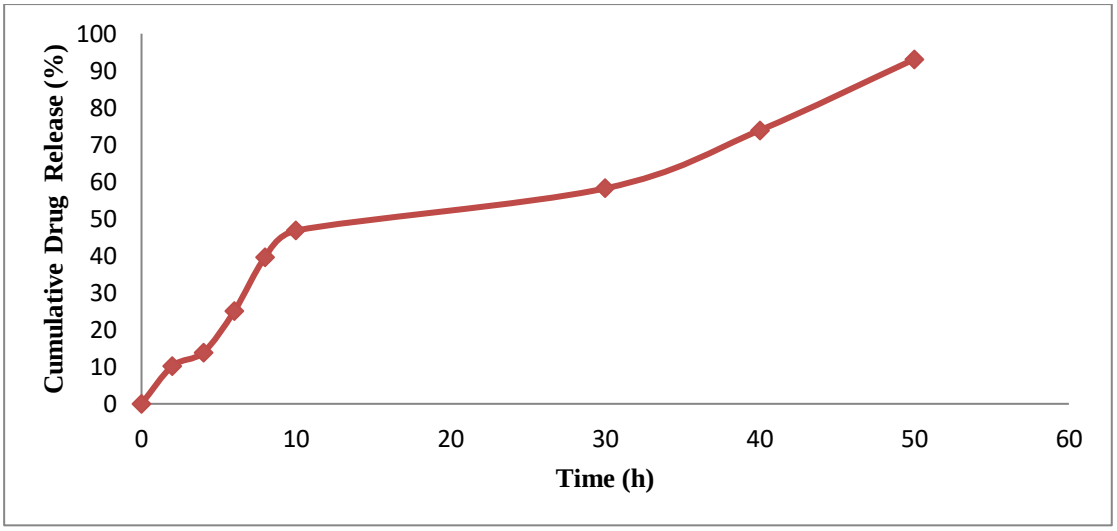

Figure 5.44: Cumulative drug release (%) of ART-NLC.

5.4.2.2 *Discussion on ART-NLCs*

The diffusion of solvent was used to prepare ART loaded NLCs. NLCs with a milky white hue were produced. The developed NLCs were then lyophilized. The NLCs were then placed inside enteric-coated capsule shells to prevent the medicine from being dissolved by acid.

A normal distribution map of the optimised ART-NLC dispersion with an average particle size of 150.3 nm and PDI = 0.016 is shown in Fig. 5.41. The low PDI value indicated homogenous NLC dispersion. The colloidal dispersion of the generated NLCs was stable and free of aggregation and settling, as shown by the zeta potential of the ART-NLC dispersion, which was -26.1 mV. Entrapment was successful in 68.2% of cases, which is a remarkable accomplishment. This might be a result of lipid crystal flaws that allow the medication to fit more comfortably. Lipid modification with the addition of lipophilic solubilizer molecules may have led to the creation of less-perfect crystals with many flaws that provided room for the dissolved medication (Westesen *et al*., 1997). The optimised ART-NLCs had a drug content of 88.6%, and their pH value was found to be 6.9, which is near to neutral, making more acceptable for oral delivery.

5.4.3 Formulation development, optimization, and characterization of SMEDDS

5.4.3.1Formulation optimization and development

5.4.3.1.1 *Equilibrium solubility studies of SMEDDS*

The equilibrium solubility of ART was determined in a range of pH values, including

1.2, 4.5, 6.8, 7.4, and pure water, as seen in Fig 5.45. The order of increasing solubility was shown to be higher with pH 6.8 phosphate buffer > pH 7.4 phosphate buffer > pH 4.5 phosphate buffer > pH 1.2 phosphate buffer. The findings suggest that AE has a pH-dependent solubility. Additionally, it is substantially more soluble at pH 6.8, followed by pH 7.4, pH 1.2, pH 4.5, and pure water, and buffer displayed a decline in solubility as the pH value decreased.

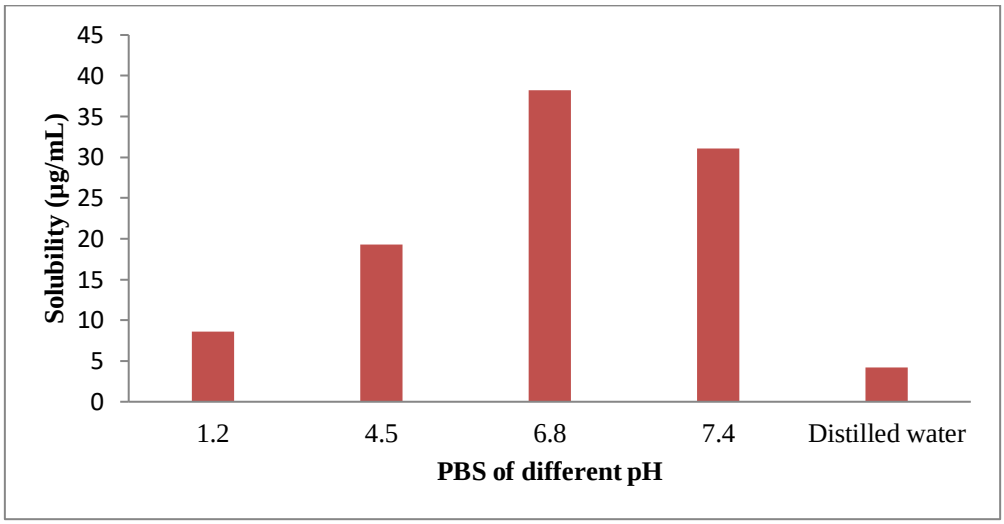

Figure 5.45: The equilibrium solubility of ART determined in a range of pH values.

5.4.3.1.2 *Solubility in solvents, oils, and surfactants of SMEDDS*

Fig.5.46-5.48, summarise the results of a solubility investigation of ART in several solvents. According to the data, ART is most soluble in ethanol, acetone, and methanol, but is almost insoluble in water. The greatest solubility of ART in different oils was determined to be 99.10±2.96 mg/mL in arachis oil, followed by oleic acid (78.70±1.94 mg/mL). ART was the least soluble in coconut oil (5.03±1.55 mg/mL). As a result, arachis oil was chosen for further screening in the preparation of new formulations including ART. Fig. 5.48 summarised the results of a solubility investigation of ART in various surfactants and co-surfactants. Tween 80 (298.26±4.67 mg/mL) was determined to have the highest solubility, followed by span 80 (248.69±5.58 mg/mL). As a result, polysorbate 80 (Tween 80) and Span 80 were chosen as a surfactant and cosurfactant, respectively, for future formulation development research.

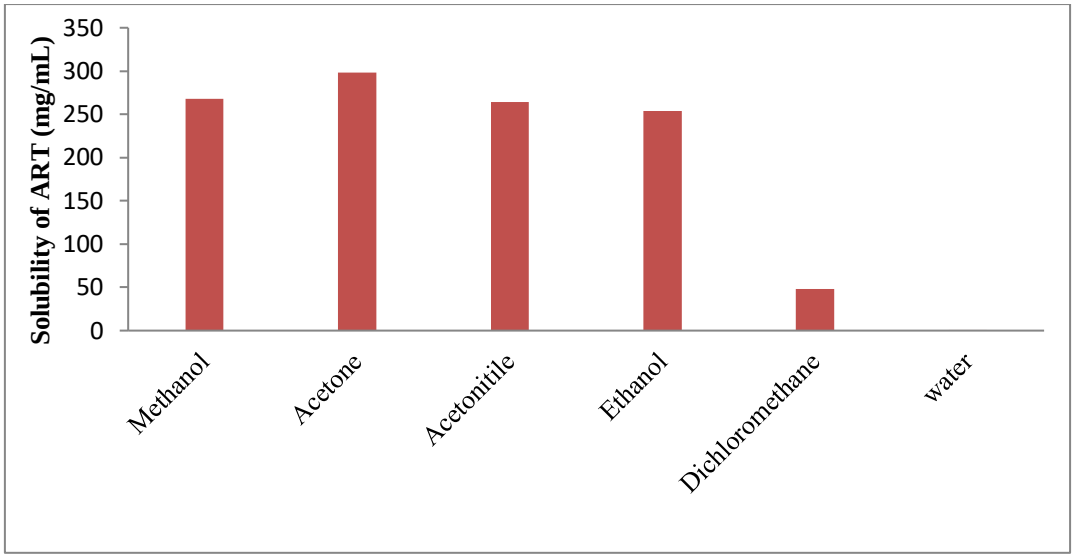

Figure 5.46: Solubility data of ART in different solvents.

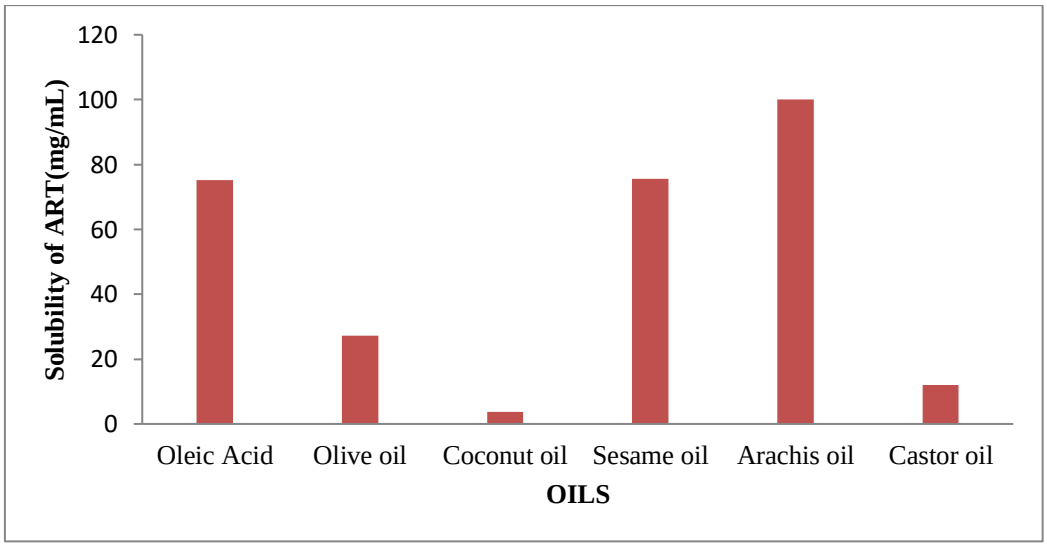

Figure 5.47: Solubility data of ART in different oils.

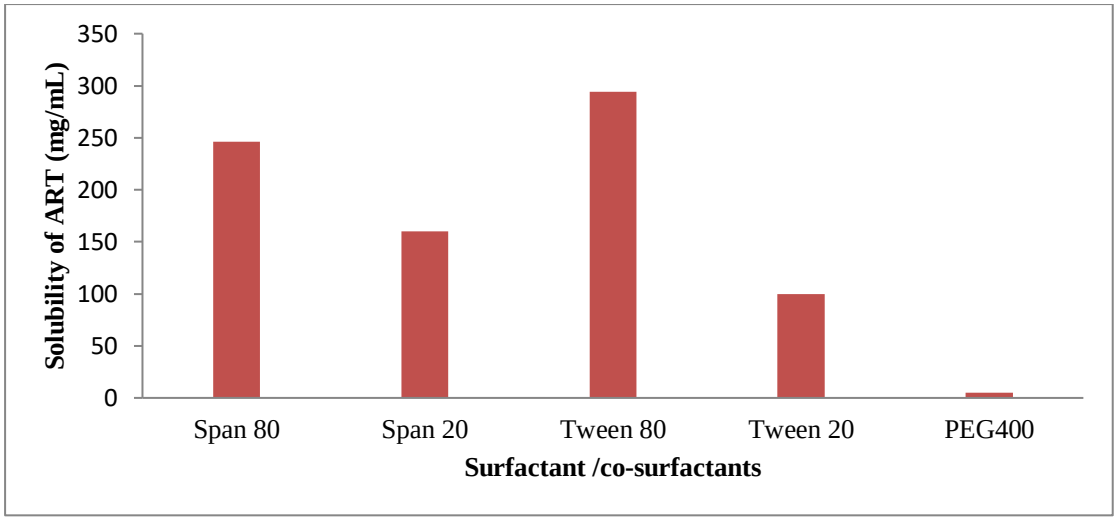

Figure 5.48: Solubility data of ART in different surfactants and co-surfactants.

5.4.3.1.3 *Construction of the ternary phase diagram of SMEDDS*

Arachis oil, tween 80, and span 80 were chosen as the three-component system for preparing ART-loaded SMEDDS based on preliminary studies, and the phase diagram of ART-loaded samples is presented in Fig. 5.49. The shaded areas indicate nano emulsification locations with a high chance of creating nanoemulsions with globule sizes of 150-200 nm, whilst the area around these areas denotes formulations with a low potential to generate nanoemulsions with larger globule sizes (Singh *et al.*, 2010). It has been reported that the drug compounds included in SNEDDS influence the device's performance (Xuemei *et al.*, 2011). Thus, the ternary phase diagram was constructed in the presence of ART (Kim *et al.*, 2010). Due to ART's limited water solubility, the drug molecules were expected to orient at the nanoemulsion interface. This may be a result of the surfactant and cosurfactant's interaction with a particular oil being altered by the medication (Patel *et al.*, 2009). Maximum solubilized oil content was 70% w/w for ART-SMEDDS, with a minimum surfactant content of 30% w/w. Notably, the ternary phase diagram for SMEDDS formed without cosurfactant was difficult to emulsify, demonstrating the critical role of cosurfactant in formulations (Mohamed *et al.*, 2009). Additionally, the following table summarises the influence of different components such as oil, surfactant, and cosurfactant.

The effect of oil concentration: The findings indicated that emulsification of ART-SMEDDS at intermediate oil concentrations was more likely. To determine the influence of oil concentration, we plotted the globule size of diluted formulations without co-surfactant against the oil concentrations. The findings demonstrated an

increase in the size of globules from 100–143 nm at 70–90% w/w arachis oil. Above and below this concentration range, a substantial increase in globule size was observed. The rise in globule size beyond these concentration ranges might be explained by a reduction in the relative quantity of surfactant, which may have resulted in the coalescence of oil globules and the loss of the emulsification potential of systems (Azeem *et al*., 2009). Below these concentration ranges, there was an increase in globule size, which might be ascribed to the formulation's decreased solubilization ability at lower oil levels.

Surfactant and co-surfactant action concentration: The influence of surfactant and co-surfactant concentrations on drug-loaded SMEDDS was assessed by graphing the globule size of SMEDDS formulations without co-surfactants and with various surfactant concentrations. When ART-SMEDDS was emulsified at a 20% surfactant concentration, the efficiency of emulsification was outstanding. Below these concentrations, a relative increase in globule size might be rationalized by surfactants' failure to emulsify the quantity of oil present. Additionally, raising the surfactant content improved the spontaneity of systems. The globule size decreased linearly with increasing surfactant concentrations from 29 to 31% w/w. This might be explained by the fact that a higher concentration of surfactant stabilizes the oil–water interface more effectively, hence reducing the globule size (Azeem *et al*., 2009). This might be explained by excessive water penetration into bulk oil, resulting in enormous interfacial disturbance and globule ejection from the aqueous phase. The rise in globule size might also be explained by a condensation process and the production of several layers of extra surfactant molecules. In comparison to cosurfactant, it was noticed that raising the concentration of co-surfactant improved the spontaneity of SMEDDS self-emulsification. This might be explained by the SMEDDS's relative drop in viscosity since SPAN 80 had a much lower viscosity than their corresponding surfactant. Increases in co-surfactant concentration resulted in a decrease in globule size. This might be explained by Span 80's capacity as a co-surfactant to reduce the interfacial tension between oil and water and enhance the interface's flexibility around oil globules (Lawrence *et al.,* 2000). This might be attributed to the fact that at high concentrations, co-surfactant does not only remain in the interfacial film but also enters the inner oil phase, causing the interfacial film to expand and the globule size to grow (Azeem *et al*., 2009)

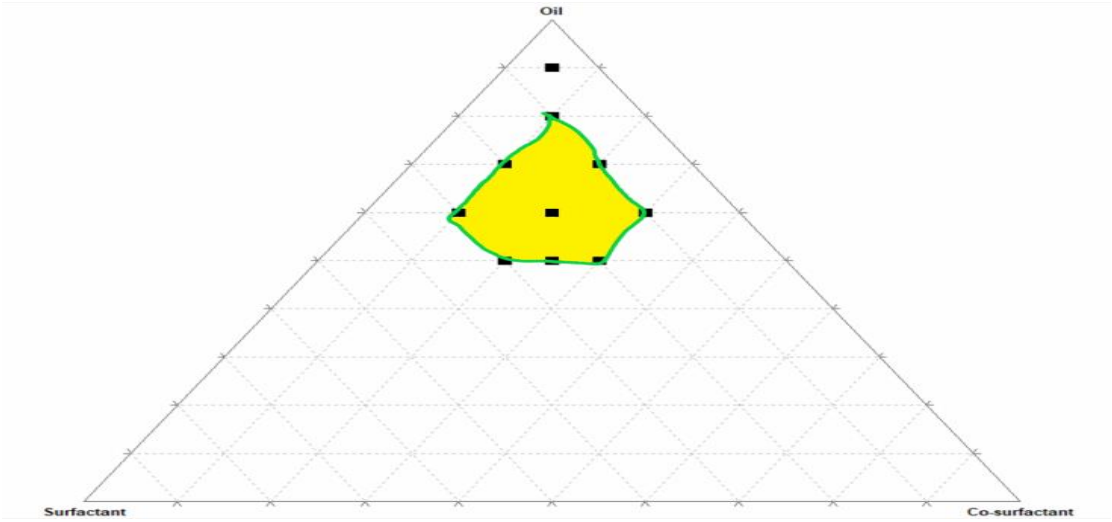

Figure 5.49: Ternary phase diagram of developed emulsion.

5.4.3.1.4 *Risk assessment studies of SMEDDS*

The Ishikawa fishbone diagram in Fig. 5.50 illustrates numerous factors that impact the CQAs of SMEDDS formulations. The fish-bone graphic illustrated the six Ms that are likely to affect CQAs: machines, men, material (API and excipients), measurements, techniques, and milieu/environment. Additionally, a risk assessment matrix (RAM) was created to track various reasons impacting the CQAs. The risk matrix for SMEDDS is given in Table 5.47, indicating the low, medium, and high-risk levels associated with each process parameter/material specification. RAM indicated that the concentrations of solid lipid, liquid lipid, and surfactant, were associated with a high-risk level, while the aqueous phase was associated with a medium-risk level, while the stirring speed, stirring time, and temperature were associated with a medium to low-risk level, respectively.

Table 5.47: Initial RAM for ART-loaded SMEDDS.

Risk estimation matrix									
CQAs for ART- Loaded SMEDDS									
Quality attributes		Globule size	Transmittance	PDI	Zeta potential	Emulsification efficiency	Drug content	Drug release	Permeation flux
Material attributes	**Drug**								
	Dose	Low	Low	Low	Low	Low	High	High	High
	Solubility	Medium	Medium	Low	Low	Low	High	High	High
	Log P	Medium	Low	Low	Low	Medium	Medium	Medium	High
	PKa	Medium	Medium	Low	Low	Medium	Medium	Medium	High
	Oil/Lipids								
	Interfacial tension	Medium	Medium	High	High	High	Medium	High	High
	Polarity	Medium	Medium	High	High	High	Medium	High	High
	Lipid concentration	High	High	High	High	High	High	High	High
	Viscosity	Medium	High	Low	Low	Medium	Low	Medium	Low
	Lipid composition	High	High	High	High	High	High	High	High
	Surfactant								
	Concentration	High	High	High	High	High	High	High	High
	Viscosity	Medium	High	Low	Low	High	Low	Low	Low
	HLB	High	High	High	High	High	High	High	High
	Melting point	Low	Low	Low	Low	Low	Low	Low	Low
	Cosurfactant								
	Viscosity	Medium	Medium	Low	Low	Medium	Low	Low	Low
	Concentration	High	High	High	High	High	Medium	Medium	Medium
	HLB	High	Medium	Medium	Medium	High	Medium	Medium	Medium
Process parameters	**Stirring**								
	Time	High	Medium	High	Medium	High	High	Medium	Medium
	Speed	Medium	Medium	High	Low	Medium	High	Medium	Medium
	Temperature	Medium	Medium	Medium	Low	Medium	High	Medium	Medium

*Red color = High risk parameter, Yellow color = Medium risk parameter, Green = Low risk parameter.

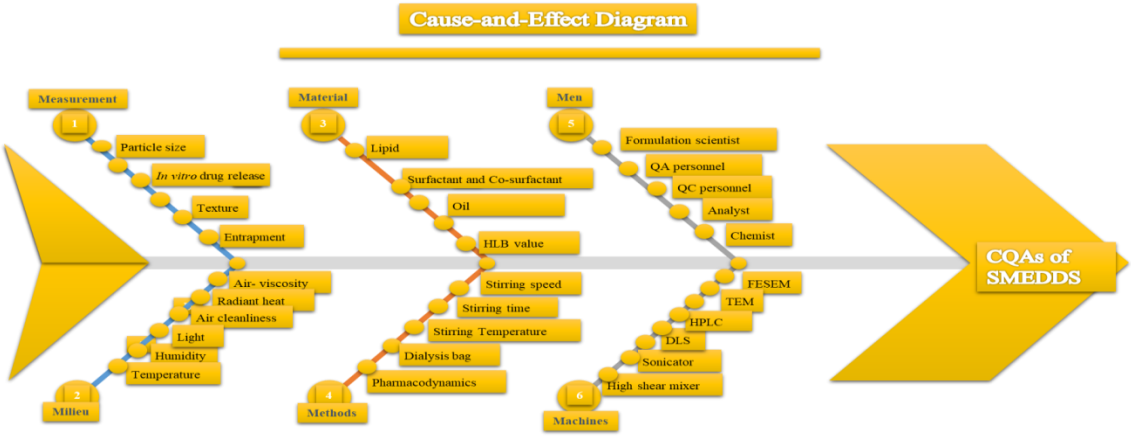

Figure 5.50: Ishikawa fish-bone diagram depicting various causes that affects the CQAs of SMEDDS.

Various QTPP and CQA components of SMEDDS are discussed in Table 5.48.

Table 5.48: QTPP components for SMEDDS along with the CQAs and their justifications.

QTPP components	**Specification**	**Justification**	
Formulation	Liquid	Bioavailability enhancement	
Novel drug delivery system designed	SMEDDS	SMEDDS selection aids in increasing drug loading and bioavailability.	
Administration route	Oral	The recommended mode of administration is intended to increase patient compliance.	
Concentration	0.025% w/w	Within ART's lowest efficacious concentrations limits as determined by the literature and preclinical studies.	
Packaging	Appropriate for dosage form	Appropriate packaging is necessary for successful extrusion and customer acceptance.	
Stability	In refrigerated storage for about 12 months	To sustain the optimal strength of ART over the storage period to maximize the drug's therapeutic effectiveness.	
Quality attribute	**Specification**	**Justification**	**Whether considered CQA or not?**
Organoleptic properties (color, odor, appearance)	Uniform and smooth appearance No unpleasant color or odor	Physical appearance is not significant since it is unrelated to safety and effectiveness.	No
Total drug content	~100%	It is a critical parameter in the design of dosage forms. Because SMEDDS is not a unit dosage system, they are classified as moderately necessary.	No
Particle size	Nanometer range (50-200 nm)	This is a crucial element since particle size significantly impacts bioavailability and solubility.	Yes
PDE	80-100%	A higher PDE value will result in improved formulation and medication stability. As a result, it is a crucial characteristic.	Yes
Entrapment Efficiency	More than 90%	Increased percent EE has a substantial influence on dosage loading and delivery.	Yes
In vitro release	Dependent on pH	Minimum in an acidic environment and maximum in basic pH.	Yes
Permeability	>80%	f ≥80% is critical for achieving therapeutically effective medication concentrations in the blood.	Yes

5.4.3.1.5 *Selection of design of SMEDDS*

5.4.3.1.5.1 *Measurement of dependent responses of SMEDDS*

After specifying ranges of all 3 components, to evaluate content uniformity data

average assay and %RSD of are measured in all 16 experimental runs of the selected design. The components of experimental design for development of SMEDDS are as shown in Table 5.49. The low and high values for the selected factors for arachis oil (60-80%), Tween 80 (10 to 30%), Span80 (5 to 25 %) was selected to get the desired experimental runs.

Table 5.49: Components with 16 experimental runs.

Run	A:Arachis oil	B:Tween 80	C:Span 80	% DR	%RSD DR
	%	%	%		
1	73.7	10.0	16.3	97.5	3.4
2	73.7	10.0	16.3	96.6	3.2
3	61.9	13.1	25.0	91.5	5.2
4	66.7	15.5	17.8	97.2	1.3
5	75.1	14.6	10.3	95.9	3.9
6	60.0	30.0	10.0	76.9	8.1
7	61.9	13.1	25.0	88.1	5.4
8	65.0	30.0	5.0	81.2	7.3
9	69.7	20.0	10.4	98.6	1.4
10	75.0	19.9	5.2	89.5	4.8
11	69.7	20.0	10.4	98.4	1.2
12	60.0	25.0	15.0	84.7	6.4
13	80.0	15.0	5.0	83.7	6.3
14	60.0	25.0	15.0	86.1	6.3
15	70.0	25.0	5.0	86.4	5.3
16	69.7	20.0	10.4	99.1	1.2

5.4.3.1.5.2 *ANOVA based statistical analysis of data* of *SMEDDS*

Various ANOVA parameters i.e., P-value, R^2 value, adequate precision, etc. were determined using the Design Expert software. Software suggested a quadratic vs linear relationship between the independent variable and dependent variable. Various ANOVA parameters were shown in Table 5.50.

Table 5.50: ANOVA-based statistical analysis parameters.

	% DR			% RSD DR			Inference
Source	**Sum of Squares**	**F-value**	**p-value**	**Sum of Squares**	**F-value**	**p-value**	
Model	732.14	59.43	< 0.0001	9.70	911.06	< 0.0001	Significant
Linear Mixture	321.58	65.25	< 0.0001	10.07	945.64	< 0.0001	
AB	271.73	110.28	< 0.0001	4.69	440.41	< 0.0001	
AC	318.19	129.13	< 0.0001	9.15	859.01	< 0.0001	
BC	139.47	56.60	< 0.0001	3.69	346.64	< 0.0001	
Residual	24.64						
Lack of Fit	17.22	2.32	0.1887				Not significant
Pure Error	7.43						
Cor Total	756.78						
R^2	0.9674				0.9990		
Adequate precision	22.895				88.0736		

After analysis of Table 5.51, all the parameters i.e., P-value., R^2 value, and adequate precision were found to be in the acceptable range to make the design significant. The design further suggested the relationship between the independent and dependent variables in the form of an equation, which is shown below:

Y = b1X1 + b2X2 + b3X3 + b4X1X2 + b5X1X3 + b6X2X3 + b7X1X2X3 ……(4)

Where, b1……b7 were the coefficients of the equations and XI, X2, and X3 are the three dependent variables.

A 2D contour plot in the form of an equilateral triangle is drawn to depict the relationship between the independent variable and dependent variable as shown in Fig. 5.51.

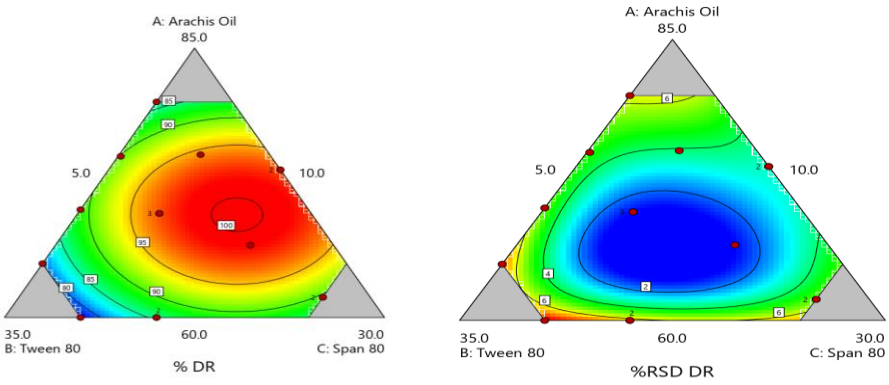

Figure 5.51: 2D counter plot in the form of an equilateral triangle to depict the relationship between the independent and dependent variables.

5.4.3.1.5.3 ***Overlay plot and validation of the model of SMEDDS***

It is important to determine the design space from the experimental area because the design space helps achieve the final target product profile more quickly and precisely. The overlay plot has been plotted for this process for showing the design space as shown in Fig 5.52.

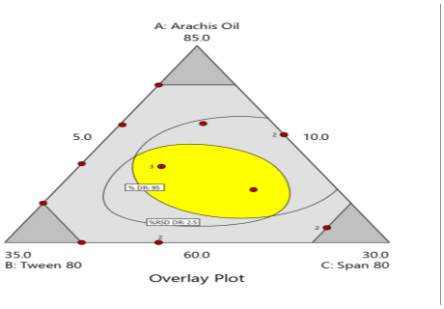

Figure 5.52: Overlay plot showing the yellow region as design space.

Validation of the model is important for checking its functionality at the experimental level as discussed in Table 5.51. The model was validated by comparing the result obtained from the lab scale to that predicted by the software and the developed model was 99.3 % similar in predicting both the responses i.e, % DR (99.27%) and % RSD DR (0.6097%) respectively.

Table 5.51: Validation value of SMEDDS.

Response	Predicted Mean	Predicted Median	Observed	Std Dev	n	SE Pred	95% PI low	95% PI high
% DR	99.2749	99.2749	99.3%	1.56973	1	1.74239	95.3926	103.157
%RSD DR	0.609793	0.609793	0.613	0.103204	1	0.124353	0.315745	0.903841

A series of SMEDDS have been formulated by dissolving ART in arachis oil (70 mL) following addition of a mixture of surfactants (20 mL) and co-surfactants (10 mL) at ambient temperature. The final mixture was vortexed vigorously for 30 min to achieve complete mixing until a clear solution was obtained. The SMEDDS were analyzed for phase separation or turbidity and were equilibrated and stored at ambient temperature.

5.4.3.2 *Characterization of SMEDDS*

5.4.3.2.1 *Visual appearance of SMEDDS*

After oral administration, the produced SMEDDS were analysed in gastro-intestinal fluid when they came into direct touch with various physiological fluids. No change in colour was detected when GI fluid was added and no turbidity was observed when 900 mL of water was added, as shown in (Fig. 5.53).

Figure 5.53: Prepared SMEDDS with no phase separation after centrifugation.

5.4.3.2.2 *Microscopic image of SMEDDS*

Microemulsion compositions were transparent and clear. The transmission electron microscopy indicated that the microemulsion droplets were spherical (Fig. 5.54).

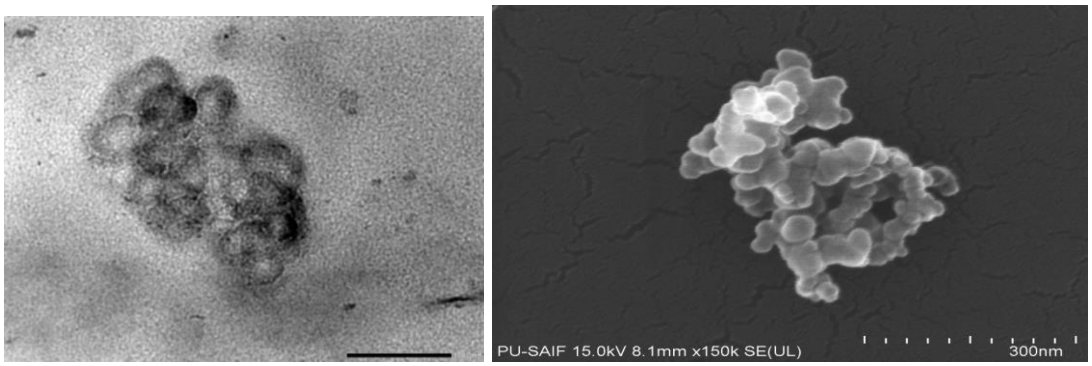

Figure 5.54: TEM and SEM images of prepared SMEDDS.

5.4.3.2.3 *Globule size analysis of SMEDDS*

The improved formulation had a mean diameter of 116.1 nm and a polydispersity index of 0.034 (Fig. 5.55). The low PDI value suggested that SMEDDS dispersion was homogeneous (Valecha *et al*., 2012). The created microemulsion's zeta potential was determined to be -29.8 mV, showing that the generated SMEDDS colloidal dispersion was stable and devoid of aggregation and settling (Fig. 5.54). The pH ranged between 6.8 to 7.0, which is close to neutral and appropriate for oral formulation. Rheological studies established the microemulsion's Newtonian character. The drug concentration of various formulations was determined to be between 98.2 ±0.26 and 99.14 ±0.32%.

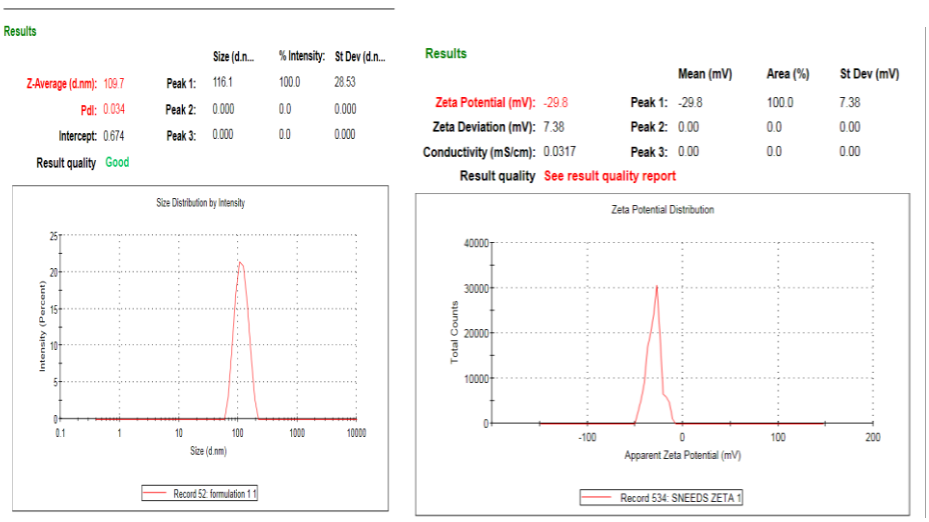

Figure 5.55: Particle size and zeta potential of prepared SMEDDS.

5.4.3.2.4 *Shape of solid SMEDDS*

The shape of powder was found to be spherical when seen under a motic microscope as shown in Fig 5.56. The spherical nature was calculated by P_{ellips}. A pellet with P_{ellips} equal to 1.0 is considered good for pharmaceutical processing.

[P_{ellips} = p/π d max = 1(Spherical)]

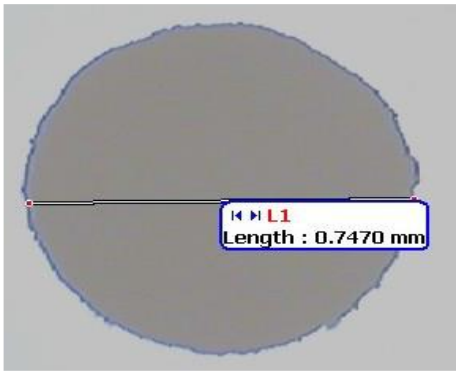

Fig 5.56: Shape of solid SMEDDS

Bulk density of S-SMEDDS

Bulk density and tapped density were used for the calculation of Hausner's ratio and compressibility index. These helped in determining the flow property and the compressibility of ingredients. A negligible variation in bulk density was observed. The bulk density of spheroids was found to be 0.79.

Tapped density of S-SMEDDS

Negligible difference was experimentally observed in the tapped density and was found to be 0.82.

Carr's Index of S-SMEDDS

Results of the compressibility study showed that the compressibility index of the S-SMEDDS was having excellent flowability as the results fell in the range of ≤10 %. The compressibility index was found to be 7.4 confirming excellent flow.

Hausner's ratio of S-SMEDDS

According to USP 2000, Hausner's ratio between 1.12 and 1.18 corresponds to good flow, and above 1.35 showed poor flow properties. The result was found to be 1.04, confirming good flow of S-SMEDDS.

Angle of repose of S-SMEDDS

The angle of repose of S-SMEDDS was found to be 24. According to I.P. this reflects very good flow.

5.4.3.2.5 *In- vitro drug release of S-SMEDDS*

A dialysis bag approach was used to examine the *in- vitro* medication release of ART-SMEDDS. Around 42% of the drug was released in first 10 h and half of the drug was released in 12 h. The maximum drug release starts after 30 h and 90% of the drug was released after 40 h. After acid degradation, each sample was examined using a UV-visible spectrophotometer set at 254 nm as shown in Fig 5.57.

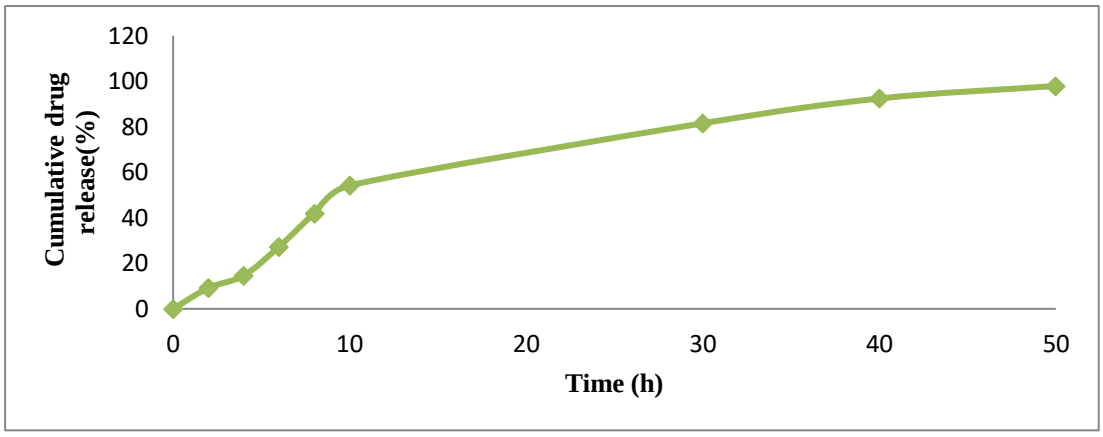

Figure 5.57: Cumulative drug release(%) of ART-SMEDDS.

5.4.3.3 *Discussion on SMEDDS formulation*

SMEDDS are lipid-based formulations that, when exposed to physiological fluid, self-emulsify, enhancing the absorption of medications like ART that are lipophilic. Since it has been shown that the inclusion of fatty acids might increase the bioavailability of lipophilic medicines, SMEDDS was our formulation of choice. Since it was discovered that the self-emulsifying characteristic of the drug reduces with increasing drug concentration in the formulation development SMEDDS, the final ART concentration selected was 6 mg. Formulations with less than 50% surfactant did not spontaneously emulsify, or exhibited turbidity or displayed phase separation during storage. At 30% w/w, the lipid ratio was optimum. Surfactants with a weight-to-weight ratio of 70% demonstrated strong self-emulsification, generating a clear emulsion with a little stirring. These transparent emulsions were discovered to have globules between 100 and 200 nm in size. Additionally, it was shown that globule size

increases when the surfactant content was reduced. The liquid-liquid extraction technique was used, and it consistently produced excellent recoveries of ART. By administering an oral dosage of 6 mg/kg in SMEDDS, the level of ART in rat plasma was determined.

The creation of the tiny emulsion droplets, following lipolysis, and the development of mixed micelles, which provide a greater surface area for ART absorption, may be attributed to the higher efficacy of SMEDDS. Tween 80 increased intestinal permeability of ART by inhibiting P-glycoprotein function, which protects the body from xenotoxins. Tween 80 and oleic acid, which also boosts chylomicron production, which ultimately enhances the lymphatic transfer of ART. However, unstable gastrointestinal fluids and restricted aqueous solubility and dissolution of ART may contribute to poor oral bioavailability of ART in GNO and ART in aqueous suspension. Pharmacokinetic studies amply demonstrated the considerable improvement in ART bioavailability in SMEDDS. Due to its high solubility in the long-chain oil found in SMEDDS and the improved mucosal permeability brought on by the presence of surfactants, the drug is expected to be more readily absorbed into the lymphatic system, increasing ART's bioavailability (Joshi *et al.*, 2008). Rapid parasite clearance was seen in mice, which may be related to ART's fast-acting schizontocide action.

5.4.4 *Formulation development optimization and characterization of spheroids containing CD complexed ART.*

5.4.4.1 *Experimental design optimization and response surface methodology for spheroids*

BBD was applied for the optimization of selected critical factors such as stirring time, stirring speed, disintegration concentration, and binder concentration in comparison to the selected response i.e., dissolution (%) BBD has been employed because it is an important optimization design that can help in the determination of the estimation relation between the independent and dependent variables.

BBD in this study for four selected critical independent variables i.e., stirring time, stirring speed, disintegration concentration, and binder concentration gave 29 runs, and % dissolution was selected as the only response. Table 5.52 depicts the value of response in comparison to various values of independent variables. The selected low

and high value of the bender concentration (100 to 200 mg), disintegrant concentration (50 to 200 mg), stirring speed (500 to 900 rpm), and stirring time 5 to 9 min) were selected to get the desired runs.

Table 5.52: Value of response in comparison of different values of independent variables.

Run	A: Stirring speed	B: Stirring time	C: Disintegrant concentration	D: Binder concentration	Dissolution
	rpm	min	mg	mg	%
1	700	7	100	150	64.5
2	500	7	50	150	58.6
3	700	5	50	150	69.2
4	900	9	150	200	90.3
5	700	5	150	150	45.6
6	700	5	100	200	54.7
7	500	9	100	150	79.6
8	*900*	*7*	*50*	*150*	*58.9*
9	700	9	100	200	37.8
10	500	5	100	150	29.3
11	500	7	100	200	40.6
12	700	9	50	150	45.8
13	700	7	150	100	50.7
14	700	7	100	150	70.9
15	700	7	100	150	76.1
16	500	7	150	150	56.8
17	700	7	50	100	78.9
18	700	7	150	200	89.4
19	500	7	100	100	57.4
20	700	5	100	100	56.4
21	900	7	100	100	67.9
22	900	7	150	150	85.9
23	700	7	100	150	61.4
24	900	8	150	200	99.6
25	700	7	100	150	56.8
26	700	7	50	200	46
27	900	9	175	200	99.2
28	700	9	200	100	45.3
29	700	9	150	150	58.6

5.4.4.2 *Equation of responses in terms of coded factors for spheroids*

The suggested non-linear quadratic model gave a coded equation for each response to depict the relationship between the possible independent variables and the response. The + in the equation shows a synergistic or positive effect while '-'depicts the negative or polynomials. The coefficients are adjusted around the average based on various factors settings. The equation for the response i.e., % dissolution generated by BBD in this study has been shown as Equation 5.

$$\% \text{ Dissolution} = +65.21 + 9.21A - 2.34B + 2.83C - 0.9403D - 24.98AB + 8.11AC + 8.83AD + 10.09BC - 2.60BD + 18.65CD + 1.50A^2 - 9.08B^2 + 0.4626C^2 - 2.75D^2 \quad \ldots\ldots\ldots\ldots\ldots\ldots\ldots\ldots (5)$$

5.4.4.3 *ANOVA-based statistical analysis of spheroids*

Analysis of variance (ANOVA) was performed to check the suitability of developed model. Various ANOVA-based statistical parameters were shown in Table 5.53. The selection of the model was done based on analysis of various parameters such as f-value, p-value, R^2 value, predicted R^2 value, Standard Deviation (SD) value, adequate precision. The precision value was very important in the significance determination of the model. A model with a p-value should be less than 0.5 for being a significant Error of the model was determined based on the significance "Lack of fit" value (Alruwaili *et al.,* 2021). A significant "Lack of fit" depicts that the developed model does not have a proper difference between the exploratory and predicted data points. The R^2 value represents how good the predicted data points fit into the experimental data points and the value of R^2 should be near 1. The value of predicted R^2 should have a difference of more than 0.2 for the model to be significant (Tome *et al.,* 2019). Adequate precision in the ANOVA measures the ratio of signal and noise in the model and a ratio of 4 or more should be necessary for a model to be noise free. SD of the developed model should have less value for the significance of the developed model.

Table 5.53: Various ANOVA-based statistical parameters.

Source	Sum of Squares	df	Mean Square	F-value	p-value	Inference
Model	8467.06	14	604.79	9.63	< 0.0001	Significant
A- Stirring speed	696.41	1	696.41	11.09	0.0050	
B- Stirring time	38.23	1	38.23	0.6087	0.4483	
C-Disintegrant concentration	103.68	1	103.68	1.65	0.2197	
D-Binder concentration	8.89	1	8.89	0.1416	0.7124	
AB	1163.39	1	1163.39	18.53	0.0007	
AC	291.64	1	291.64	4.64	0.0491	
AD	264.73	1	264.73	4.22	0.0592	
BC	514.31	1	514.31	8.19	0.0126	
BD	19.25	1	19.25	0.3064	0.5886	
CD	1935.66	1	1935.66	30.82	< 0.0001	
A^2	12.03	1	12.03	0.1916	0.6683	
B^2	442.04	1	442.04	7.04	0.0189	
C^2	1.82	1	1.82	0.0290	0.8673	
D^2	45.79	1	45.79	0.7291	0.4075	
Residual	879.21	14	62.80			
Lack of Fit	645.16	10	64.52	1.10	0.5041	Not significant
Pure Error	234.05	4	58.51			
Cor Total	9346.27	28				
Std. Dev	**R^2**	**C.V.**	**Predicted R^2**	**Adeq Precision**		
7.92	0.9059	12.59	0.4738	13.480		

As per Table 5.54, the p-value and SD of the model were found to be less than 0.0001 and 7.92 respectively which showed the significance of the developed model. The non-significant "lack of fit" of the developed model showed that the developed model has a proper difference between the exploratory and predicted data points. The value of R^2 was found to be 0.9059 and has a difference of more than 0.2 to that of predicted R^2 (0.4738). Adequate Precision was found to be 13.480, whose value was found to be much more than 4. Thus, by analyzing most of the statistical parameters, it could be said that the developed model was significant in predicting the optimized value of independent variables.

Fig.5.58 depict the normal plots of residuals for all the selected independent variables showing that the irregular distribution of the data points to that of the best-fit line without much deviation from the best-fit line. Close of data points to the best-fit line confirmed the suitability of the developed QbD model for the optimization of selected independent variables.

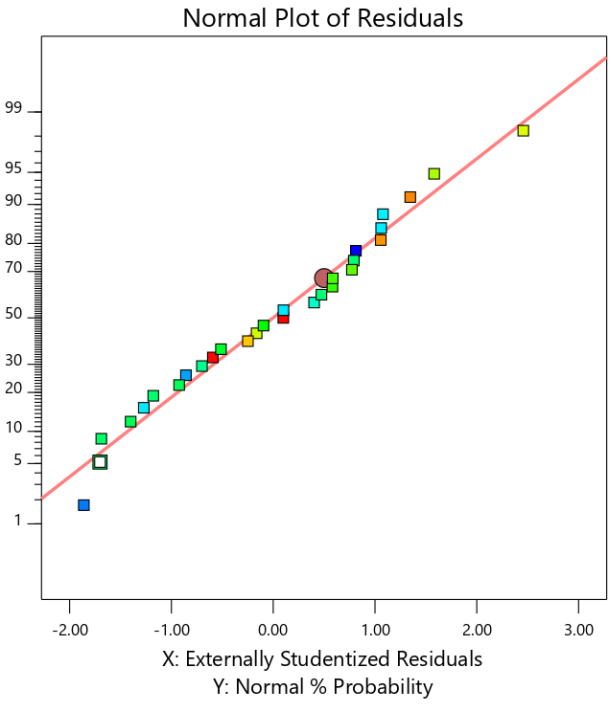

Figure 5.58: Normal Plot of residuals for the various data points of independent variables.

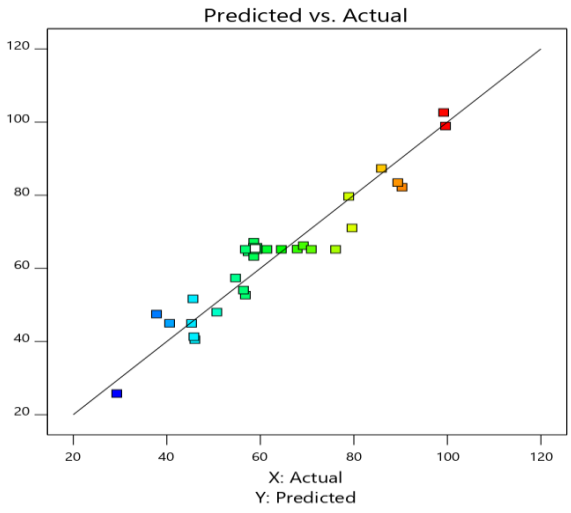

Figure 5.59: The predicted vs actual plot, showing how close the predicted data points are to the experimental data points.

The inter-variation, interdependence, and co-dependence among the selected independent variables and their possible relationship with the response/dependent variable were shown by drawing the response surface diagram as shown in Fig 5.59.

Fig 5.60 depict the 2-dimensional contour plot and depict the 3-dimensional response surface plot for the selected independent variable and dependent variable i.e., % dissolution.

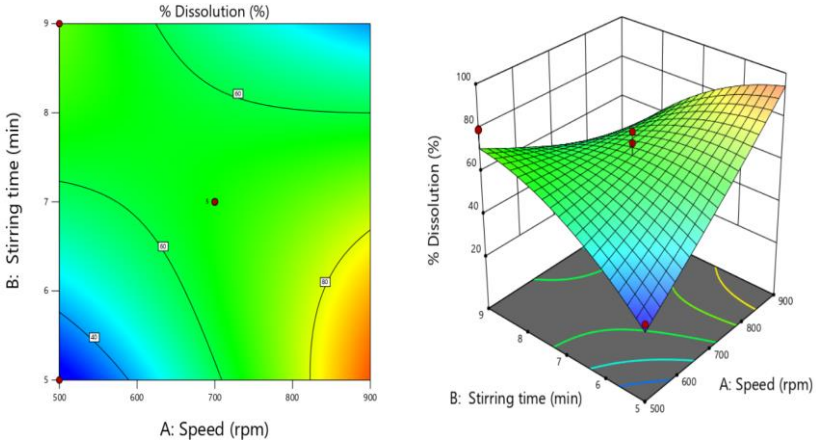

Figure 5.60: 2-D contour plot and 3-D response surface plot for selected variables.

After analysis of the 2D contour plot it was concluded that % dissolution (response) for the selected independent variables (i.e., stirring time, stirring speed, disintegration concentration, and binder concentration) increases to some extent with increasing value but starts decreasing when the values of independent variables keep increasing.

5.4.4.4 *Overlay plot and defining the design space of spheroids*

The developed model worked in an experimental domain, which was created with the help of various ranges of independent variables (i.e., stirring time, stirring speed, disintegration concentration, and binder concentration). But it is necessary to determine the design space, which helps in achieving the final quality profile for our formulation. Fig. 5.61 depicts the overlay plot showing the experimental area in grey colour and design space which was important for achieving the final quality target profile in the yellow region.

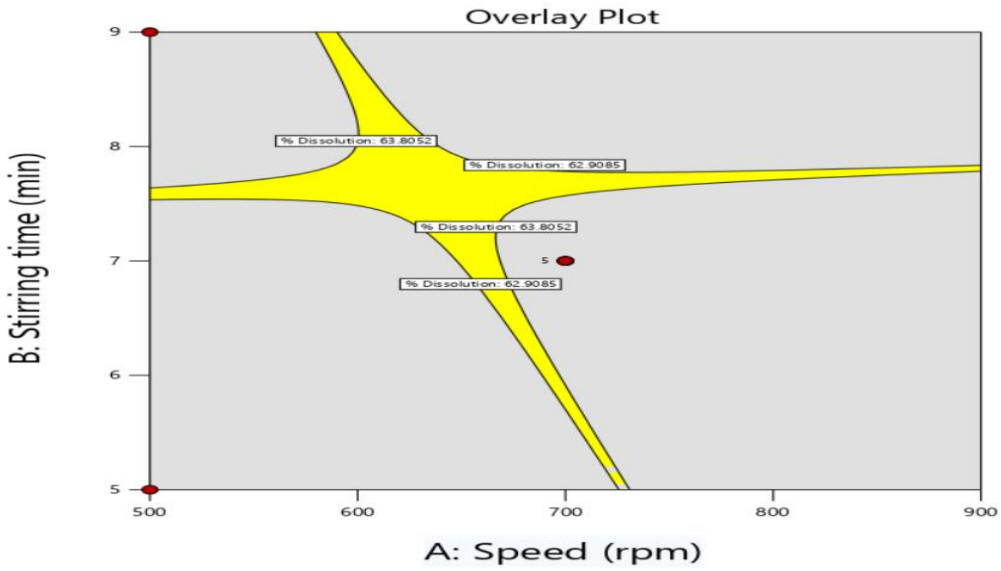

Figure 5.61: Overlay plots showing the design and experimental space.

5.4.4.5 *Point prediction and validation of developed model for spheroids*

The point prediction feature of the Design Expert software was employed for determining the optimized value of independent variables (i.e., stirring time, stirring speed, disintegration concentration, and binder concentration) for achieving the quality target profile as given in Table 5.54. The validation model confirmed the predicted value (65.2144 %) and the observed value (62.819 %) are near to each other which confirm the 96.32%.

Table 5.54: Validation of developed model.

Response	Predicted Mean	Predicted Median	Observed	Std Dev	SE Mean	95% CI low for Mean	95% CI high for Mean	95% TI low for 99% Pop	95% TI high for 99% Pop
% Dissolution	65.2144	65.2144	62.819	7.9247	3.22161	58.3047	72.124	29.7439	100.685

5.4.4.6 Flow properties of spheroids

Particle size distribution of spheroids

The particle size of the prepared spheroids is mentioned in Table 5.55.

Table 5.55: Particle size distribution.

S.no.	Sieve No.	% weight retained (uncoated)
1	18	0
2	22	1.7
3	25	4.9
4	30	86

Shape of spheroids

Shape of the spheroid was found to be spherical when seen under a motic microscope as shown in Fig 5.62. The spherical nature of the spheroid was calculated by P_{ellips} (which is a characteristic of pellet shape). A pellet with P_{ellips} equal to 1.0 is considered spherical and good for pharmaceutical processing.

$$P_{ellips} = p/\pi\ d\ max = 1(Spherical)$$

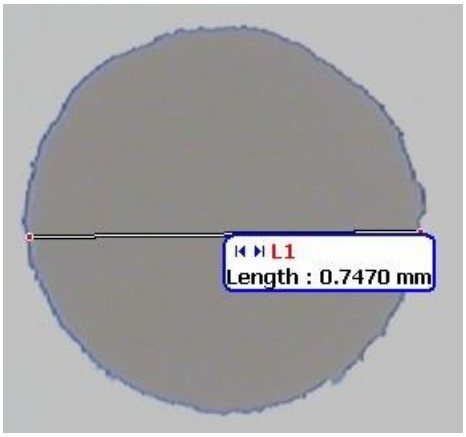

Figure: 5.62: Shape of spheroids

Size of spheroids

Size pellets were calculated by digital vernier caliper and the reported size is 0.7470 mm.

Bulk density

Bulk density and tapped density were used for the calculation of Hausner's ratio and compressibility index. These help in determining the flow property and the compressibility of ingredients. A negligible variation in bulk density was observed. The bulk density of spheroids was found to be 0.72.

Tapped density of spheroids

A negligible difference was experimentally observed in the tapped density and was found to be 0.84.

Carr's index of spheroids

Results of the compressibility study showed that the compressibility index of the spheroids was having excellent flowability as the results fell in the range of ≤10 %. The compressibility index was found to be 7.1, which shows excellent flow.

Hausner's ratio of spheroids

According to USP 2000, spheroids with Hausner's ratio between 1.12 and 1.18 exhibit good flow, and above 1.35 showed poor flow properties. The result which was found to be 1.14, reflecting good flow property of prepared spheroids.

Angle of repose of spheroids

The angle of repose of spheroids was found to be 20 again confirming very good flow (IP, 2007).

Friability of spheroids

Friability was observed to lie in the range of 0.74% of spheroids which fell within the acceptable limit as per I.P. 2007. The result of friability showed that the formulation had sufficient hardness for its safe shipment.

5.4.4.7 ***In-vitro drug release for spheroids containing CD complexed ART***

The dissolution rate of the pure drug was very slow, owing to the poor solubility and hydrophobic nature of the drug. The increased apparent solubility of ART stemming from the interaction of the drug with βCD led to an evident improvement in the dissolution rate. As expected, spheroids filled in enteric-coated capsule shell were not disintegrated upon exposure to 0.1 N HCl for 2 h. But when exposed to phosphate buffer pH 6.8, disintegration was observed within 1 hour. So this proved that the enteric coating was uniform and acid resistant enabling protection of the drug content from degradation in the acidic environment at the stomach. Furthermore, release in simulated intestinal fluid supported the hypothesis of increasing absorption of the drug. *In vitro* dissolution studies for the first 2 h in 0.1 N HCl revealed the acid resistance capacity of spheroids. The dissolution behavior of spheroids in phosphate buffer pH 6.8 revealed the drug release characteristics. The similarity factors (f2)

between the couples ART, ART-CD spray dried complex and ART-CD spheroids filled in enteric-coated capsule shell were 7.29, 12.18, and 44.20, respectively, indicating that the dissolution profiles were significantly different from each other. The release of the drug was rapid up to some extent and after a certain time, it showed sustained release. The % cumulative drug release of ART, ART-CD, ART-CD spheroids showed that around 30% of the drug was released during 3 h and maximum drug release i.e. 96% which is mentioned in Fig 5.63.

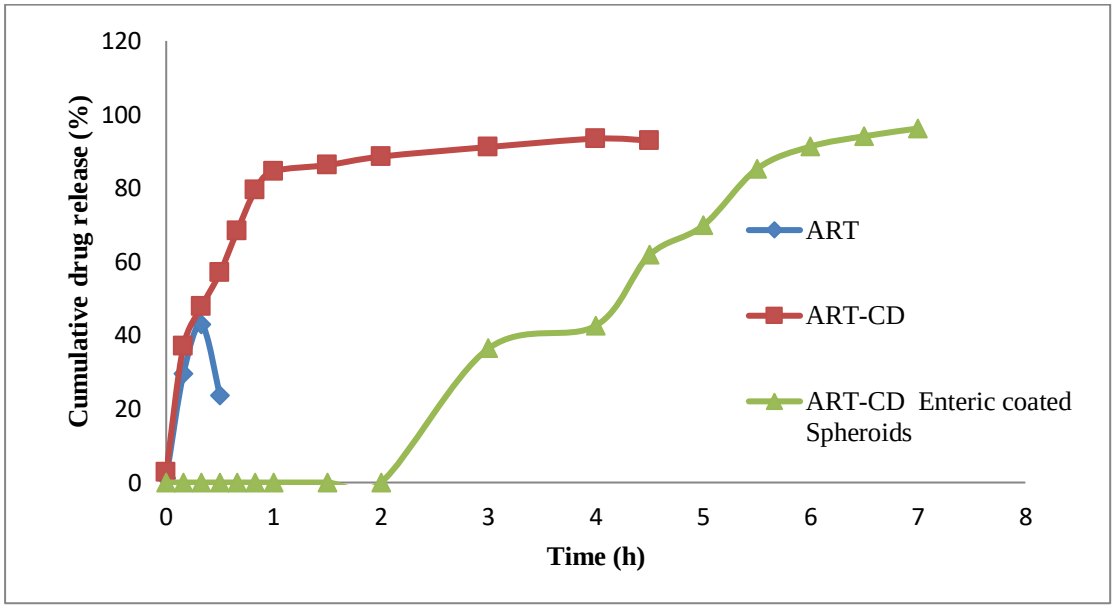

Figure 5.63: Cumulative drug release (%) of ART, ART-CD, and ART-CD loaded enteric coated spheroids.

5.4.4.8 *Morphology of CD complex spheroids*

ART, CD, Physical mixture of CD and ART, and lyophillized ART-CD complex were examined by scanning electron microscope (SEM) to visualize the surface topography as shown in Fig 5.64. Samples were prepared by preparing the film on aluminium stub. The stubs were then coated with gold to the thickness of 200-500Å under the argon atmosphere using a gold sputter module in a high vaccum evaporator. The coated samples were scanned and photographs were taken with SEM camera (Jeol-1761, Cmbridge, UK).

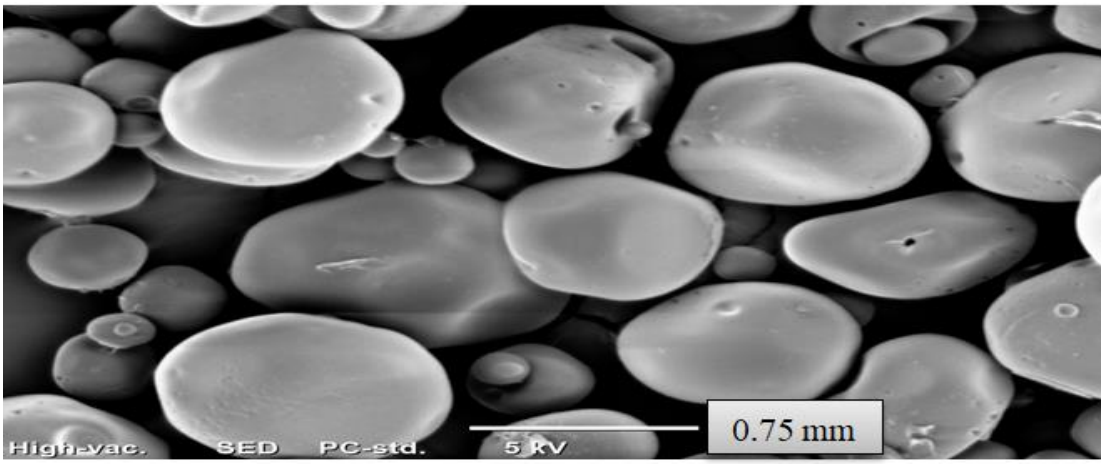

Figure 5.64: SEM Image of spheroids.

5.4.4.9 *Discussion on spheroids formulation*

ART-CD inclusion complexes in a 1:1 molar ratio using the spray drying method were successfully prepared. Spheroids of the ART-CD complex were made using the extrusion spheronization technique. The statistically optimized recipe was used to make the spheroids, which were then placed into enteric-coated capsule shells and evaluated for various characteristics such as size, shape, flow characteristics, disintegration time, release profile, etc. Angles of repose for the various formulations were compared to those of the formulation, which demonstrates that the formulation flow characteristics were good after pelletization. The results of the weight variation test for spheroids were within the permitted ranges. FT-IR spectra showed their spectra were similar to the ones recorded for pure CD, strengthening the idea that ART was successfully included in their cavity. The morphologies, evaluated by SEM analysis, revealed important changes in the structure and shape of the binary lyophilized systems, proving that new compounds were formed. The recorded DSC curves showed that the complexation was complete in the case of ART-CD spheroids/ pellets drug delivery systems that presented a good mechanical resistance with a low friability, and a weight variation within the compendial limits. A rapid disintegration was registered for both series of tables and it can be considered that the main purpose of this study was completely achieved, as disintegration is the critical quality attribute for tablets. The dissolution rates were satisfying and within the imposed pharmacopeial limits for prepared formulations. As the performances were very similar for the formulation, the conclusion is that the pharmaco-technical properties present a higher dissolution rate. When compared to pure medication, the inclusion of

complex permeability experiments is more favorable. This could be because the medication is trapped in the complex and all of it permeates through the skin of the gut. The produced spheroids filled in enteric-coated capsule shell pharmacokinetic experiments verified the improvement in oral bioavailability. 51.89 percent more of the bioavailability was made available. This is because, upon oral administration, only negligible quantities of intact CDs—due to their bulky and hydrophilic nature—are absorbed from the gastrointestinal system.

Evaluation parameters for enteric coated capsule shells

The prepared SLNs, NLCs, SMEDDS, spheroids were filled in enteric coated capsule shell. The enteric coated capsule shells filled with formulations were evaluated on the basis of parameters, as given in Table 5.56.

Table 5.56: Evaluation parameters for enteric coated capsule shells filled with different formulations.

Parameters for evaluation	**Various formulations**			
	SLNs	**NLCs**	**SMEDDS**	**Spheroids**
Size/ Volume (mL)	0.61	0.61	0.61	0.61
Weight loss/gain	Less than 2%	Less than 2%	2-3%	Less than 2%
Moisture	0.02%	0.01%	0.3%	0.01%
Weight variation	±0.94%	±0.89%	±0.67%	±0.91%
Content Uniformity	400 mg	390 mg	280 mg	520 mg

5.4.5 *Formulation development, optimization, and characterization of enteric coated tablets.*

The enteric coated tablets were prepared by direct compression method as discussed in detail in chapter-4 (section 4.5.5.3).

5.4.5.1 *Statistical optimization of enteric-coated tablets*

Applications of statistical experimental designs are useful techniques to optimize the formulation and process variables. Traditionally, pharmaceutical formulators used to change one single variable at a time but that did not give an idea about the interaction among the other variables so optimization of formulations was a tedious process. The

statistical experiment designs overcome the limitations of the conventional approach and require less number of experiments to achieve an optimum formulation, yielding the ‘‘best solution’’ in the presence of competing objectives which results in saving time, cost, and manpower. Moreover, it helps in understanding the interactions among factors. There are numerous types of experimental designs including factorial designs (FD), fractional factorial designs (FFD), central composite designs (CCD), star designs, center of gravity designs, and Box-Behnken designs. The formulation-by-design concept is recently used in the pharmaceutical industry for formulation optimization and quality control. In design-based optimization, the influences of all experimental variables, factors, and interaction effects on the response are investigated. An experimental design is chosen to estimate the influence of the different variables on the result. In screening studies, linear or second-order interaction models are common, such as in full factorial or fractional factorial designs. The former design is limited to the determination of the linear influence of the variables, while the latter allows for interaction terms between variables to be evaluated as well (Maneesha *et al.*, 2006).

5.4.5.2 *Selection of critical ingredients using Plackett-Burman design for enteric coated tablets*

The Plackett–Burman screening design was used to screen different ingredients based on the magnitude of their effect on critical quality attributes for effervescent formulation. Low and high values for each factor tested in the screening design were identified in preliminary experiments to define PARs. The magnitudes of responses for each of the 8 experiments are given in Table 5.57.

Table 5.57: Box –Behnken design-based limits for selected factors using Design-Expert software.

Factor	Name	Units	Minimum	Maximum	Coded Low	Coded High	Mean	Std. Dev.
A	Microcrystline cellulose	mg	20.00	60.00	-1 ↔ 20.00	+1 ↔ 60.00	40.00	13.09
B	Magnesium stearate	mg	5.00	15.00	-1 ↔ 5.00	+1 ↔ 15.00	10.00	3.27
C	Lactose monohydrate	mg	20.00	60.00	-1 ↔ 20.00	+1 ↔ 60.00	40.00	13.09
D	PVP	mg	5.00	25.00	-1 ↔ 5.00	+1 ↔ 25.00	15.00	6.55

5.4.5.3 *Response surface methodology for enteric coated tablets*

For optimization of the most effective variables (MCC, lactose, sodium starch glycolate) to get selected response (percentage release of drug in 2-6 hours) in PARs, CCD of response surface methodology was applied by using Design Expert software. The recipe of 20 experimental runs of dependent and independent variables and the most effective response *i.e*. release of drug (2-6 h) by the central composite design is presented in table 5.31. Different combinations of MCC, lactose, and sodium starch glycolate had given the result of effective response *i.e.* release of drug as low as 58.47 % (Run 10) and as high as 87.67% (Run 1). This indicated the significance of the interaction of effectors and their effect on the overall response.

5.4.5.4 *Statistical analysis of mathematical model for enteric coated tablets*

Statistical testing of the models (percentage drug release) was done by the analysis of variance (ANOVA) test to check model accuracy and the results are summarized in Table 5.58. The goodness of the drug release can be checked by the determination coefficient (R^2) and correlation coefficient (R). The coefficient of determination (R^2= 0.7554) indicated that the sample variation of 75.54 % was attributed to the independent variables and only about 24.46 % of the total variation cannot be explained by the selected model. The closer the value of R^2 to 1.0, the better the correlation between the experimental and predicted values. In the present study, the value of R^2 (0.755) being close to 1.0 indicated a close agreement between the experimental results and theoretical values predicted by the model. Quadratic terms of release of drug (2-6 h) were highly significant as reflected by Prob>F values of 0.0500.

Table 5.58: Experimental recipe and observed responses of 3 level central composite design

Std	Run	A:Microcrystline cellulose	B:Magnesium stearate	C:Lactose monohydrate	D:PVP	Drug release
		(mg)	(mg)	(mg)	(mg)	Percentage
19	1	20	10	60	15	77.87
27	2	40	10	40	15	73.53
25	3	40	10	40	15	73.53
10	4	60	10	40	5	70.95
20	5	60	10	60	15	63.67
23	6	40	5	40	25	69.8
24	7	40	15	40	25	69.1
16	8	40	15	60	15	70.05
1	9	20	5	40	15	80.95
3	10	20	15	40	15	79.82
26	11	40	10	40	15	73.16
4	12	60	15	40	15	66.108
11	13	20	10	40	25	75.96
28	14	40	10	40	15	73.47
6	15	40	10	60	5	75.038
2	16	60	5	40	15	67.55
22	17	40	15	40	5	77.6
17	18	20	10	20	15	82.85
18	19	60	10	20	15	70.1128
14	20	40	15	20	15	76.14
9	21	20	10	40	5	84.8
8	22	40	10	60	25	66.96
13	23	40	5	20	15	76.75
15	24	40	5	60	15	71.48
21	25	40	5	40	5	78.54
5	26	40	10	20	5	80.86
29	27	40	10	40	15	73.47
12	28	60	10	40	25	62.81
7	29	40	10	20	25	72.02

5.4.5.5 *ANOVA for quadratic model of enteric coated tablets containing ART-CD complex*

Values of 't' coefficients for each of the selected parameters were calculated by performing an ANOVA test and are given in Table 5.59.

Table 5.59: Analysis of variance test (ANOVA) for release of drug (2-6 h)

Source	Sum of Squares	df	Mean Square	F-value	p-value	Inference
Model	864.32	14	61.74	2973.27	< 0.0001	Significant
A-Microcrystalline cellulose	547.41	1	547.41	26363.49	< 0.0001	
B-Magnesium stearate	3.26	1	3.26	156.87	< 0.0001	
C-Lactose monohydrate	94.44	1	94.44	4548.39	< 0.0001	
D-PVP	217.92	1	217.92	10495.25	< 0.0001	
AB	0.0243	1	0.0243	1.17	0.2973	
AC	0.5349	1	0.5349	25.76	0.0002	
AD	0.1225	1	0.1225	5.90	0.0292	
BC	0.1681	1	0.1681	8.10	0.0130	
BD	0.0144	1	0.0144	0.6935	0.4190	
CD	0.1452	1	0.1452	6.99	0.0193	
A^2	0.0214	1	0.0214	1.03	0.3269	
B^2	0.0816	1	0.0816	3.93	0.0675	
C^2	0.0665	1	0.0665	3.20	0.0952	
D^2	0.2122	1	0.2122	10.22	0.0065	
Residual	0.2907	14	0.0208			
Lack of Fit	0.1946	10	0.0195	0.8102	0.6432	Not significant
Pure Error	0.0961	4	0.0240			
Cor Total	864.61	28				

Factor coding is **Coded**.

Sum of squares is **Type III - Partial**

The **Model F-value** of 2973.27 implies the model is significant. There is only a 0.01% chance that an F-value this large could occur due to noise.

P-values less than 0.0500 indicate model terms are significant. In this case, A, B, C, D, AC, AD, BC, CD, and D^2 are significant model terms. Values greater than 0.1000 indicate the model terms are not significant. If there are many insignificant model

terms (not counting those required to support hierarchy), then model reduction is essential to improve the model.

The **Lack of Fit F-value** of 0.81 implies the Lack of Fit is not significant relative to the pure error. There is a 64.32% chance that a Lack of Fit F-value this large could occur due to noise.

Model equation for release of drug of enteric coated tablets

Release (2-6 h) = 73.432 + -6.7541 * A + -0.521 * B + -2.8054 * C + -4.2615 * D + -0.078 * AB + -0.3657 * AC + 0.175 * AD + -0.205 * BC + 0.06 * BD + 0.1905 * CD + 0.0574833 * A^2 + 0.112133 * B^2 + 0.101233 * C^2 + 0.180883 * D^2 ……. (6)

Where, A=Microcrystalline cellulose, B= Magnesium stearate, C=Lactose, D=PVP

- The magnitude and direction of the factor coefficient in the equation explained the nature of the effect of factors on the response.

- Factors with a coefficient of greater magnitude showed a high effect on the response suggesting that concentration of MCC, Lactose, and sodium starch glycolate demonstrated a very significant effect on response.

5.4.5.6 Contour plots and optimization of enteric coated tablets

The contour diagrams were plotted using the polynomial equation to study the interaction of major effective variables and critical quality attributes. The contour plots affirmed the unimodal nature of the objective function showing an optimum in the boundaries. These plots also revealed that there were no saddle points within the design space. Contour plots were then generated to study the effect of the interaction of different variables i.e. MCC, lactose monohydrate, PVP and magnesium stearate on the release of the drug. The statistically optimal values of variables were obtained by moving the major and minor axis of the plots and using the "Point Optimum" feature of the software by independent variation of one parameter at a time. As MCC concentration was not affecting the selected quality attributes significantly after a certain level, its concentration was kept constant at 20 mg for further optimization studies. Release of the drug was obtained between 2-6 h under the same conditions. An increase in concentrations of lactose and magnesium stearate above 108 mg and

9.4 mg respectively were not affected the release profile significantly. So the optimum values of the ingredients, as obtained by the design, were: MCC (20 mg), lactose monohyderate (108 mg), and magnesium stearate (9.4 mg). The model predicted values of release of drug by Design Expert Software were 88.09%. The interrelationships of the two major ingredients, lactose monohyderate and MCC on the release of the drug are shown as 2-D contour plots and 3-D response surface plots in Fig. 5.63.

5.4.5.7 Validation of model of enteric coated tablets

To confirm the optimal concentration, a set of three replicate experiments with the optimal combination of major variables and responses were used as confirmation of the forecasted formulation of enteric-coated tablets. The confirmatory experiment showed 86.23 % drug release of the formulation as given in Table 5.60. This represented 97.88 % similarity of the predicted models for drug release respectively.

Table 5.60: Composition of checkpoint formulation, expected and observed values for response variables of drug release (2-6 h).

Composition (mg)				**Model predicted values**	**Observed Values**
Microcrystalline cellulose	Lactose	Magnesium stearate	PVP	Drug release (2-6 h) %	
40	40	10	15	73.43	80.23

Application of FbD using statistical design allowed the reliable shortlisting of a few most significant factors from a long list of probable factors affecting the formulation process. This method also features studies of different rare interactions between variables which is not possible by the One-Variable-At-a-Time (OVAT) procedure as shown in Fig. 5.65. Linear correlation plots between the actual and the predicted response variables of drug release showed the scatter of the residuals versus actual values for better representing the spread of the dependent variables under present experimental settings. The overlay plot is as shown in Fig. 5.66 shows the effective region for formulation development.

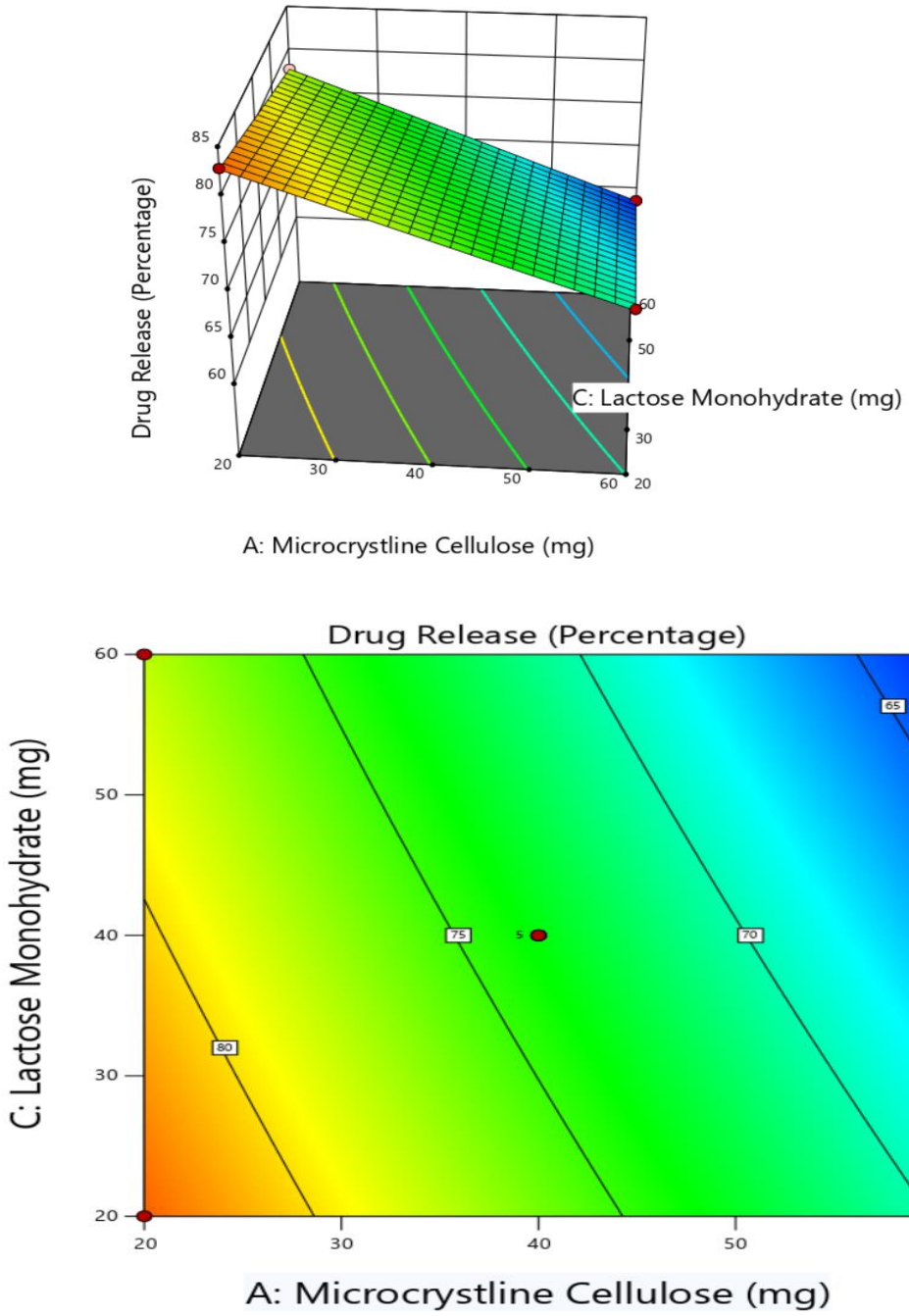

Figure 5.65: 3D & 2D contour plots for the interactive effect microcrystalline cellulose and magnesium stearate on drug release.

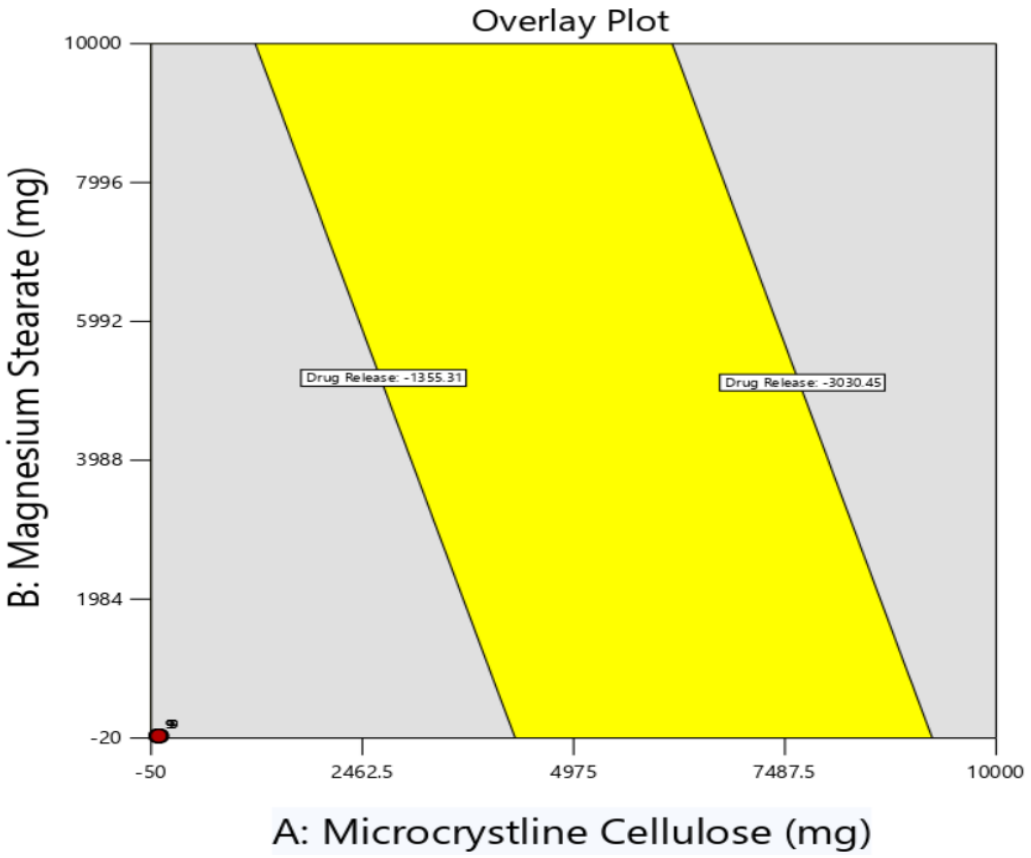

Figure 5.66: Overlay plot of optimized enteric-coated tablets.

5.4.5.8 Evaluation of enteric-coated tablet formulation

5.4.5.8.1 Particle Size Distribution

The particle size distribution of the enteric coated tablet premix powder is mentioned in Table 5.61.

Table 5.61: Particle size distribution.

S No.	Sieve No.	% weight retain (uncoated)
1	18	0
2	22	1.1
3	25	5.3
4	30	87

5.4.5.8.2 Flow properties of powder

Bulk density

Bulk density and tapped density were used for the calculation of Hausner's ratio and compressibility index. These help in determining the flow property and the

compressibility of ingredients. A negligible variation in bulk density was observed. The bulk density of spheroids was found to be 0.81.

Tapped density

A negligible difference was experimentally observed in the tapped density and was found to be 0.88.

Carr's index (%)

Results of the compressibility study showed that the compressibility index of the premix powder of tablets was having excellent flowability as the results fell in the range of ≤10 %. The compressibility index was found to be 6.8 which shows excellent flow.

Hausner's ratio

According to USP 2000, spheroids with Hausner's ratio between 1.12 and 1.18 had good flow, and above 1.35 showed poor flow properties. The result which was found to be 1.14.

Angle of repose

The angle of repose of spheroids was found to be 26 According to I.P. this is a very good flow.

5.4.5.9.3 *Finished Product Quality Control (FPQC) Evaluation* of enteric coated tablets

Friability

Friability was observed to lie in the range of 0.75% of tablets which fell within the acceptable limit as per I.P. 2007. The result of friability showed that the formulation had sufficient hardness for its safe shipment.

Hardness test

The hardness of tablets was found to be in the ranges of 6.8±0.95 to 8.5±0.82 kg/cm^2

Friability

Three batches of optimized formulations were evaluated for friability and the % weight loss in the friability test was found to be less than 1% for all batches indicating that prepared tablets can withstand mechanical shock or during handling.

Weight variation test

The average weight of tablets was found to be 215.42 mg for all batches and % deviation was also observed within specified value. Overall the all prepared formulations were of good quality with reference to consistency.

Drug content uniformity of enteric coated tablets

Good uniformity in drug content was found among all the batches of tablet formulations and the percentage of drug content was more than 95%. Hence it complies with the official specification.

Confirmation of coating of enteric coated tablets

The confirmation of the coating was done by visual inspection and by checking the dispersion of the colour on the surface by which we can make sure that the coating of the polymer was proper and equal. Uniformity of coating was further confirmed by coating with Eudragit S100 up to a consistent weight gain of 10%.

In vitro drug release from optimized formulation of enteric coated tablets

The *in vitro* drug release profile of the entrapped drug was determined in different simulated fluids to mimic the gut environments using USP apparatus I and is shown in Fig. 5.67. The release study of ART-CD containing enteric-coated tablets was repeated thrice to check the reproducibility. *In vitro* drug release profile indicated that there was no release of drug for the initial 2 h. and after 2 h. there was a burst release of drug from the formulation, which may be due to the pH-dependent polymer used for the enteric coating. In following 4 h the cumulative release percentage reached 86.23%. The release pattern was in a sustainably increased manner, which provided the possibility to continually exhibit therapeutic effect.

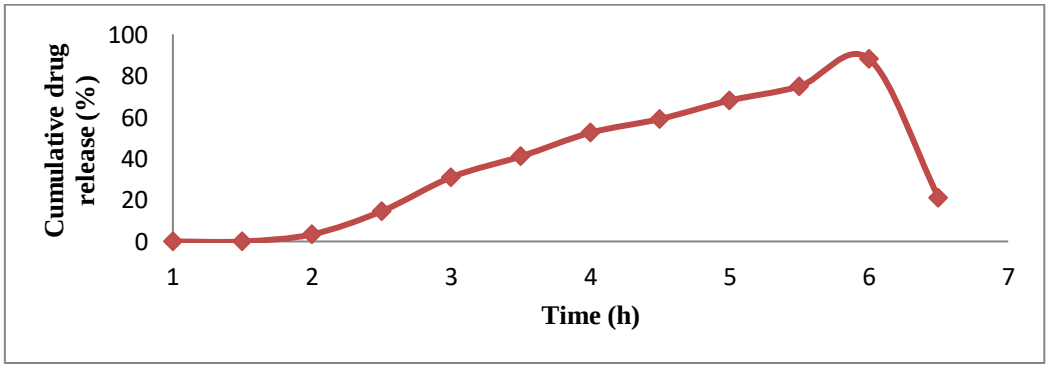

Figure 5.67: *In vitro* release profile of CD complexed ART from the enteric coated tablets.

5.4.5.9.4 *Discussion on enteric coated tablet formulation*

Cyclodextrin inclusion complexes may be formed to increase aqueous solubility, and enteric coated tablets were created to prevent stomach breakdown A barrier used with oral medications that is pH dependent regulate the drug absorption in GIT. Using a pH-dependent polymer (enteric coating) retards drug release before it reaches the small intestine, preventing the drug's decomposition in the stomach.

The problem of low solubility of arteether was addressed by preparation of inclusion complex with β-cyclodextrin (AE-β-CD 3º). Arteether complexes were formed by lyophilization technique. Ternary complexes with polyvinyl pyrrolidone were used to prepare equimolar inclusion complexes. The complexation was furthur confirmed on the basis of NMR, Mass, XRD, DSC, FT-IR. On the basis of solubility studies it was confirmed that the solubility of drug by complexation using co-evaporation technique was maximally increased by 77.05 folds. The results suggested that large cavity of β-CD can form inclusion complex with bulky molecule like arteether for improvement of its solubility profile.

The purpose of this study was to increase arteether's solubility and stop it from degrading in the stomach in order to increase its antimalarial activity. Arteether's limited solubility was a difficulty that was solved by creating an inclusion complex with cyclodextrin (ART-CD). When compared to pure drug, the release profile of ART tablet formulations demonstrated greater release. This could be a result of the medication being enclosed in cyclodextrin, which, in addition to the solubilization effect, has a greater water solubility than the crystalline form. According to in-vivo tests, enteric-coated tablets' oral bioavailability increased by a maximum of 48.29 percent. Only negligible quantities of intact CDs are absorbed from the gastrointestinal system due to their bulky and hydrophilic character, reducing the improved bioavailability of ART on oral administration.

5.4 Comparative permeability studies of prepared formulations

The Franz diffusion cell approach was used to investigate the permeability of prepared formulations of ART, which correlates enhanced bioavailability as a component of improved dissolvability. Absorption of drug via the intestine's humid environment is limited by the diffusion limit through the lipophilic apical layer, and the drug must be dissolved to maximise bioavailability. Additionally, the drug

solubility is determined by its solid state features, such as molecule size, internal energy, glasslike or nebulous structure, atomic mobility, and wettability. The concentration of ART distributed over the pig's colon using ART-loaded SMEDDS, ART-SLN, and ART-NLCs vs pure ART (Fig. 5.68).

The findings demonstrated a maximum improvement (7.1 fold) in the permeabtion concentration measure of ART, with SLNs in comparison to ART in its pure form. The findings corroborate previous equilibrium solubility studies. The enhanced penetrability nanoformulations may be used to confirm the existence of microcrystalline and amorphous ART fragments in the lipid phase. A nearly 7.1 fold, 6.8 fold, 7 fold, 4.6 fold increase in permeability compared to ART in its pure form was observed with SLNs, NLCs, SMEDDS, ART-CD inclusion complex respectively also showed positive effect on permeability of drug across membrane. The findings support the feasibility of various formulations approaches for enhancing the bioavailability of ART.

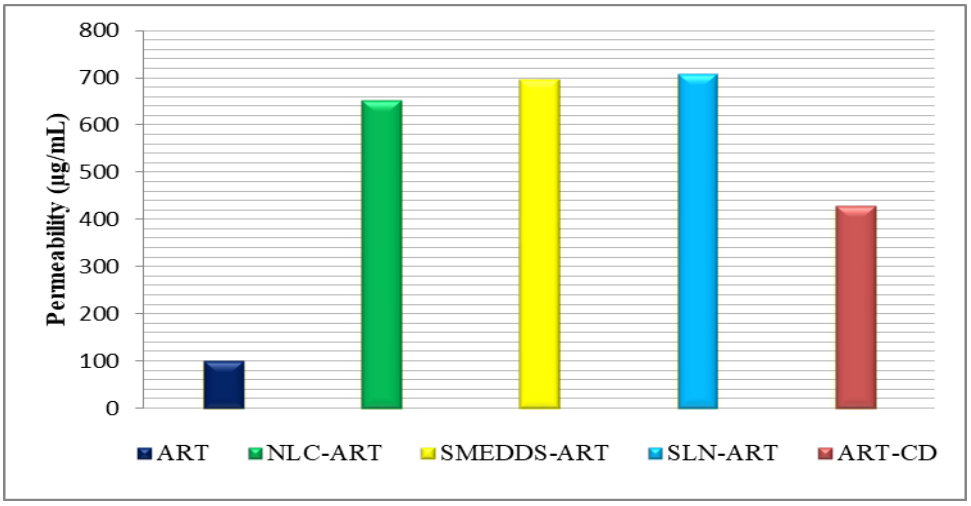

Figure 5.68: The permeability studies of prepared formulations.

5.6 Pharmacokinetic study of ART containing formulations

Plasma drug concentration–time profile of pure drug suspension, ART-CD enteric-coated tablets and formulations encapsulated in enteric capsule shell (lyophilized ART-SLN, lyophilized ART-NLC, solid ART-SMEDDS, ART-CD spheroids) administered orally in rabbits are represented as Fig. 5.69, Table 5.61 represents various pharmacokinetic parameters of the same. The data showed the maximum

enhancement of oral bioavailability through spheroids. Additionally it was found that all formulations approaches adopted in present study have resulted in significant improvement in bioavailability after oral administration in comparison to pure drug.

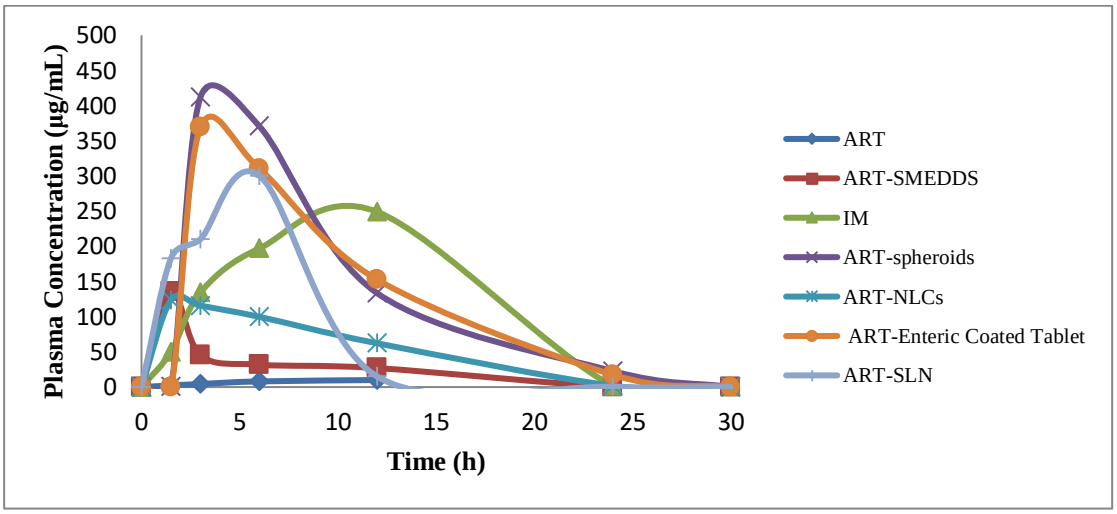

Figure 5.69: Concentration vs. time profile of plain drug suspension and different formulations.

Following oral administration of all developed formulations equivalent to 6 mg/Kg to three rabbits for each batch, the mean pharmacokinetic parameters are shown in Table 5.61 along with the plasma concentrations versus time profile curve in Fig. 5.69. It was observed that the ART-CD enteric coated tablet's C_{max} was lower than that of the pure drug suspensions. The curve also demonstrated that the plasma concentration of ART was lower in the early hours. The results also confirmed that the absolute bioavailability was enhanced as given in Table 5.62. The physicochemical properties of nanoparticles, such as size, shape, surface charge, and surface chemistry, play a critical role in determining their bioavailability (Fang *et al.*, 2013). However nanoformulations exhibited slightly lesser bioavailability enhancement in comparison to spheroids containing ART-CD complex. Nanoparticles with unfavorable physicochemical properties may be rapidly cleared by the immune system or may not be able to penetrate biological barriers, leading to low bioavailability. Also, nanoparticles can aggregate in the body, leading to decreased bioavailability. Also nanoparticles have limited drug loading capacity due to their small particle size and high surface area, which can lead to drug expulsion or degradation during the manufacturing process (Rashidzadeh *et al.*, 2019). Nanoparticles are unstable in biological fluids, leading to drug release and

degradation before reaching the target site. These formulations have very limited tissue penetration (Puttappa *et al.,* 2017). Moreover, cyclodextrins are cyclic oligosaccharides that can enhance the bioavailability of drugs by improving their solubility and stability (Szejtli *et al.,* 1998). Cyclodextrins have a hydrophobic cavity that can encapsulate hydrophobic drugs, forming inclusion complexes that increase the solubility and stability of the drug. This increases the concentration of the drug in the bloodstream, leading to improved bioavailability (Santos *et al.,* 2021).

Table 5.62: Pharmacokinetic comparative study of formulations and plain drug suspension.

Parameters	Encapsulated in enteric coated capsule shells					ART-CD Enteric coated tablets	Intravenous injection	Intra muscular injection
	Plain Drug	ART-SLN	ART-NLC	ART-SMEDDS	ART-CD-spheroids			
Dose	6 mg/kg	6 mg/kg	6 mg/kg	6 mg/kg	6 mg/kg	6 mg/kg	1 mg/kg	150 mg/2mL
slope	-0.02703	-0.162	-0.042758	-0.18868	-4.10844	-0.112541	-0.01033	-0.64556
AUC	79.8	2241.399	1496.278	691.2823	4208.103	3915.949	1081.218	3546.419
AUMC	117.8074	2731.7845	2752.077	1002.81	4251.655	3915.972	97448.9	3636.752
V_d	2.045708	0.01471	28100.23	0.034423	0.000373	0.014777	0.00647	2456.235
$T_{1/2}$	11.13289	1.8579	7.037557	1.594822	0.073242	2.673799	0.44	0.466124
Total clearance	0.127326	0.00549	2767.077	0.014958	0.003528	0.00383	0.000154	3651.752
MRT	1.47919	1.2187	1.839282	1.450652	1.01035	1.0005	90.12881	1.025472
C_{max}	2.361879	182.9138	123.6606	135.3684	412.0776	0.006117	2292.009	134.3005
% Absolute bioavailability	0.9828%	27.64043%	18.45176%	8.524735%	51.89337%	48.29059%	100%	43.73363%

5.7 Antimalarial activity

The IC_{50} values of ART and ART-CD were also determined. The fractional inhibitory concentration (FIC) was determined for both in each combination (FIC=concentration of a compound that caused 50% inhibition in the combination/concentration of the compound required for 50% inhibition when used alone). The FICs at different ratios for ART and ART-CD combinations were plotted using linear regression analysis to construct an isobologram using GraphPad Prism.

The IC_{50} value of ART and ART-CD complex was estimated to be 0.76 ng/mL and 0.733 ng/mL equivalent to 3.4 ng/mL(calculated by molar ratios) in dimethylsulfoxide solvent respectively. The IC_{50} value of ART-CD complex is almost equivalent to ART in dimethylsulfoxide solvent which showed the acceptability of antimalarial

activity of ART-CD complex drug. The results in Fig. 5.70 shows the experiments were repeated three times for accuracy of result.

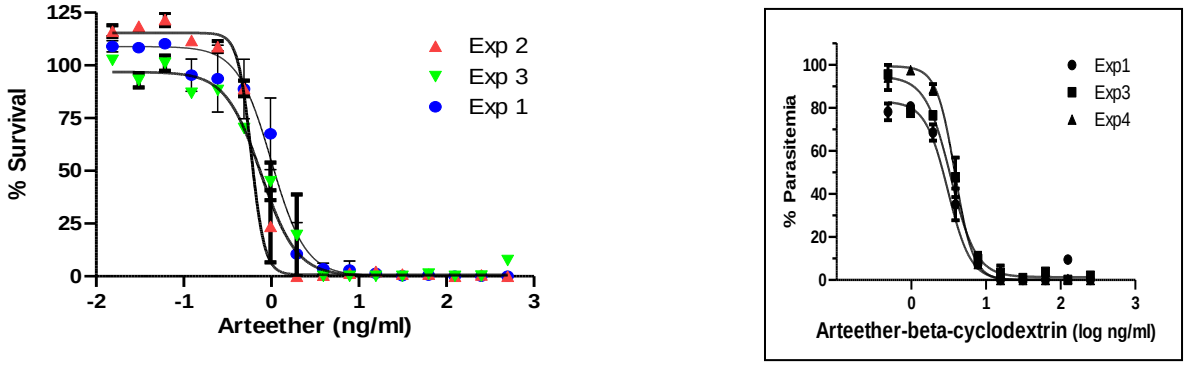

Figure 5.70: Mean % parasitemia for plain ART and ART-β-CD.

Based on the IC_{50} values, it appears that the inhibition rate of ART-CD complex was comparable for ART with pure drug (Prasad *et al.*, 2013). This suggested that ART-CD complex may be effective in inhibiting the target. However, as mentioned earlier, it's important to consider other factors such as drug delivery and pharmacokinetics when evaluating the effectiveness of a drug.

With benefits including higher acceptability, particularly among children and female patients, enhanced compliance, cheap production cost, and many dose-related difficulties, the proposed formulation may offer a new vista in the treatment of malaria worldwide utilising artemisinin derivatives.

The results of solubility studies, oral bioavailability and antimalarial activity confirmed that the ART-CD complexation techniques showed best results compared with prepared nanoformulations. Enteric coated tablets also offered a reliable delivery system for the enrichment in poorly aqueous soluble drugs bioavailability. The significance of this research is that it will provide economic, safe, patient compliant formulation for effective management of malaria with several advantages when compared with the available marketed formulation. It will help the rearchers to know the methods of solubility and bioavailability enhancement techniques for such BCS class of drugs. The present work is a comprehensive study for development of industry acceptable and patient compliant oral dosage form of arteether by implementing Quality –by- Design principles.